Conducting Polymers for Electronic Nose Applications

A dissertation submitted to the Faculty of Science of the University of Neuchâtel, in fulfilment of the requirements for the degree of "Docteur ès Sciences"

by

M.G.H. Meijerink

Institute of Microtechnology
University of Neuchâtel
P.O. Box 3
CH-2007 Neuchâtel

1999

IMPRIMATUR POUR LA THÈSE

Conducting Polymers for electronic nose applications

de M. Marcus Gerhardus Hendrikus Meijerink

UNIVERSITÉ DE NEUCHÂTEL

FACULTÉ DES SCIENCES

La Faculté des sciences de l'Université de Neuchâtel sur le rapport des membres du jury,

Mme. M. Koudelka-Hep (directrice de thèse), N. de Rooij, D.J. Strike, V. Neumann (CSEM, Neuchâtel) et W. Schuhmann (Bochum, D)

autorise l'impression de la présente thèse.

Neuchâtel, le 21 mai 1999

Le doyen:

F. Stoeckli

Summary

This thesis deals with the characterisation and further development of conducting polymer based gas sensors for electronic nose applications.
The electrodeposition process of conducting polymers for the fabrication of chemo-resistors is examined and the influence of several deposition parameters are examined by comparison of the vapour responses of the resulting sensors.
The electrical phenomena, and especially the influence of sorbed vapour heron is studied with chemo-resistors and with newly developed FET based devices. The FET structures are also suitable for vapour recognition. This is demonstrated with some organic vapours, and Swiss cheeses.
The vapour sorption, which was found to be a critical step in the sensor response, was studied by comparison of experimental data to a theoretical model.
At the end of this thesis, a feasibility study for a dielectric vapour sensor is presented.

Table of Contents

1 Introduction

1.1 Electronic noses

1.1.1 History

Liquid and many solid samples release gaseous substances at ambient temperature. For many products we are exposed to in every day life, the resulting mixture of volatile components can be perceived as an odour, which can give important information about the product they are released from. A human being can for example easily distinguish between spoiled and fresh meat.

Also for laboratory analysis and product screening, the analysis of a product odour can be interesting. A controlled vapour composition can be obtained by leaving samples in a closed thermostatted vial until the equilibrium between vapour and sample is reached. This equilibrium vapour mixture is often referred to as the headspace of the sample [1]. If the product parameters of interest can be derived from an analysis of the sample headspace, this if often more cost effective then a product analysis because of the ease of handling of gaseous samples. In consequence there has been an interest in headspace analysis as a characterisation method [1-3], since the early days of gas chromatography. The area got a new impulse after the publication of a sensor based electronic nose by Persaud & Dodd in 1982 [4]. Claimed advantages over conventional techniques include speed of analysis, ease of sample preparation, and price.

Since then a lot of research in the field of electronic noses has resulted in the appearance of a large number of research papers on electronic noses and the realisation of several commercially available instruments. Published applications are mainly in quality control [5-7], but also include fields like health screening [8] and micro-organism identification [9].

1.1.2 Working principle

The principle of operation of an electronic nose is often compared to the mammalian olfactory system [4,10-12]. This is based on a widely sensitive array of non-specific receptor cells (the olfactory bulb) which all lead their signal to a central processing unit (the brain). In an electronic nose, the function of the olfactory bulb is performed by an array of non-specific gas sensors. Their signals are fed into a computer, which treats the data, and compares it to previously acquired data in a database, to recognise the odour. For a successful recognition of the odour, the sensors need to give a stable and reproducible signal, when exposed to the odours of interest.
An important distinction between the nose approach and more established analytical techniques like head-space chromatography [2] is that the electronic nose gives a typical 'image' of an odour instead of the concentrations of the individual components present in the odour.
Although at a first glance, this lack of composition data seems like a disadvantage, in many applications only the ability to observe a change in the odour is required.

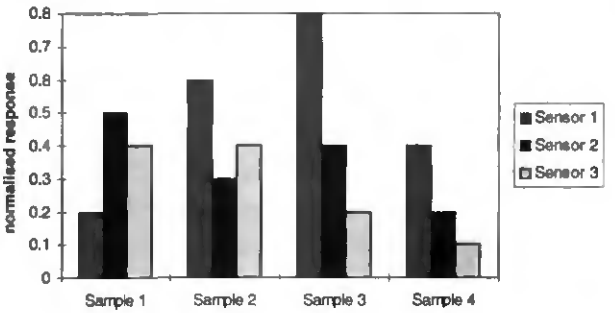

Fig. 1.1: An example of a possible output pattern for a 3 sensor system exposed to 4 different samples.

To obtain a 'image', an array of sufficiently different sensors should be used. Figure 1.1 gives an example of sensor responses which are sufficiently different to allow for a distinction between the samples. It can be observed that sample 3 and 4 have the same response patterns, but

different amplitudes. In the case of linearly responding sensors, this would correspond to the same vapour mixture with a different concentration.
More details and more examples can be found in one of the review papers and books [10,14-18] in this field.

1.1.3 Data treatment

The data treatment is an important part of the electronic nose concept. Independent of the sensor type used, two phases can always be distinguished in the data treatment: the feature extraction, also called pre-processing, and the pattern recognition [12,18,19]. The feature extraction reduces the transient sensory data of every sensor, to one or a few typical values characteristic for the odour. The values of every individual sensor are then collected in a 'feature vector' [12] or -matrix which is used as input for the pattern recognition procedure.

Feature extraction

The choice of the feature extraction depends on the sensor type used. Although other normalisation procedures like auto-scaling [20,21] have also been used, normalisation can be considered to be the standard procedure for conducting polymer based chemo-resistors [22-25].
A simple normalisation procedure consisting of division of the sensor resistance by the base-line resistance R_0 (equation 1.1) has been used throughout this thesis. Although simple, this treatment has previously been shown to reduce the influence of sensor drift [25].

$$Normalised\ response = \frac{R_t - R_0}{R_0} \tag{1.1}$$

In more sophisticated measurements protocols, feature extraction may furthermore involve a normalisation with values obtained with reference samples, to further compensate for sensor drift [26,27].

Pattern recognition

Depending on the purpose and characteristics of specific odour analysis, different pattern recognition techniques (Table 1.1) can be applied to the feature matrix. For some simple applications where the system is only used to detect an incidental outlyer, a simple visualisation with a principle component analysis (PCA) might be sufficient [5,9,18]. This method allows to visualise a maximum of the data variance, by a base-transformation [16,28,29].

Table 1.1: Three types of pattern recognition techniques.

	Type of technique	Typical example
1	visualising techniques	• Principle Component Analysis • Cluster analysis
2	linear calibration methods	• Partial Least Squares • Linear Discriminant Analysis
3	neural nets	• Multi-layer Perceptron • Kohonen

When in a more developed stage with an optimised sensor choice, odour release and exposure method a good separation between the data sets is obtained, the training data can be obtained. This training set can then be modelled by a linear learning technique like partial least squares (PLS) [16,25,28], or with a neural net [20]. The choice of a more defined technique like PLS or a more 'fuzzy' technique like a neural net fully depends on the application and the required output format[13].

Multidimensional data treatment techniques, are not only used for electronic noses, but also for evaluating multi-spectral data (chemometrics) and pattern recognition problems outside chemistry. Consequently there is a large amount of literature available concerning the optimisation of these techniques under specific conditions[28,29].

1.1.4 Detection principles for electronic noses

Electronic noses can be realised with many different sensor technologies. These technologies are described in review articles [10,12,17]. The main requirement is a set of reproducible and stable sensors which are sensitive to a sufficiently large range of volatiles. The most common sensors used are conducting polymer based chemo-resistors, metal-oxide sensors and Quartz Crystal Microbalances. They are found in the most successful commercial instruments: Alpha MOS, AromaScan, Lennartz-Electronic, Neotronics/EEV and Perkin Elmer/HKR [30]. Table 1.2 gives an overview of the most important sensing principles with their advantages and disadvantages.

Conducting polymers are especially interesting as sensor materials since they can be made simply and inexpensively and conducting polymer based chemo-resistors are easily miniaturised. Based upon previous experience at IMT [37-39] and the available substrate technology, the conducting polymer based sensors were chosen as a research subject for this thesis.

Table 1.2: **Overview of the sensor technologies used in electronic noses.**

Sensor type	physical quantity	advantages	disadvantages
intrinsically conducting polymers (chapter 3,4,6)	resistance	• wide range of available types • low power due to room temperature operation	• water sensitivity • irreproducibility
Metal-Oxide gas sensors [4]	resistance	• high sensitivity to a range of organics • commercially available	• high power consumption
Quartz Crystal Microbalances [31,32]	mass	• chemical selectivity (Langmuir- Blodgett films) • wide rage of available types	• expensive substrates • water sensitivity • poor sensitivity
Surface Acoustic Wave sensors [31,32]	mass elasticity	• chemical selectivity (Langmuir - Blodgett films) • high sensitivity	• limited stability • interface electronics
GASFETs (chapter 5)	Work Function	• wide range of available types	• expensive substrates
insulating polymers with conducting filler [33]	swelling changes resistance	• wide range of available types	• irreproducibility
dielectric gas sensors (chapter 7)	dielectric constant	• better stability	• low selectivity
optical sensors [34]	fluorescence	• no electrical interferences • miniaturisation	• irreproducibility
Mass spectrometry [35,36]	mass-charge ratio	• physical property • analytical accuracy	• expensive

1.2 Conducting polymers

Since their original discovery in the 1800s, intrinsically conducting polymers have received a vast amount of attention. Applications have since ranged from matrices for enzyme immobilisation [40] to RF-shielding [41]. Due to their charge storage properties (they can exist in different oxidation states), these materials can also be used in rechargeable batteries [46]. For all these applications, the absolute value of conductivity is not critical, the arguments for the choice of the material are the advantageous weight to conductivity ratio or processing advantages allowing for inclusion of catalytic chemistry in a conducting matrix.

The semi-conducting nature of the material makes the modulation of the electrical properties of the polymers also suitable as a transduction principle in sensor applications. The electrical properties are easily changeable by the inclusion of materials with a different work-function. They cause a partial electron transfer [42,43], which changes the work-function and the directly related conductivity of the polymer. Because the polymer also interacts with sorbed gases, the materials can conveniently be used in gas sensing applications.

Polypyrrole (ppy) is widely used for gas sensing applications, as it is relatively stable in ambient atmosphere [44]. It was first prepared in a powder form by chemical oxidation in 1916 [45]. Wider interest in the material was initiated by the discovery of electrochemically prepared polypyrrole by Dall'Olio [41,45] in 1968, which was further developed by Diaz et al. [45-47].

Other extensively examined polymers for gas sensing applications have been prepared from indole, thiophene, aniline and their derivatives [6,44,48,49].

1.3 Outline

Chapter 2 of this thesis discusses the design of the gas handling system, after three years of evolution throughout the project, and a characterisation of its sampling behaviour. Chapter 3 discusses the observations made during the preparation of conducting polymers on IDA substrates and the influence of the most important deposition parameters. The electrical characteristics including contact resistance, noise and temperature dependency in the so prepared chemo-resistor devices are presented in chapter 4.

Chapter 5 discusses the behaviour of conducting polymers when they are used as a gate contact on GASFETs. The work function based operation of these devices allows the polymer's behaviour to be examined without the passage of current.

Sorption of the vapour playing an important role in the vapour-polymer interaction, is discussed in chapter 6. Chapter 7 discusses the feasibility of the use of dielectric sensors based on the same IDA supports as used for the chemo-resistors.

The last chapter gives a global discussion of the work and an outlook into conducting polymers and electronic noses.

1.4 References

1. B. Kolb and L.S. Ettre, Static Headspace-Gas Chromatography, Wiley-VCH, New York, 1997.
2. M. Leino, *Applicotion of headspace gas chromatography complemented with sensory evaluation to analysis of various foods*, Ph. D. Thesis, University of Turku, Finland, 1983.
3. R. Mariaca and J.O. Bosset, *Instrumental analysis of volatile (flavour) compounds in milk and dairy products*, Lait 76 (1996).
4. K. Persaud and G. Dodd, *Analysis of discrimination mechanisms in the mammalian olfactory system using a model nose*, Nature 299 (1982) 352-355.
5. M. Holmberg, F. Winquist, I. Lundström, J.W. Gardner and E.L. Hines, *Identification of paper quality using a hybrid electronic nose*, Sensors and Actuators B26-27 (1995) 246-249.
6. P. Mielle, *'Electronic noses': Towards the objective instrumental charocterization of food aroma*, Trends in Food science & Technology 7 (1996) 432-438.
7. V. Vernat-Rossi, C. Garcia, R. Talon, C. Denoyer, J.-L. Berdagué, *Rapid discrimination of meat products and bacterial strains using semiconductor gas sensors*, Sensors and Actuators B37 (1996) 43-48.
8. W. Ping, T. Yi, X. Haibao and S. Farong, *A novel method for diabetes diagnosis based on electronic nose*, Biosensors and Bioelectronics 12 (1997) 1031-1036.
9. T.D. Gibson, O. Prosser, J.N. Hulbert, R.W. Marshall, P. Corcoran, P. Lowery, E.A. Ruck-Keene and S. Heron, *Detection and simultoneous identification of microorganisms from headspace samples using and electronic nose*, Sensors and Actuators B44 (1997) 413-422.
10. H.T. Troy Nagle, S.S. Schiffman and R. Gutierrez-Osuna, *The How and Why of Electronic Noses*, IEEE Spectrum, Sept. 1998.
11. W. Göpel, Ch. Ziegler, H. Breer, D. Schild, R. Apfelbach, J. Joerges and R. Malaka, *Biolelectronic noses: a status report. Part I*, Biosensors & Biolelectronics 13 (1998) 479-493.
12. Ch. Ziegler, W., Göpel, H. Hämmerle, H. Hatt, G. Jung, L. Laxhuber, H.-L. Schmidt, S. Schütz, F. Vögtle and A. Zell, *Bioelectronic noses: a stotus report. Part II*, Biosensors & Bioelectronics 13 (1998) 539-571.
13. E. Kress-Rogers, Handbook of Biosensors and Electronic Noses, CRC Press, Inc., Boca Raton (USA) 1997.
14. J.W. Gardner and P.N. Bartlett, *Sensors and Sensory Systems for and Electronic Nose*, edited by J.W. Gardner and P.N. Bartlett, NATO ASI Series E vol. 212, Kluwer Academic Publishers, London, 1992.
15. J.W. Gardner and P.N. Bartlett, *A brief history of electronic noses*, Sensors and Actuators B18-19 (1994) 211-220.
16. J.W. Gardner and P.N. Bartlett, Electronic Noses, Principles and Applications, Oxford University Press, Oxford (UK), 1999.
17. D.J. Strike, M.G.H. Meijerink, M. Koudelka-Hep, *Electronic Noses, A Mini-Review*, Accepted for publication in Fresenius' Journal of Analytical Chemistry, in press.

18. J.W. Gardner and P.N. Bartlett, *Pattern Recognition in Gas Sensing*, in Techniques & Mechanisms in Gas Sensing, Edited by P.T. Moseley, S.O.W. Norris and D.E. Williams, The Adam Hilger series on sensors, Bristol (UK), 1991.
19. D. Gnani, V. Guidi, M. Ferroni, G. Faglia and G. Sberveglieri, *High-precision neural pre-processing for signal analysis of a sensor array*, Sensors and Actuators B47 (1998) 77-83.
20. C. Di Natale, F. Davide and A. D'Amico, *Pattern recognition in gas sensing: well-stated techniques and advances*, Sensors and Actuators B23 (1995) 111-118.
21. J.W. Gardner, M. Craven, C. Dow and E.L. Hines, *The prediction of bacteria type and culture growth phase by and electronic nose with a multi-layer perceptron network*, Meas. Sci. Technol. 9 (1998) 120-127.
22. E. Stussi, R. Stella and D. De Rossi, *Chemoresistive conducting polymer-based odour sensors: influence of thickness changes on their sensing properties*, Sensors and Actuators B43 (1997) 180-185.
23. M. De Wit, E. Vanneste, F. Blockhuys, H.J. Geise, R. Mertens and P. Nagels, *Application of Polythienylene vinylene) as a chemiresistor for organic vapours*, Synthetic Metals 85 (1997) 1303-1304.
24. M.E.H. Amrani, P.A. Payne and K.C. Persaud, *Multi-frequency measurements of organic conducting polymers for sensing of gases and vapours*, Sensors and Actuators B33 (1996) 137-141.
25. T.C. Pearce, J.W. Gardner, S. Friel, P.N. Bartlett and N. Blair, *Electronic Nose for Monitoring the Flavours of Beers*, Analyst 118 (1993) 371-377.
26. M. Fryder, M. Holmberg, F. Winquist and I. Lundström, *A Calibration Technique For an Electronic Nose*, Technical digest Eurosensors IX/Transducers '95, Stockholm, June 1995.
27. M. Holmberg, F.A.M. Davide, C. Di Natale, A. D'Amico, F. Winquist and I. Lundström, *Drift counteraction in odour recognition applications: lifelong calibration method*, Sensors and Actuators B42 (1997) 185-194.
28. K. Esbensen, T. Midtgaard, S. Schönkopf, Multivariate analysis in practice, Camo A/S, Trondheim, 1994.
29. R.G. Brereton, Multivariate pattern recognition in chemometrics, Elsevier, Amsterdam, 1992.
30. http://nose.uia.ac.be/
31. J.W. Grate, S.J. Martin and R.M. White, *Acoustic Wave Microsensors, Part I*, Anal. Chem. 65 (1993) 940A-948A.
32. J.W. Grate, S.J. Martin and R.M. White, *Acoustic Wave Microsensors, Part II*, Anal. Chem. 65 (1993) 987A-995A.
33. B.J. Doleman, R. D. Sanner, E.J. Severin, R.H. Grubbs and N.S. Lewis, *Use of Compatible Polymer Blends To Fabricate Arrays of Carbon Black-Polymer Composite Vapor Detectors*, Anal. Chem. 70 (1998) 2560-2564.
34. S.R. Johnson, J.M. Sutter, H.H. Engelhardt, P.C. Jurs, J. White, J.S. Kauer, T.A. Dickinson and D. Walt, *Identification of Multiple Analytes Using an Optical Sensor Array and Pattern Recognition Neural Networks*, Anal. Chem. 69 (1997) 4641-4648.
35. http://www.smartnose.com.
36. http://chem.external.hp.com/cag/products/hp4440.html.
37. D.J. Strike, *Gas Analysis Systems for Consumer Products Industry*, Proceedings of the Minast Convention, Project 1.04, Bern (Switzerland), April 1998.

38. D.J. Strike, N.F. de Rooij, M. Koudelka-Hep, M. Ulmann and J. Augustynski, *Electrocatalytic oxidation of methanol on platinum microparticles in polypyrrole*, Journal of Applied Electrochemistry 22 (1992) 922-926.
39. D.J. Strike, N.F. de Rooij and M. Koudelka-Hep, *Electrochemical-Based Immobilization of Enzymes*, in Immobilization of Enzymes and Cells ed.: G.F. Bickerstaff, Humana Press, Totowa, New Jersey, 1997.
40. N.C. Foulds and C.R. Lowe, *Enzyme entrapment in electricolly conducting polymers*, J. Chem. Soc. Faraday Trans. 182 (1986) 1259-1264.
41. T.A. Skotheim, *Handbook of conducting polymers*, Vol. 1, Marcel Dekker Inc., New York, 1986.
42. J. Janata, *Chemical Modulation of the Electron Work Function*, Anal. Chem. 63 (1991) 2546-2550.
43. G. Gustafsson and I. Lundström, *The Effect of Ammonia on the Physical Properties of Polypyrrole*, Synthetic Metals 21 (1987) 203-208.
44. P.N. Bartlett and K. Ling-Chung, *Conducting Polymer Gas Sensors, Part III: Results for Four Different Polymers ond Five Different Vapours*, Sensors and Actuators 20 (1989) 287-292.
45. G.K. Chandler and D. Pletcher, *The Electrochemistry of Conducting Polymers*, Specialist Periodical Report, Electrochemistry, vol. 10, Edited by D. Pletcher, Royal Soc. of Chemistry, Burlington House, London, 1985.
46. K.K. Kenazawa, A.F. Diaz, R.H. Geiss, W.D. Gill, J.F. Kwak, J.A. Logan, J.F. Rabolt, G.B. Street, *'Organic Metals': polypyrrole, a stable synthetic 'Metallic' polymer*. J.C.S. Chem. Comm. (1979) 854-855.
47. A.F. Diaz, K. Keiji Kanazawa and G.P. Gardini, *Electrochemical Polymerization of Pyrrole*, J.C.S. Chem. Comm. (1979) 635-636.
48. N. Blair, *The development and characterisation of conducting polymer based sensor for use in an electronic nose*, Ph.D. Thesis, University of Southampton, United Kingdom, 1994.
49. T. Hanwa, S. Kuwabata, H. Hashimoto and H. Yoneyama, *Gas Sensitivities of Electropolymerized Polythiophene Films*, Synthetic Metals 30 (1989) 173-181.

2 Gas handling

2.1 Introduction

2.1.1 General

The performance of an electronic nose system not only depends on the quality of the sensors, but also critically on the gas handling system used to bring the sensors into contact with the odour. The design of such a system, which in the scope the IMT nose project needs to function as a tool for sensor characterisation, as well as a part of a complete electronic nose system, is non-trivial and requires thorough consideration.
To place the different parts required by such a system in context, a global scheme of the working principle of an electronic nose will be presented.

2.1.2 Working principle of an electronic nose

In every electronic nose system, 3 critical system aspects (Fig. 2.1) can be identified: the sensor array, the sample preparation and the reference gas. During operation of the nose, the sensor array is used to compare the reference gas to the actual sample, which is preferably prepared using this same reference gas.

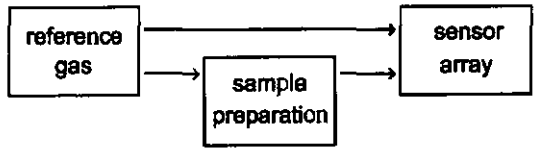

Fig. 2.1: The sensor array compares the reference gas to the prepared sample in the same reference air.

The reference gas is important since it establishes a base-line for the sensor signal, from which the samples are measured. The way the sample

is contacted with the sensor array is another important aspect. It involves system configuration and parameters like flow rate, temperature and mixing characteristics, all of which have to be considered in the optimisation of the system behaviour.

Early electronic noses consisted of a sensor head which was inserted in the equilibrated headspace of a sample [1-3]. This approach is simple, and sufficient for the evaluation of the sensory values for simple applications. However, most current electronic noses, including the commercial ones, are based on a flow-through system [4-7]. The odour is led through a sensor chamber by means of a system of tubing (Fig. 2.2). Odour exposures are alternated with purges of reference air.

Fig. 2.2: A flow through sensor chamber.

The most important advantage of such a flow system is the ease of purging of the sensor array with reference air to promote a stable baseline. Furthermore it allows control of environmental parameters like temperature and humidity to which most commonly used sensors are sensitive. This approach requires however extensive control equipment and is therefore used in bench-top electronic nose instruments.

2.1.3 Sample preparation

Before the execution of a measurement in an electronic nose, the volatile components of the sample have to be released in the sample chamber. In the case of pure chemicals, the equilibrium vapour concentration can be calculated from the gas law (Appendix A).

For real samples the vapour release is a complex process depending on different parameters. It will depend on the filling ratio in the sample bottle [8], the surface area of the sample, and some system parameters like the

temperature, the equilibration time and the composition of the atmosphere in the chamber. The resulting composition of the headspace is thus difficult to calculate, even if all the volatile components in the sample are known. To assure the reproducible liberation of the volatiles, necessary for a repeatable odour measurement, special care must be taken with the sample preparation [9]. The initial atmosphere in the chamber needs to be of a defined composition (reference air), and the amount of sample which is supplied to the system has to be kept as constant as possible. For solid samples the surface area must also be controlled, which can be problematic for certain samples, such as cheese. Careful grating of the sample is in these cases a possibility.

2.1.4 Outline

This chapter will deal with system aspects of an electronic nose excluding the sensor array, which is discussed elsewhere. It is split up in two sections: section 2.2, describing the implementation of the different aspects of the developed nose system and section 2.3, describing validation experiments of this system.

2.2 The IMT flow system

2.2.1 Layout

Fig. 2.3 shows a schematic drawing of the components of the IMT flow-system. After pre-treatment of the gas in a carbon filter and a Drierite® column, the flow passes through two mass-flow controllers. One of them regulates the flow through the sampling system, the other regulates the diluting flow. The two combine in a T-piece before they are fed into the sensor chamber.

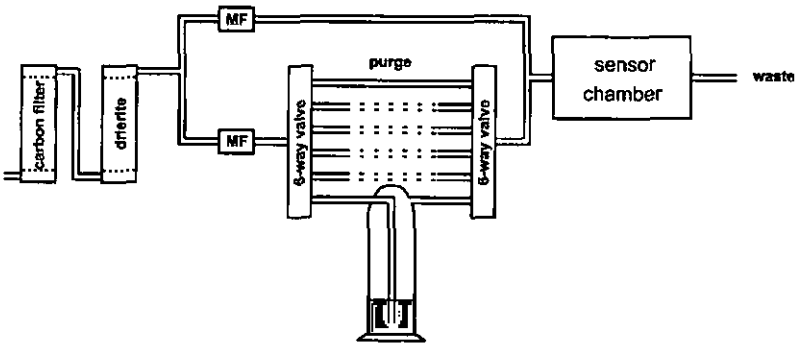

Fig. 2.3: Schematic overview of the IMT flow-system. The Mass Flow controllers are marked with MF. Only 1 of the 5 sample containers is shown.

The sampling system consists of two Bio-Chem Valve™ Corp. model 105T 6 12-125 6-way valves. One of the lines is connected straight through to create a purge line, the other 5 allow to insert wash bottles containing samples (only one displayed). By regulating the flow between the two mass-flow controllers it is possible to dilute the headspace sample, allowing it to be assessed at various concentrations.
The whole flow system starting from the carbon filter unit is operated in a temperature controlled (25°C) container (not shown).

2.2.2 Carrier gas

In our electronic nose, compressed air, obtained from the building's compressed air system was used as the reference gas. It was passed through a Wilkerson oil filter (not shown) to remove residual pump oil before entering the nose system. In the system the air is passed through two laboratory gas drying units (acrylic model, W.A. Hammond Drierite company) the first filled with 4-12 mesh activated carbon (Aldrich) to serve as an additional filter for any remaining organic components and the second was filled with "8 Mesh indicating Drierite®", which dries the air to -100°F dew point [10]. The air obtained has a relative humidity of less then 0.1 % (this was confirmed by measurements, see section2.3).
The flow rate of the carrier gas defines the mixing properties, and is therefore an important parameter. It was controlled with 2 mass flow controllers obtained from Brooks Instrument Div. Emerson Electric Co. Veenendaal (Holland) type 5850S/BC1HA1AA0BA1A1, 0-1.0 l/min (accuracy: ± 0.75% of rate accuracy ± 0.25% full scale).

2.2.3 Sample containers

Wash-bottles were used as sample containers. These were especially convenient to generate vapours from liquid test samples. These components do not loose their odour, and can be used for repeated measurements over periods as long as multiple days long.
The wash bottles were 250 ml Drechsel type gas wash bottles from borosilicate glass (DURAN®) with a frit with porosity 1. They were obtained from Merck Switzerland. They were filled with 100 ml sample to keep a sufficiently large headspace above the sample [5].

2.2.4 Sensor chamber and mixing

The sample chamber is the place were the sensors contact with the sample headspace. Because of the laminar flow in the tubing (section 2.3.3), this is also the place where the gas streams from the sampling and diluting line mix.

Whilst for practical electronic nose measurements the repeatability of the gas flow and mixing in the cell is sufficient, for the fundamental study of the gas polymer interactions it is desirable to have a defined gas composition at all times. When the sensor chamber is relatively small compared to the flow rate, the concentration changes are approximated by step changes, facilitating the study of the dynamic behaviour of the sensors enormously.

Apart from the small dimensions of the sensor chamber, a symmetric position of all the sensors relative to the gas inlet is preferable to reduce any influence of the sensor position on the response dynamics. Furthermore dead corners have to be avoided at all times, to guarantee a fast recovery of the sensor whilst purging the chamber.

The sensor chamber used in this study was a 32 ml cylindrical PVC container (5 cm length, 3 cm diameter) with the sensors positioned on the circular wall. The in- and outlet were placed at the top and the bottom ends respectively of the chamber.

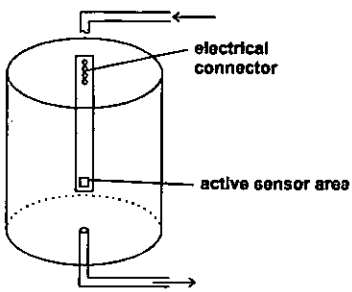

Fig. 2.4: The sensor chamber with only 1 of the 8 radially positioned sensors displayed.

2.2.5 Materials

Interaction of gases with the flow system can also decrease its performance in several ways: Firstly the sorbed species may not reach the sensor chamber, possibly eliminating specific characteristic compounds from the odour and thus disturbing the recognition.
Secondly the sorbed gases might slowly desorb during the purge phase, slowing down the recovery of the sensors after their exposure or in extreme cases disturbing successive measurements.
Although adsorption in the tubing can never be fully prevented, it can be limited by the right choice of materials. Dense inert materials like stainless steel and glass have low absorbency values for common vapours, and are therefore most suitable for the critical parts of the flow system. Unfortunately these materials are not as easy to machine and modify under laboratory conditions as common plastic materials. When the system is kept under a sufficiently high continuous flow, the interaction time between the tubing and the passing vapour is low. Consequently, sorption should have minor influences on the resulting vapour concentration.
All the interconnections in the flow system were made of 1 mm internal diameter nylon tubing, which was chosen for its low water permeability.

2.2.6 Humidity sensor

In some experiments, a P570 Humidity probe (Temperature Products gmbh) mounted in a flow through cell was inserted in the waste line directly after the sensor chamber. The probe has an accuracy of ±1% relative humidity. The response time was found to be approximately 2 minutes.
The humidity sensor, which is of the dielectric type, was found to also be sensitive to diverse organic vapours like methanol and acetone, with responses equivalent to 70% RH for the saturated organic vapours. The responses of the sensor therefore have to be evaluated with grate care when they were obtained in the presence of complex vapours.

2.2.7 Computer Control

The 6-way valves are controlled by an in-house built interface, which allowed the valves to be switched using the parallel port of the PC. To control the mass flow controllers, a HP E1328A D/A-converter was employed. Both valves and mass flow controllers were controlled by a computer program written in Visual Basic, which allowed a test sequence composed of different samples, separated by defined purges to be employed. This was used in combination with a Visual Basic data acquisition program, to give a completely automatic system.

2.3 System characterisation

2.3.1 Introduction

This section describes the characterisation of the flow system properties. It will serve as a reference for the observations made during sensor characterisation.

2.3.2 Sample containers

The samples were placed in wash bottles. During sample retrieval, the carrier gas is bubbled through the liquid sample to obtain a vapour. This presents a dynamic situation, different from the static situation presented in Appendix A. This section describes the characterisation experiments for this type of dynamic measurements, to examine how much this disturbs the calculated static concentrations.

Experimental

To verify the validity of the quasi static assumption whilst passing a carrier stream through a sample bottle, the flow system was tested using water as a sample. The humidity directly at the wash bottle outlet was measured with the humidity sensor (section 2.2.6). The static equilibrium concentration is represented by a relative humidity of 100%.
The flow rate was varied between 0.0 and 1.0 l/min, in a stair-case shape, with a time interval of 10 minutes without any purging in between. This relatively long time interval was chosen to allow a plateau value for the relatively slow humidity sensor to be reached.
As explained above (Fig. 2.3) the obtained saturated stream from a sample bottle can be diluted with a second stream to vary the vapour concentration. The performance of this dilution system was assessed by measuring the humidity resulting from mixtures of the sample stream and the diluting stream. This was done with humidity pulses of different concentrations, alternated with dry air purges, similar to the situation in

practical nose measurements. In this case the pulses and the purges also had lengths of 10 minutes to allow the humidity sensor to equilibrate. The total combined flow rate of the two streams was controlled at 1.0 l/min.

Results and discussion.

Fig. 2.5 shows the humidity obtained from the water sample at different flow rates through the water sample bottle. A maximum was observed in the relation between flow rate and relative humidity. At intermediate flow rates the carrier is almost saturated with water. At flow rates above 0.4 l/min, the gas does not fully reach saturation. The gas flow is apparently too high to allow for full equilibration between the liquid water and the carrier.

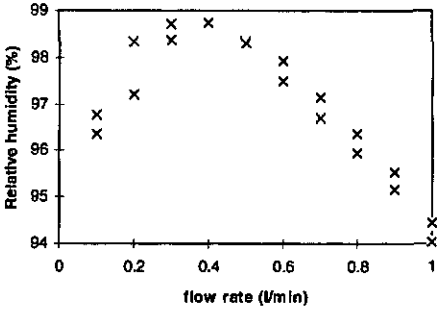

Fig. 2.5: Vapour saturation as a function of flow rate through a wash bottle containing water.

Below 0.4 l/min the relative humidity of the resulting carrier is also lower. This may be caused by a loss due to sorption in the tubing between the sample bottle and the humidity sensor, or by a lower bubbling efficiency. It was observed that after 12 hours of continuous measurement, which presumably saturates the tubing with water, the humidity at the low flow-rate remained lower than expected. It is therefore probable that the efficiency of the bubbler is reduced at the lower flow rate. This is probably caused by the straight trajectory of the air bubbles through the liquid in the

sample bottles at lower flow rates, whereas for higher flow rates a more turbulent flow was obtained which apparently improves the efficiency.
The results of the characterisation of the performance of the diluting system are shown in Fig. 2.6. As can be seen measurements made at the same dilution overlap, demonstrating the high reproducibility of the system.

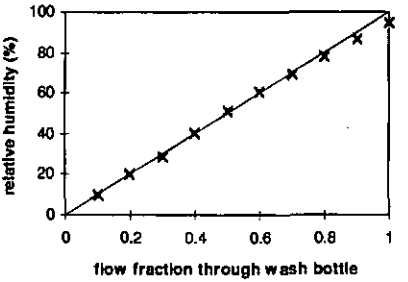

Fig. 2.6: Humidities obtained by dilution of a saturated stream with a dry air stream. Represented data was obtained during 16 hours of continuous measurements, which allowed to repeat every data paint 4 times.

Furthermore a good linearity (correlation coefficient 0.9987 ± 0.0001) was obtained. Above a flow ratio of 0.7, a small deviation from linearity due to the decreased efficiency of the bubbler (Fig. 2.5) was observed. The decreased efficiency at lower flow rates is not observed in this curve because the contribution of the sample flow to the total flow is in this case very low, which decreases the influence of incomplete saturation accordingly.
Experiments with water, which could be characterised with a humidity sensor, showed nearly 100 % saturated vapour after the sample bottle. It is expected that similar results will be obtained for the organic compounds used in this thesis, because they are more volatile then water. The vapour concentrations of sample headspaces are therefore in all cases assumed to equal the equilibrium concentration calculated from the vapour pressure.

2.3.3 Mixing properties

The maximum flow rate used was 1 l/min. At the minimum channel diameter of 1 mm, the mean gas velocity <v> is the quotient of the flow and the surface area of the tube: $1.67*10^{-5}$ m^3/s / $7.9*10^{-7}$ m^2= 21 m/s.

$$Re = \frac{\rho \cdot \langle v \rangle}{\eta} \cdot D \qquad (2.1)$$

ρ:	density	($\approx$1.2 kg/m^3 for air)
η:	viscosity	($\approx 17*10^{-6}$ Pa.s for air)
<v>:	mean velocity	[m/s]
D:	diameter	[m]

When this is substituted in equation (2.1) this results in a Reynolds number of 1500, which is too low for turbulent flow [11]. Since the product of diameter and mean velocity decreases with the channel diameter, the Reynolds number in the larger parts in the system was even lower.
This flow behaviour however is only applicable for the case of smooth circular channels. Especially at interconnections between different types of tubing, and in the sensor cell there will be a turbulent flow due to an abrupt change in diameter. Thus the flow in the system will be laminar, and that the mixing will occur at some mixing points, predominantly in the sensor chamber, where there is an abrupt change in channel diameter.

Experimental

The mixing behaviour in the sensor chamber was characterised with 1 minute exposures of saturated water vapour separated by 30 minutes purges with dry air at different flow rates. For this purpose a hexane sulfonic acid doped polypyrrole chemo-resistor (section 3.6) was used because of its fast response. The response transients were fitted to the model obtained using the Langmuir isotherm (equation 6.4) and the resulting parameters were studied.

Results and discussion

Fig. 2.7 shows the time constants k as a function of flow rate. It can clearly be observed that the time constant increases with flow rate. At 0.5 l/min which corresponds with 8.3 ml/s, a time constant of 32/8.3=3.9 s corresponding with k=0.25 would be expected. Due to the sorption process in the sensors, an almost 10 times slower process is observed. The sensor response obviously is the slowest part of the system. It is however believed that the sensor responses are rather flow rate independent. This implies that the observed flow dependency is due to the mixing.

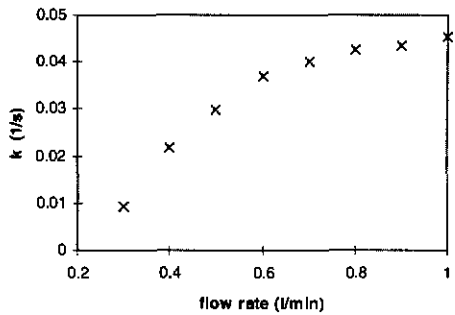

Fig. 2.7: Fitted time constants obtained with a 4 mC hexanesulfonic acid doped polypyrrole sensor for repeated water exposures at different flow rates.

Because at flow rates approaching 1 l/min, the flow rate dependency is greatly reduced, it is assumed that at this flow rate the vapour concentration becomes almost stepwise. This allows the sorption of the vapour in the sensors (chapter 6) to be studied without influences of mixing.

2.3.4 Sorption

Sorption in the tubing was noticed, especially in the connections to the sample bottles where the tubing is continuously exposed. Fortunately the sorbed species could easily be removed from the system by purging with reference air. Purge times required were dependent on the nature of sample which caused the contamination, but were typically less then 2 hours.

2.4 References

1. N. Blair, *The development and characterisation of conducting polymer based sensor for use in an electronic nose*, Ph.D. Thesis, University of Southampton, 1994.
2. H.V. Shurmer, J.W. Gardner and P. Corcoran, *Intelligent Vapour Discrimination Using a Composite 12-Element Sensor Array*, Sensors and Actuators B1 (1990) 256-260.
3. H. Shurmer, A. Fard, J. Barker P. Bartlett, G. Dodd and U. Hayet, *Development of an electronic nose*, Phys. Technol. 18 (1987) 170-176.
4. An introduction to electronic nose technology, Neotronics Scientific Ltd., Essex, United Kingdom, 1996.
5. http://www.leeds.ac.uk/ulis/Bloodhound/Frames/index.htm
6. H. Troy Nagle, S.S. Schiffman and R. Gutierrez-Ossuna, *The HOW and WHY of ELECTRONIC NOSES*, IEEE Spectrum, September 1998.
7. http://inch.uia.ac.be/struct/review/
8. B. Kolb and L.S. Ettre, Static Headspace-Gas Chromatography, Wiley-VCH, New York, 1997.
9. P. Mielle and F. Marquis, *An alternative way to improve the sensitivity of Electronic Olfactometers ('Electronic Noses')*, Eurosensors XII (1998) 1119-1122.
10. Drierite® drying column for air and gases, product data sheet, W.A. Hammond Drierite Company, 138 Dayton Avenue, Xenia, Ohio 45385 (USA).
11. W.J. Beek and K.M.K. Muttzall, Transport Phenomena, Wiley and Sons, London, 1975.

3 Fabrication of chemo-resistors

3.1 Introduction

3.1.1 General

Conducting polymers can be synthesised from their monomers by chemical or electrochemical oxidation. Chemically prepared polymers have to be pressed to pellets [1,2] or deposited on sensor substrates by dip-coating, spin-coating or related techniques before the resistance of the polymer can be measured. These coating techniques require the chemically prepared polymer to be dissolved or ground and mixed with another polymer matrix [3-5]. Although there is an increasing interest in soluble conducting polymers [6-8], most conducting polymers, including the ones generally used for sensor applications, are not soluble in commonly used solvents [9,10]. The deposition of chemically prepared polymers is therefore difficult and their application to sensor technologies limited.

Electro-polymerisation is an attractive alternative and is therefore frequently used for sensor preparation [11-13]. The polymerisation can be performed directly on the conducting regions of the sensor substrate, without the need of an additional coating procedure. The principle is as follows: The monomer is oxidised to give radical cations, which react to give insoluble oligomers. These deposit on the electrode. After this initial nucleation process, the growth proceeds on the oxidised polymer formed on the electrode when the oxidation potential is maintained [14-18]. Fig. 3.1 illustrates the electro-polymerisation of pyrrole.

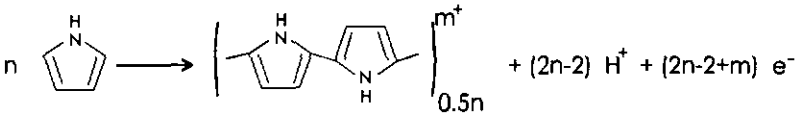

Fig. 3.1: Overall reaction of the polymerisation of pyrrole.

Extensive literature exists upon the influence that polymerisation conditions have on polymer properties like morphology [19-21], conductivity [2,22,23] and electrochemical behaviour [14,24-27]. However, these properties are difficult to relate to the gas response, which is of interest for our application. The characterisation of influence of the polymerisation conditions on the gas sensing properties of the resulting polymer, is issued in only few publications [9,28] and was therefore chosen as one of the aims of this work.

3.1.2 Parameters of electrochemical polymerisation.

Many different types of conducting polymers with widely different gas sensitivities can be prepared by the polymerisation of suitable monomers. The variety of available monomers can almost infinitely be expanded by the introduction of a pendent group on the monomer [9,11,13,15-17,27,29-34].

Depending on the type of monomer used, the backbone of the polymer is oxidised or sometimes reduced [7,9,17,30,32,35,36] to become conductive. This results in a charged polymer, and therefore it incorporates ions from the deposition electrolyte to maintain electro-neutrality. These ions are often referred to as counter ions and can also be used to vary the polymer properties [10,17,22-24,28,30,31,37-41].

Apart from the monomer and the counter ions, the solvent from which the deposition is performed [42], its pH [19,42,43], and other electrochemical deposition conditions during the polymerisation, including for example applied potential, temperature and cell configuration, can be varied [24,43,44]. The main deposition parameters are summarised inTable 3.1.

Table 3.1: Principal deposition parameters.

1.	monomer
2.	counter ions
3.	solvent
4.	potential/current
5.	temperature
6.	cell configuration

Polypyrrole is one of the mostly used conducting polymers in electronic noses. Electro-polymerisation results in a p-doped polymer with negative counter ions incorporated in it. The polymer is rather stable in air and therefore particularly suitable for gas sensing applications [2,9,10,13,31]. The pyrrole monomer is soluble in various solvents, including water and acetonitrile, which allows a large range of doping salts to be used. In aqueous deposition solutions, especially sulfonate salts [14,45] proved to be suitable electrolytes to obtain chemo-resistors with a favourable gas sensing behaviour.

3.1.3 Outline

This chapter starts with a general experimental section dealing with the preparation of the chemo-resistors, mostly polypyrrole doped with bsa. Observations made during the deposition of the bsa doped polypyrrole are described in section 3 and section 4 describes the reproducibility of this preparation. The following sections consider the influence of thickness, doping ions and deposition potential on the behaviour of the obtained chemo-resistors.

3.2 Experimental

3.2.1 Substrates for sensor fabrication

In the literature various types of sensor substrates have been described for the preparation of chemo-resistors for gas sensing applications [4,11,13,46-50]. Substrate materials are in general passivated silicon or alumina, the first has the advantage of being more compatible with high resolution lithography for the patterning of the electrodes in a standard IC process facility, whilst the second technology is less expensive but allows only a limited lithographic resolution.
The reported electrode designs vary from a simple gap between two square electrodes [14,31] to sophisticated circular structures [51] which allow HF-measurements. Interdigitated electrodes [12,52] allow a low base-line resistance of the prepared sensors and are therefore frequently used. The polymer is electrodeposited on both electrodes until the gap between them is crossed (Fig. 3.2).

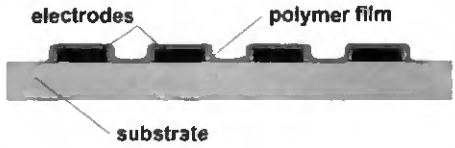

Fig. 3.2: A schematic drawing of a cross-section through a set of interdigitated electrodes covered with a polymer layer.

The chemo-resistors were prepared on in-house fabricated InterDigitated electrode Array (IDA) [52] structures. These structures consist of a silicon nitride passivated silicon substrate with two sets of IDAs with 2 & 5 or 5 & 10 µm spacing. Although the IDAs with a 10 µm spacing were also used, the IDAs with a 5 µm spacing were preferred, because they result in chemo-resistors with a lower baseline resistance, which facilitates the resistance measurements. IDAs with a 2 µm spacing, which were also available, can in principle give an even better performance, but

the yield of the fabrication of those structures was too low for their systematic use. Furthermore it is possible that on this very small scale of 2 µm the irregularity of the electrode borders [52] would become significant.

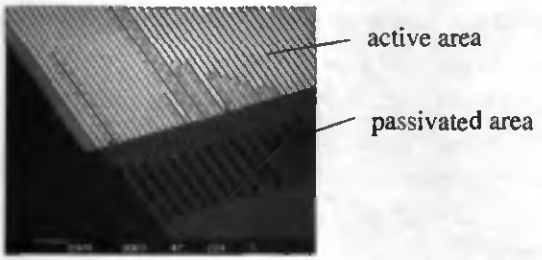

Fig. 3.3: A SEM photograph of a detail of an IDA structure with passivated connection leads.

IDA substrates were fabricated with Pt and Au electrodes. The connection leads of platinum electrodes were passivated with silicon nitride (Fig. 3.3). In the case of gold electrodes, the connection leads to the actual IDA structures were initially not passivated because gold is not allowed in the LPCVD nitride process running in the IMT clean room. Later a new PECVD nitride process became available, which can also be performed on wafers with gold electrodes. This was in some cases used for passivation to result in structures where only the actual interdigitated gold electrodes were exposed during polymer deposition (Fig. 3.3). In other cases the polymer was also deposited on a part of the connection leads.

3.2.2 Equipment

For the electrodeposition, an EG&G potentiostat/galvanostat model 273A was used. The instrument was connected to either a Kipp & Zonen x-y/t recorder or an HP54600A digital oscilloscope to monitor the current.
All counter and reference electrodes were obtained from Metrohm Switzerland. The counter electrode was a Pt foil electrode with a surface area of 128 mm^2 (6.0305.100). In aqueous solutions a Saturated Calomel

Electrode (SCE) (6.0701.100) was used as a reference. In acetonitrile this was replaced by a Ag/AgCl reference (6.0726.100) with a double junction. The inner compartment of the electrode was filled with saturated aqueous LiCl. The outer compartment was during storage also filled with saturated aqueous LiCl. Before every deposition it was thoroughly rinsed and filled with the background electrolyte used for the deposition.

For gas phase measurements, the resistance of the prepared chemo-resistors was measured with an in house made current source circuit with integrated output amplifier (Fig. 3.4) that was able to deliver currents between 0.12 mA and 12 nA. The circuit is based on a design described by Bartlett [5].

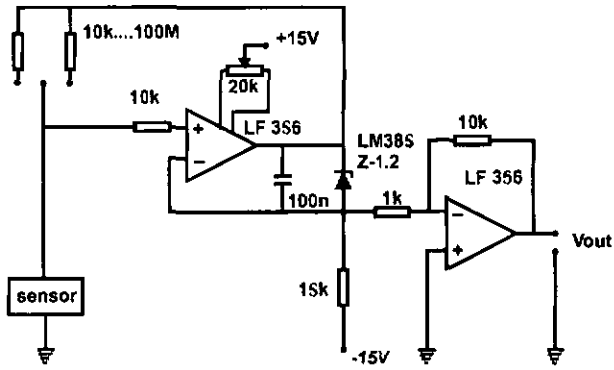

Fig. 3.4: Electrical scheme of the circuit used for the resistance meosurement. The output is connected to the A/D converter.

After the off-sets of the amplifiers were carefully regulated at zero, the outputs of a series of these circuits were connected to a HPE1313A 16 bit scanning A/D converter. The A/D converter was controlled by a dedicated program written in Visual Basic®, which was synchronised with the sampling system control program (section 2.2.7).

3.2.3 Procedure

Pre-treatment of the working electrode

Immediately before polymer deposition there was a pre-treatment step as follows:

- Gold electrodes were thoroughly rinsed with MOS-grade isopropanol and then dried with nitrogen.
- Platinum electrodes were cycled 4 times in 1 M sulphuric acid between -0.2 and 1.2 V vs. SCE at a scan speed of 100 mV/s. The middle two scans were taken up to 2.0 V during which the electrode was tapped to remove gas bubbles. If the last voltammogram of the four cycles did not have the typical platinum shape [53] as displayed in Fig. 3.5, this procedure was repeated. After the treatment the electrodes were rinsed with demineralised water and dried with nitrogen.

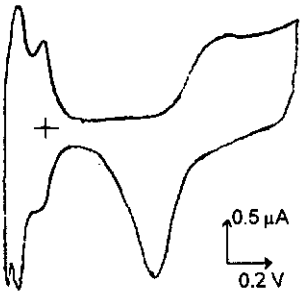

Fig. 3.5: A typical voltammogram vs. SCE for a pre-treated platinum IDA. The cross indicates the origin.

Purification of the monomer

The pyrrole used (Aldrich 98 %) was stored in the dark at 4°C. Even under these conditions, it proved unstable, as could be seen from the formation of a brown colour which darkens with time [44]. Pyrrole required for the deposition was therefore purified. This was carried out by passage through a 7 cm Al_2O_3 column (Aldrich, activated, neutral, Brockmann I, ~150 mesh), where the first fraction was discarded. The procedure resulted in a colourless liquid.

Solution preparation

The deposition was performed in a Metrohm single compartment electrochemical cell (volume 100 ml) containing 30 ml of electrolyte which was 0.1 M of the counter-ion in an appropriate solvent. Oxygen was removed by bubbling nitrogen through the solution for at least 30 minutes. Then 0.204 ml of the purified pyrrole was added with a micro-pipette to give a pyrrole concentration of 0.1 M. After adding the pyrrole the solution was mixed by at least another 5 minutes of bubbling, then the electrodes were put in place and the deposition was performed according to the deposition protocol.
Salts used for the electrolyte preparation were 1-Butanesulfonic acid, sodium salt, 98% (bsa) and Tetraethylammonium tetrafluoroborate, 99% (teatfb). Both were obtained from Aldrich.
Demineralised water was taken directly from the in-house purification system. Acetonitrile (HPLC grade) was obtained from Aldrich. After opening of the bottle, it was stored over 4 Å molecular sieve.

Deposition protocol

Previous experiments with the deposition of polypyrrole chemo-resistors [45] resulted in a standard deposition protocol based on a train of potential pulses. For bsa doped polypyrrole, it consisted of 0.5 s long pulses of 1.0 V separated by 5 s resting periods at 0.0 V. This was applied until the required charge was reached. Then the sensors were held at 0.0 V for 30 s. The deposition protocol for teatfb doped sensors consisted of 2 s long pulses of 1.5 V separated by 5 s resting periods at 0.0 V. On non-passivated IDAs, pulses were applied until a total charge of 1.3 mC was passed.

Fig. 3.6 shows an example of a finished device.

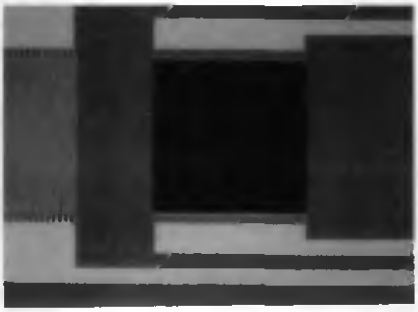

Fig. 3.6: An optical picture of a passivated IDA with 5 µm electrode spacing. The bsa doped polypyrrole film (5mC) is visible as the 1 mm^2 black square. On the left an unused IDA with 10 µm spacing is visible.

3.3 Characterisation of growth

3.3.1 Introduction

The growth of the conducting polymer films was studied via the deposition current, by Atomic Force Microscopy (AFM) and by observation through an optical microscope after partial and complete deposition. This section describes the observations during the preparation of bsa doped polypyrrole on 5 μm spaced gold IDAs.

3.3.2 Current profiles

Fig. 3.7 shows the current profile during the first two pulses of the deposition of bsa doped polypyrrole on a non-passivated 5 μm gold IDA substrate. A significant difference between the shapes of the first and the following pulses can be observed. The form of the first peak may be explained as follows. At the start of the pulse a current spike is observed, which then decays due to local depletion of the pyrrole concentration in the solution close to the electrode. Once the polymer deposits on the electrode, the current increases again due to nucleation and growth of the polymer [1,14,18,40,54].

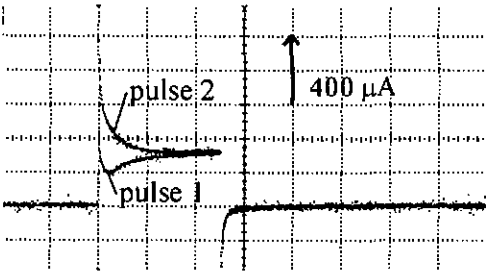

Fig. 3.7: The first two deposition pulses of a bsa doped ppy deposition. The pulses are 0.5 s long.

The second pulse shows a different form, presumably since the nucleation is now complete, and a decaying current transient due to the depletion of pyrrole in the solution is seen. The subsequent transients all have this form, except that each is higher than the one before due to increasing surface area.

3.3.3 Spatial distribution of the growth.

Fig. 3.8 shows the polypyrrole after two 0.5 s long deposition pulses on a non-passivated IDA. Here it is clearly observed that the polypyrrole does not deposit homogeneously over all the bands of the IDA. Instead it nucleates in a certain area, and then preferably grows in that area. The initial growth of the polymer is apparently quite a random process, as previously reported by Partridge [48].

Fig. 3.8: A 2 µm spaced IDA after two deposition pulses of bsa doped ppy.

After the deposition of a larger amount of polymer however, this initial irregularity largely vanishes. Fig. 3.9 shows a zoom in on the edge of the IDA with a finished film prepared using 5 mC of charge, which corresponds to ca. 50 pulses. Although the polymer has now expanded across all the electrodes, the image still clearly shows the irregularity of a finished film. Especially at the extremities or the electrodes, where the distance between two electrodes is 15 µm, irregularities as large as a few microns can be observed.

Fig. 3.9: A 5 μm spaced IDA without lead passivation covered with polypyrrole (5mC).

On passivated structures the influence of the irregularities largely disappears. Fig. 3.10 shows a zoom on a passivated gold IDA with 3 mC passed charge, which is in this configuration the required amount for complete bridging (section 3.5.3). This is the same device as shown completely in Fig. 3.6.

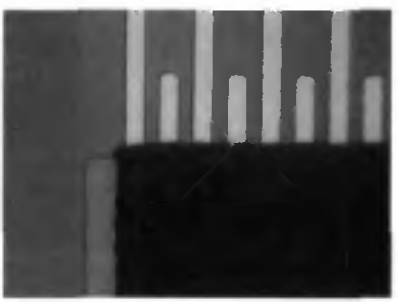

Fig. 3.10: Polypyrrole doped with bsa (5mC) on a 5 μm passivoted IDA.

3.3.4 AFM

The polymer films were also imaged with an Atomic Force Microscope (AFM). These measurements were performed with a Nanoscope® IIIa from Digital Instruments, operated in tapping mode. Fig. 3.11 shows a typical image obtained in on one of the electrodes. The typical polymer grain size is estimated to be 300 nm.

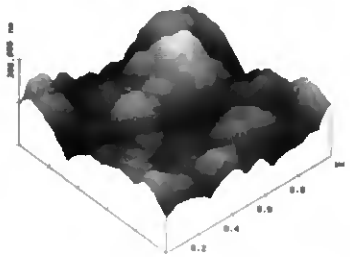

Fig. 3.11: An AFM image of a bsa doped polypyrrole film (5mC).

Another image was taken on the edge of the same polypyrrole film (Fig. 3.12). Here it can be observed that the polymer grains continue until the edge, until they abruptly stop, to reveal the very smooth silicon nitride surface.

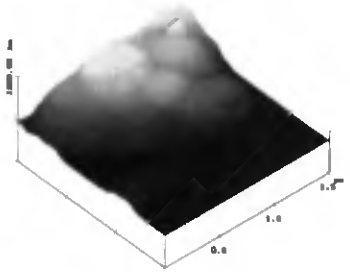

Fig. 3.12: An AFM image of edge of a bsa doped polypyrrole film (5mC).

Fig. 3.13 shows an image of a teatfb doped polypyrrole film. The surface appears very similar to the bsa doped polypyrrole. This image is made on the edge of one of the covered IDA electrodes. Some features bigger than the typical grain size can be observed. These features may be nucleation sites or lift off 'ears' [52] originating from the IDA fabrication. Such 'ears' have been observed on uncovered electrodes with the same visualisation technique.

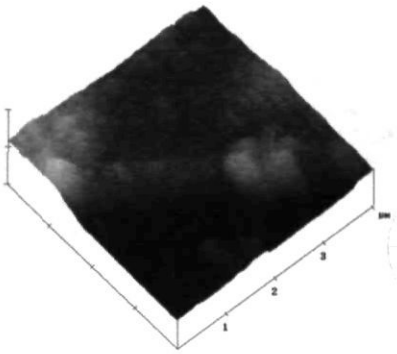

Fig. 3.13: An AFM image of a teatfb doped polypyrrole film (1.3 mC).

3.4 Reproducibility

3.4.1 Introduction

Reproducibility is a general requirement for comparative studies of different materials, and of course is also an important issue for the comparison of different chemo-resistors. This section describes experiments for an evaluation of the reproducibility of the deposition process. This is particularly important to validate the approach in the following sections, which describe the influence of different preparation parameters.

Some earlier reproducibility studies concerned the electrochemical behaviour during cyclic voltammetry of sensors [14], however a variation in electrochemical behaviour is difficult to relate to a variation in vapour response behaviour. A series of in situ tests was therefore performed, i.e. the vapour response behaviour of different prepared sensors was determined. This is hoped to a give more relevant image of the reproducibility of the polymer properties required for our application.

3.4.2 Experimental

The vapour responses of polypyrrole chemo-resistors with bsa doping prepared from independently prepared deposition baths were compared in the flow system.

Sensor preparation

A detailed description of the fabrication of chemo-resistors is described in section 3.2 of this thesis. In this series of experiments 5.0 mC bsa doped polypyrrole was deposited on 5 μm spaced non-passivated gold IDAs. Pyrrole was purified according to the standard procedure described in section 3.2 or by distillation. Distillations were performed at ambient pressure and the 128 °C fraction was collected.

Sensor characterisation

The sensors were mounted in the test system which was modified by the incorporation of a wash bottle containing saturated aqueous $CaCl_2$ in the carrier stream, to give it a relative humidity of 30 %. The dilution bypass was not present. The sensors were characterised by 1 minute exposures to 4 different samples: 50% aqueous methanol, water, 50% aqueous ethanol and a saturated aqueous LiCl solution (gives a relative humidity of 11%). The flow rate was 0.5 l/min.
Sensors were tested both directly after preparation and after a few days, to check for any change in sensor behaviour during the first few days after fabrication.

3.4.3 Results and discussion

The reproducibility between different depositions was tested whilst using the alumina column for pyrrole purification.

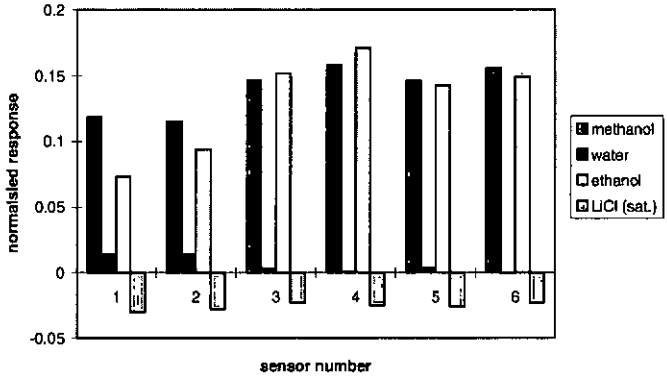

Fig. 3.14: Sensor responses directly after preparation from two lots of solution. Sensor 1 and 2 are prepared from lot 1. Sensors 3-6 from lot 2, where sensor 6 was prepared 1 hour after sensor 5 whilst the deposition bath was continuously bubbled with nitrogen.

The results are presented in Fig. 3.14. Although the data set is rather small, the results strongly suggest that sensors prepared from the same deposition bath are quite similar, even with time intervals as large as 1 hour, whilst there is a difference between sensors fabricated from different deposition baths.

To examine the evolution of the responses, the sensors were tested continuously for a period of 3 days using the same 4 samples. The response behaviour at the end of this period is presented in Fig. 3.15.

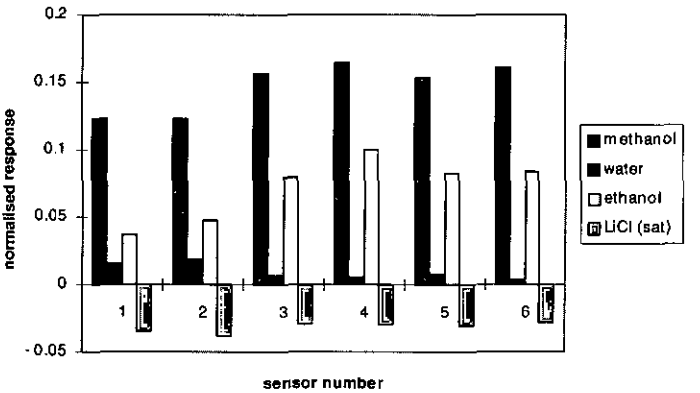

Fig. 3.15: Responses of the sensors from Fig. 3.14 after 3 days of continuous exposure.

The data from Fig. 3.14 and Fig. 3.15 is collected in a principle component analysis (pca) of the sensors in Fig. 3.16. Here it is clearly observed that the sensors prepared from the same baths show a more similar behaviour after three days, whilst the sensors prepared from different baths remain different. Apparently it is favourable to store freshly prepared sensors for a few days before using them.

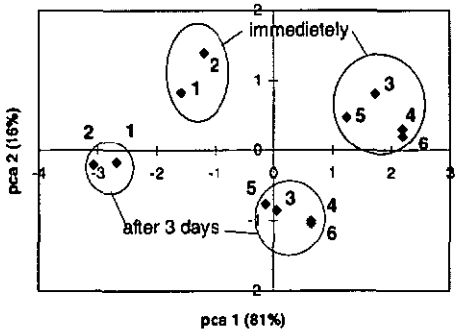

Fig. 3.16: Principle component analysis of the sensors, with the response to the 4 different vapours in Fig. 3.14 and Fig. 3.15 as input variables. The bold numbers indicate the sensor numbers.

The deposition solutions were prepared using the same chemicals, and yet they clearly give different results. A possible reason for this could be the purified pyrrole used. This possibility was investigated by using 2 deposition baths which were both made up from the same stock of purified pyrrole, which was stored at 4°C in the dark between the 2 depositions (approximately 1.5 hours).

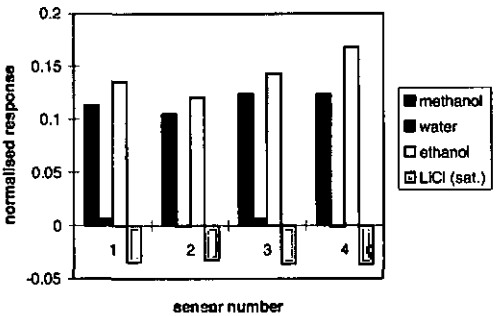

Fig. 3.17: Sensor responses directly after preparation from the same purified pyrrole stock. Sensor 1 & 2 prepared from a different lot of solution than sensor 3 & 4.

The sensors were characterised under the same conditions directly after preparation. The results are presented in Fig. 3.17.

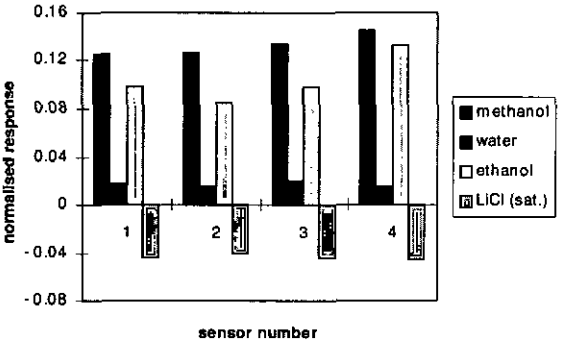

Fig. 3.18: Reproducibility of the sensors in Fig. 3.17 two days after preparation.

Also for this experiment the response evolution was studied (Fig. 3.18) and a pca was performed (Fig. 3.19).

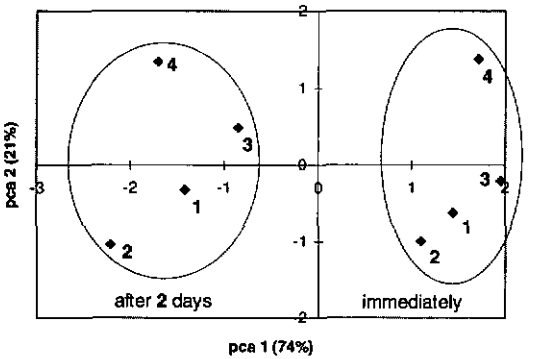

Fig. 3.19: Principle component analysis of the sensors, with the response to the 4 different vapours in Fig. 3.17 and Fig. 3.18 as input variables. The bold numbers indicate the sensor numbers.

Although data set is again limited it can from the pca be observed the difference between the sensors prepared from different baths is similar to

the variance betwcen the sensors prepared from the same bath. The similarity of the sensors did in this case not improve with time. It is observed though that an initially almost absent water response does appear with time. This can be explained by the drying out of the initially very wet sensor material deposited from an aqueous solution.

The better reproducibility between baths prepared from the same polypyrrole stock suggests that the purity of the pyrrole itself is the origin of the irreproducibility. A more rigorous purification procedure might therefore be required.

Sensors prepared from different deposition solutions prepared from two lots of distilled pyrrole were compared (Fig. 3.20).

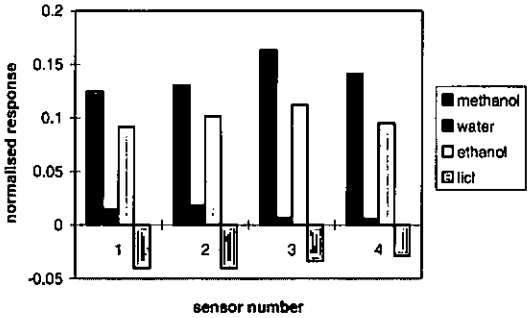

Fig. 3.20: Sensor responses 2 days after preparation from 2 different lots of deposition solution. Sensor 1 & 2 prepared from lot 1, sensor 3 & 4 from lot 2. The two lots of pyrrole were distilled before the experiment.

From the pca in Fig. 3.21 it can bc observed that the variation between the sensors made from the 2 lots of deposition solution is in this case smaller than when the pyrrole was purified with alumina (Fig. 3.16), there is however still a significant difference. The variation between different batches of purified polypyrrole can apparently not be completely eliminated by the distillation procedure used in this experiment.

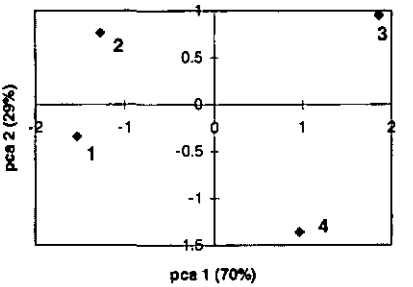

Fig. 3.21: Principle component analysis of the sensors, with the response to the 4 different vapours in Fig. 3.20 as input variables. The bold numbers indicate the sensor numbers.

3.4.4 Conclusions

Unfortunately the reproducibility of the preparation of the chemo-resistors is limited, but it is clear that sensors prepared from the same deposition solution are reasonably similar, even at time intervals as large as an hour between the depositions. The experiments suggest that the variation observed between different deposition baths might be caused by the irreproducibility of the pyrrole purification. The reproducibility between independently prepared baths could be improved by distillation, but a small variation nevertheless remains.

To study of the influence of the deposition parameters it was decided to take advantage of the reproducibility of the sensors prepared from the same deposition solution. Comparative studies on sensors in this thesis are therefore performed on sensors prepared from the same deposition bath.

3.5 Influence of the deposition charge on the sensing properties

3.5.1 Introduction

One of the obvious parameters of the preparation of a chemo-resistor is the thickness of the final polymer film. Thicker films may for example be more stable and have a lower resistance, whilst thinner films might be more gas permeable and thus give faster responses [11,49]. This section describes experiments to examine the influence of the film thickness on the performance of bsa doped polypyrrole films, to determine the optimum thickness for this type of chemo-resistor. Throughout this section, the deposition charge is used as an indicator of the film thickness. Previous experiments [55] indicated a thickness of 2.3 $\mu m.cm^2/C$.

3.5.2 Experimental

A series of chemo-resistors were prepared by electrodeposition of bsa doped polypyrrole on 5 μm spaced, passivated Au IDAs. The sensors were all prepared from the same deposition bath and were prepared with total charges varying between 2 and 7 mC. The so obtained chemo-resistors were mounted in the flow system and characterised with 1 minute exposures to various saturated vapours separated by 30 min. purges with dry air.

3.5.3 Results and discussion

Fig. 3.22 shows the baseline resistance of the chemo-resistors as a function of passed deposition charge. It can clearly be seen that at deposited charges greater then 4 mC the resistance becomes independent of the charge, whilst below this value it shows a rapid increase.

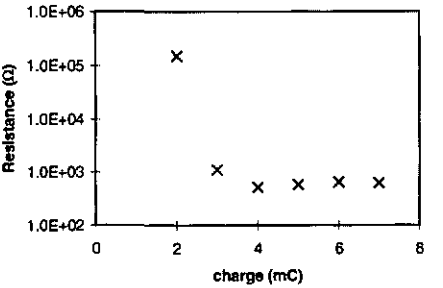

Fig. 3.22: The baseline resistance as a function of deposition charge.

Fig. 3.23 shows an optical microscope picture of a part of the chemo-resistor prepared with only 2 mC of charge. It is clearly observed that the electrodes are not fully bridged. The contact only exists at some individual points where the polymer bridged the electrodes.

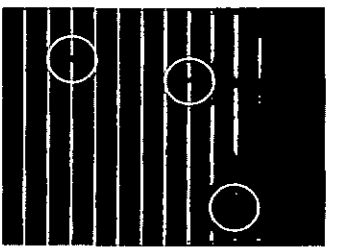

Fig. 3.23: Optical microscope picture of the chemo-resistor with 2 mC of charge. The bridged areas are marked with white circles. The electrodes are 5 μm wide.

At higher charges when the gap between the electrodes is fully covered, the thickness apparently does not have a significant influence on the base-line resistance. This might be due to a relatively high contact resistance (see also section 4.4), a decreased contribution to the conductivity of the outer part of the film [48], or a conductivity taking place mainly at the polymer surface [9].

Fig. 3.24 - Fig. 3.27 show transient responses of the different sensors to the various vapours. Considering first the water vapour response, it can be seen to increase with film thickness. The sensors all show similar rise and fall times. This may result from the mixing time in the sensor chamber, which may be slower then the sensors response.

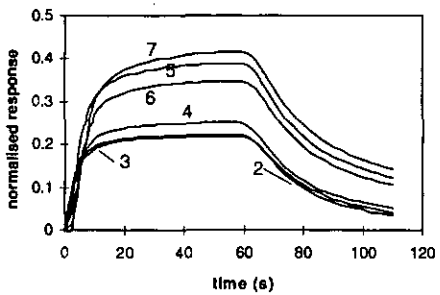

Fig. 3.24: Normalised responses to saturated water vapour. The deposition charge in mC corresponding to the different sensors is indicated on the graph.

For organic vapours a more complex behaviour is observed. There is a tendency in the opposite direction to water, i.e. the sensors prepared with thinner films show a larger positive response. The thicker films also show a longer rise - and fall time, strongly suggesting some diffusion limitation.

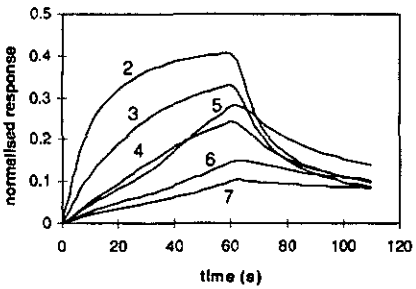

Fig. 3.25: Normalised responses to methanol vapour. The deposition charge in mC corresponding to the different sensors is indicated on the graph.

In the case of methanol, the slow response of the thicker films suggest that the exposure time is not sufficient for equilibration and the maximum response is not reached. This can explain the smaller response for the thicker films.

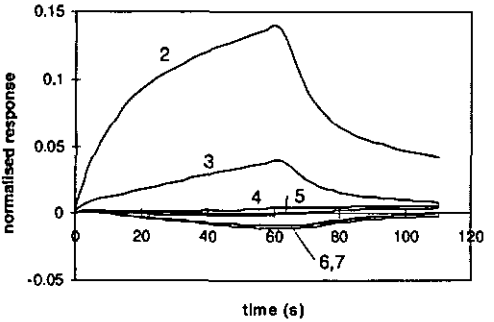

Fig. 3.26: Normalised responses to acetonitrile vapour. The deposition charge in mC corresponding to the different sensors is indicated on the graph.

For acetonitrile and ethanol vapour, the situation is more complicated. The very thin film does in this case give the biggest and fastest response, but it is not clear why the thicker films give a response in the opposite direction. A second response mechanism might be interfering with the main mechanism.

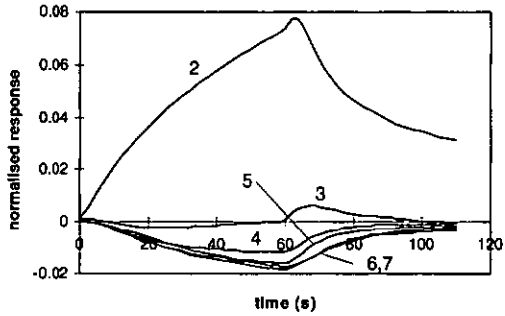

Fig. 3.27: Normalised responses to ethanol vapour. The deposition charge in mC corresponding to the different sensors is indicated on the graph.

Another cause for the different response directions of the different sensors might be the different oxidation state of the different films. During extended deposition the already deposited material may become over-oxidised resulting in a final material having different properties [56]. The consecutive polymer layers may so have different response properties.

For fast diffusing components, like water, the response will be an average of the response of the different part of the polymer layer. When diffusion is limiting however, which is likely to be the case for ethanol and acetonitrile, the vapour reaches the differently responding polymer layers with different delays, causing a complicated response transient. In this way the effects of thickness may be superimposed over a variation in the polymeric material, and the final response behaviour is a result of both effects.

3.6 Performance of chemo-resistors doped with different sulfonic acid counter ions

3.6.1 Introduction

The negative ions from the deposition solution are incorporated into the polymer during its growth to give charge neutrality of the oxidised polymer. In the fully oxidised form there is ca. 1 so called counter ion (assuming it has only a single electron charge) per 3-4 pyrrole units [37]. Especially since the counter ion may be comparable in size or even larger than a pyrrole unit [14], it may be seen that it can exert a considerable influence upon the properties of the polymer film. As for previous polymer characterisation experiments, bsa doped polypyrrole was studied. Here we shall compare the properties of this polymer with similar materials made using other alkane sulfonates as doping.

3.6.2 Experimental

Polypyrrole was deposited on 5 μm spaced passivated Au IDAs from 30 ml 0.067 M aqueous salt solution of the counter ion with 0.204 ml pyrrole. The IDAs were pulsed between 0.0 and 1.0 V versus SCE until a total charge of 4 mC. Different alkane sulfonates (see Table 3.2) were used as counter ions. The different sulfonate ions were obtained as 98% sodium salts from Aldrich, and were used as received.
The prepared sensors were tested in the flow system with various vapours.

3.6.3 Results and discussion

The normalised vapour responses of bsa and hexanesulfonate (hsa) doped sensors are presented in Fig. 3.28 and Fig. 3.29. The response values at t=60 s are together with the response values of sensors doped with other sulfonate ions and their base-line resistance presented in Table 3.2.

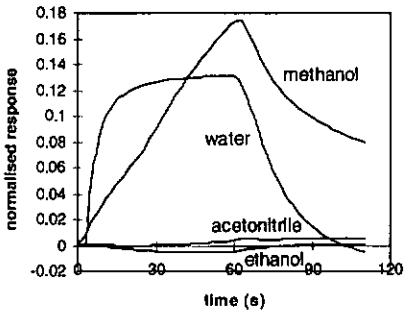

Fig. 3.28: Vapour responses of the bsa doped sensor.

Comparison of Fig. 3.28 and Fig. 3.29 show distinct differences between the two sensor materials, with the material having the longer carbon chain being more sensitive to the non-aqueous solvents.

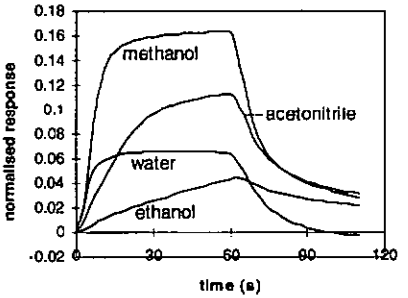

Fig. 3.29: Vapour responses of the hsa doped sensor.

Table 3.2 shows several trends. Firstly, the response to both water and methanol clearly decreases with the chain length of the counter ion [14].

Secondly, the responses of ethanol and acetonitrile show an increase with chain length. This behaviour causes a distinct change in material's selectivity profile, as evidenced from the response ratios to water of the various vapours also presented in Table 3.2. Hexane sulfonic acid is off the trend in this series, in that it displays a large acetonitrile response.
This series which was repeatable for several series of deposition baths shows that changing the counter ions does allow some degree of selectivity of the material.

Table 3.2: Normalised vapour responses for the differently doped sensors, taken 60 s after the start of the vapour exposure.

		Response							
doping	length carbon chain	water	methanol	ethanol	acetonitrile	ratio methanol water	ratio ethanol water	ratio acetonitrile water	baseline (Ω)
methane sulfonic acid	1	0.52	0.50	0.0004	0.0043	0.96	0.0008	0.008	89
butane sulfonic acid	4	0.13	0.16	-0.0055	0.0025	1.23	-0.042	0.02	122
hexane sulfonic acid	6	0.066	0.16	0.038	0.11	2.42	0.58	1.67	72
octane sulfonic acid	8	0.0014	0.004	0.0035	0.0034	2.87	2.45	2.38	53
decane sulfonic acid	10	0.0019	0.006	0.0044	0.0048	3.07	2.34	2.56	52

For practical applications, in which water is a frequent environmental variable, it is interesting to note that the water response can be suppressed by increasing the hydrophobic nature of the counter ion. However, the small size of the responses with the larger counter ions may cause measurement problems and result in a poor signal to noise ratio.
Considering these factors, butane and hexane sulfonate doped polypyrrole appear to be particularly promising materials.

3.7 Deposition potential

3.7.1 Introduction

Polypyrrole may be electrochemically deposited in several ways: at a constant potential or current, or at a variable but controlled potential or current [34]. We have found that the best results were obtained when bsa doped polypyrrole was deposited under pulsed potential conditions [57]. An important variable in this protocol is the potential of the pulse at which polypyrrole is deposited. It can strongly influence its properties, for example depositing at excessively high potentials can lead to over-oxidised, insulating films.

3.7.2 Experimental

The experiments in this section were all performed from the standard composition deposition bath (section 3.2.3). All sensors were prepared by depositing bsa doped polypyrrole on 5 μm spaced non-passivated gold IDAs with 10 mC of charge. The pulse height of the deposition pulse train was varied between 1.0 and 1.3 V.
After preparation the sensors were mounted in the flow system and characterised with water vapour.

3.7.3 Results and discussion

Different sensor series prepared from different deposition baths did not always show consistent results. In general there was a tendency to larger baseline-resistances and larger vapour responses for the sensors deposited with higher potential pulses. Pulses with an amplitude between 1.0 to 1.2 V showed a sharp charging peak at the beginning of the pulse followed by a decaying current due to diffusion limited polymerisation according to Fig. 3.7. Sensors deposited with 1.3 V pulses showed an increasing current during the deposition pulse.

Fig. 3.30 shows the normalised response to different humidities of 4 sensors, deposited from the same deposition solution with pulses from 1.0, 1.1, 1.2 and 1.3 V respectively. The sensors had baseline resistances of 184 Ω, 141 Ω, 150 Ω and 275 Ω respectively. With exception of the film deposited with 1.0 V pulses, there is a tendency of a larger response with higher oxidation pulses. It is not clear however why the sensor deposited at 1.0 V does not follow this trend.

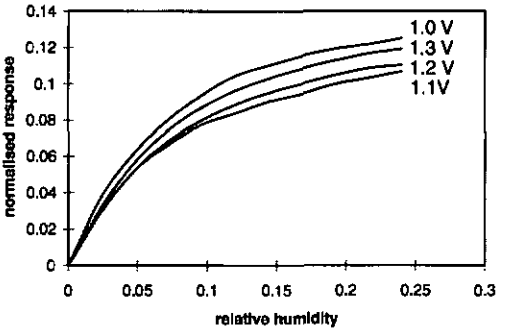

Fig. 3.30: Calibration curves of the sensors prepared with different pulse heights.

It should be concluded the deposition potential has a rather significant influence, and can so be used to trim the deposition process, to obtain sensors with the desired response properties. However, before this can be done, a reproducible deposition process should be obtained.

3.8 Conclusions and outlook

This chapter has investigated the deposition parameters of polypyrrole. It was shown that the relative water sensitivity of the sensors could be suppressed by the incorporation of more hydrophobic counter ions. It was furthermore demonstrated that for bsa doped polypyrrole films the water response increases with film thickness, whilst the response to organic vapours decreases with film thickness. Also because of a reduced response time polymer films should therefore be as thin as possible. Other parameters, such as deposition potential are also of great importance, but were much more difficult to quantify.

As other authors [14], we have found that reproducibility is problematic, although it may, at least partially, be improved when all the depositions are made from a single bath. Experimental results indicate that purity of the pyrrole monomer is critical if reproducible bath-to-batch results are to be obtained, and this area needs greater study. In the case of bsa doped polypyrrole films it has been shown that growth and subsequent bridging occurs only at a few localised areas, which may also impact upon reproducibility.

3.9 References

1. R. Greef, R. Peat, L.M. Peter, D. Pletcher and J. Robinson, Instrumental Methods in Electrochemistry, Ellis Horwood Limited, Chichester, a division of Wiley & Sons, New York, 1985.
2. X. Chen, J. Devaux, J.-P. Issi and D. billaud, *Chemically Oxidized Polypyrrole: Influence of the Experimental Conditions on Its Electrical Conductivity and Morphology*, Polymer engineering and Science 35 (1995) 642-647.
3. G. Appel, A. Yfantis, W. Göpel and D. Schmeisser, *Highly conductive polypyrrole films on non-conductive substrates*, Synthetic Metals 83 (1996) 197-200.
4. M. De Wit, E. Vanneste, F. Blockhuys, H.J. Geise, R. Mertens and P. Nagels, *Application of Polythienylene vinylene as a chemiresistor for organic vapours*, Synthetic Metals 85 (1997) 1303-1304.
5. X.B. Chen, J. Devaux, J.-P. Issi and D. Billaud, *The Conducting Behavior and Stability of Conducting Polymer Composites*, Polymer Engineering and Science 35 (1995) 637-641.
6. E.E. Havinga, L.W. van Horssen, W. ten Hoeve, H. Wynber and E.W. Meijer, *Self-doped water-soluble conducting polymers*, Polymer bulletin 18 (1987) 277-281.
7. E.E. Havinga, W. ten Hoeve, E.W. Meijer and H. Wynberg, *Water-Soluble Self-Doped 3-Substituted Polypyrroles*, Chemistry of Materials 1 (1989) 650-659.
8. S.C. Ng, H.S.O. Chan, H.H. Huang and P.K.H. Ho, *Poly(o-aminobenzylphosphonic acid): a Novel Water Soluble, Self-doped Functionalized Polyaniline*, J. Chem. Soc., Chem. Commun. (1995) 1327-1328.
9. P. Pelosi and K. Persaud, *Gas Sensors: Towards an artificial nose*, Sensors and Sensory Systems for Advanced Robots, Edited by Paolo Dario, Springer, Berlin, 1988.
10. E.-L. Kupila and J. Kankare, *Influence of electrode pretreatment, counter anions and additives on the electropolymerization of pyrrole in aqueous solutions*, Synthetic Metals 74 (1995) 241-249.
11. P.N. Bartlett, P.B.M. Archer and S.K. Ling-Chung, *Conducting polymer gas sensors. Part I: Fabrication and characterisation*, Sensors and Actuators 19 (1989) 125-140.
12. A. Guiseppi-Elie, A.M. Wilson, J.M. Tour, T.W. Brockmann, P. Zhang and D.L. Allara, *Specific Immobilization of Electropolymerized Polypyrrole Thin Films onto Interdigitated Microsensor Electrode Arrays*, Langmuir 11 (1995) 1768-1776.
13. P.N. Bartlett and K. Ling-Chung, *Conducting Polymer Gas Sensors. Part III: Results for Four Different Polymers and Five Different Vapours*, Sensors and Actuators 20 (1989) 287-292.
14. N. Blair, *The development and characterisation of conducting polymer based sensor for use in an electronic nose*, Ph.D. Thesis, University of Southampton, UK, 1994.
15. T.A. Skotheim, Handbook of Conducting Polymers, Vol. 1, Marcel Dekker, Inc. New York, 1986.

16. T.A. Skotheim, Handbook of Conducting Polymers, Vol. 2, Marcel Dekker, Inc. New York, 1986.
17. G.K. Chandler and D. Pletcher, *The Electrochemistry of Conducting Polymers*, Specialist Periodical Report, Electrochemistry, vol. 10, Edited by D. Pletcher, Royal Soc. of Chemistry, Burlington House, London, 1985.
18. W. Schuhmann, *Conducting Polymer Based Amperometric Enzyme Electrodes*, Mikrochim. Acta 121 (1995) 1-29.
19. S.J. Sutton and A.S. Vaughan, *On the morphology and growth of electrochemically polymerized polypyrrole*, Polymer 36 (1995) 1849-1857.
20. H. Eisazadeh, G.G. Wallace and G. Spinks, *Influence of steric stabilizers on the electropolymerization and properties of polypyrroles*, Polymer 35 (1994) 1754-1758.
21. J.W. Gardner and P.N. Bartlett, *Potential Applications of electropolymerized thin organic films in nonotechnology*, Nanotechnology 2 (1991) 19-32.
22. K. Imanishi, M. Satoh, Y. Yasuda, R. Tsushima and S. Aoki, *The effects of electrolyte on electrical conductivity of electrochemically prepared polypyrrole and polythiophene films*, J. Electroanal. Chem. 260 (1989) 469-473.
23. A. Talaie and G.G. Wallace, *The effect of the counterion on the electrochemical properties of conducting polymers - a study using resistometry*, Synthetic Metals 63 (1994) 83-88.
24. D.A. Kaplin and S. Qutubuddin, *Electrochemically synthesized polypyrrole films: effects of polymerization potential and electrolyte type*, Polymer 36 (1995) 1275-1286.
25. Y. Lin and G.G. Wallace, *Electropolymerisation of pyrrole under hydrodynamic conditions - effect of solution additives*, Electrochimica Acta. 39 (1994) 1409-1413.
26. G. Zotti, G. Schiavon, A. Berlin and G. Pagani, *The role of water in the electrochemical polymerization of pyrroles*, Electrochimica Acta 34 (1989) 881-884.
27. R.J. Waltman and J. Bargon, *Electrically conducting polymers: a review of the electropolymerization reaction, of the effects of chemical structure on polymer film properties, and of applications towards technology*, Can. J. Chem. 64 (1986) 76-95.
28. R. Cabala, V. Meister and K. Potje-Kamloth, *Effect of competitive doping on sensing properties of polypyrrole*, J. Chem. Soc., Faraday Trans. 93 (1997) 131-137.
29. A.F. Diaz and J.C. Lacroix, *Synthesis of electroactive/conductive polymer films: electrooxidation of heteroaromatic compounds*, New J. Chem. 12 (1988) 171-180.
30. S. Roth, H. Bleier and W. Pukacki, *Charge Transport in Conducting Polymers*, Faraday Discuss. Chem. Soc. 88 (1989).
31. P.N. Bartlett, J.W. Gardner, C. Beriet, J. Elliott and A. Duke, International Patent, PCT/GB96/01724, 1996.
32. R.J. Waltman, A.F. Diaz and J. Bargon, *Substituent Effects in the Electropolymerization of Aromatic Heterocyclic Compounds*, J. Phys. Chem. 88 (1984) 4343-4346.

33. Z. Deng, C. Stone and M. Thompson, *Characterization of Polymer Films of Pyrrole Derivatives for Chemical Sensing by Cyclic Voltammetry, X-ray Photoelectron Spectroscopy and Vapour Sorption Studies*, Analyst 122 (1997) 1129-1138.
34. M.D. Inmisides, R. John, P.J. Riley and G.G. Wallace, *The Use of Electropolymerization to Produce New Sensing Surfaces: A Review Emphasizing Electrodeposition of Heteroaromatic compounds*, Electronanalysis 3 (1991) 879-889.
35. A.O. Patil, Y. Ikenoue, N. Basescu, N. Colaneri, J. Chen, F. Wudl and A.J. Heeger, *Self-doped Conducting Polymers*, Synthetic Metals 20 (1987) 151-159.
36. A.N. Chowdhury, Y. Harima, Y. Kunugi and K. Yamashita, *p-and n-type conductance of electrochemically synthesized poly(3-methyl thiophene) films*, Electrochimica Acta 41 (1996) 1993-1997.
37. H. Zhao, W.E. Price and G.G. Wallace, *Effect of the counterion employed during synthesis on the properties of polypyrrole membranes*, J. Membrane Sci. 87 (1994) 47-56.
38. P. Marque, J. Roncali and F. Garnier, *Electrolyte effect on the electrochemical properties of poly(3-methyltiophene) thin films*, J. Electroanal. Chem. 218 (1987) 107-118.
39. M. Brie, R. Turgu and C. Neamtu, *Polypyrrole films, The effect of dopant molecules on the electrical properties and molecular organisation of polypyrrole films*, Revue Roumaine de Chimie 38 (1993) 1317-1325.
40. J.S. Wainright and C.A. Zorman, *Rutherford Backscatttering Studies of Polypyrrole Films. I. Effect of Electrolyte on Deposition Efficiency*, J. Electochem. Soc. 142 (1995) 379-383.
41. J.S. Wainright and C.A. Zorman, *Rutherford Backscattering Studies of Polypyrrole Films. II. Effect of Electrolyte on Deposition Efficiency*, J. Electrochem. Soc. 142 (1995) 379-383.
42. T.F. Otero, C. Santamaria and R.K. Bunting, *Kinetic studies of polypyrrole electrogeneration in three solvents*, J. of Electroanal. Chem. 380 (1995) 291-294.
43. A. Bhattacharya, A. De and S. Das, *Electrochemical preparation and study of transport properties of polypyrrole doped with unsaturated organic sulfonates*, Polymer 37 (1996) 4375-4382.
44. P. Dyreklev, M. Granström, O. Inganäs, L.M.W.K. Gunaratne, G.K.R. Senadeera, S. Skaarup and K. West, *The influence of polymerization rate on conductivity and crystallinity of electropolymerized polypyrrole*, Polymer 37 (1996) 2609-2613.
45. D.J. Strike, *personal communication.*
46. B.P.J. de Lacy Costello, P. Evans, R.J. Ewen, C.L. Honeybourne and N.M. Ratcliffe, *Novel composite organic-inorganic semiconductor sensors for the quantitative detection of target organic vapours*, J. Mater. Chem. 6 (1996) 289-294.
47. P.N. Bartlett, J.W. Gardner and R.G. Whitaker, *Electrochemical Deposition of Conducting Polymers onto Electronic Substrates for Sensor Applications*, Sensors and Actuators A21-A23 (1990) 911-914.
48. A.C. Partridge, P. Harris and M.K. Andrews, *High Sensitivity Conducting Polymer Sensors*, Analyst 121 (1996) 1349-1353.

49. E. Stussi, R. Stella and D. De Rossi, *Chemoresistive conducting polymer-based odour sensors: influence of thickness changes on their sensing properties*, Sensors and Actuators B43 (1997) 180-185.
50. P.A. Payne, J.G. Bartlett and N.K. Harris, UK Patent GB 2 203 553 B, 1997.
51. M.E.H. Amrani, K.C. Persaud and P.A. Payne, *High-frequency measurements of conducting polymers: development of a new technique for sensing volatile chemicals*, Meas. Sci. Technol. 6 (1995) 1500-1507.
52. J.C. Fiaccabrino, *Thin-Film Microelectrode Arrays: Materials & Designs*, Ph.D. Thesis, University of Neuchâtel, Switzerland, 1996.
53. A.J. Bard and L.R. Faulkner, *Electrochemical methods, Fundamentals and Applications*, Wiley & Sons, New York, 1980.
54. Chr. Froeck, A. Bartl and L. Dunsch, *The growth and the surface properties of polypyrrole on single crystal graphite electrodes as studied by in-situ electrochemical scanning probe microscopy*, Electrochemical Nanotechnology, In-situ Local Probe Techniques at Electrochemical Interfaces, Edited by W.J. Lorenz and W. Plieth, Wiley-VCH, New York, 1998.
55. D.J. Strike, N.F. de Rooij, M. Koudelka-Hep, M. Ulmann and J. Augustynski, *Electrocatalytic oxidation of methanol on platinum microparticles in polypyrrole*, Journal of Applied Electrochemistry 22 (1992) 922-926.
56. D. Blackwood and M. Josowicz, *Work Function and Spectroscopic Studies of Interactions between Conducting Polymers and Organic Vapors*, J. Phys. Chem. 95 (1991) 493-502.
57. C. Kranz, M. Ludwig, H.E. Gaub and W. Schuhmann, *Lateral Deposition of Polypyrrole Lines by Means of the Scanning Electrochemical Microscope*, Adv. Mater. 7 (1995) 38-40.

4 Conductivity of polypyrrole

4.1 Introduction

4.1.1 General

Polypyrrole is different from more common electron conductors, like metals, because it consists of a closely wrapped clod of conducting chains which are not interconnected [1,2]. Therefore the electrons need to transfer from one chain to another, when a current is passed through the material. For the overall conductivity of the bulk material, both the conductivity of the individual semiconducting chains and the transfer between the different chains have to be considered.

4.1.2 Theoretical

Semiconductors

A common feature about conducting polymers is the existence of long strands of conjugated double bonds [1]. They exhibit semiconductor properties [3] such as a conductivity modulation by the doping level, and frequently a positive temperature coefficient of conductivity. Their typical conductivity ranges from 10^{12} to 50 S/cm [1,4-6].
This semiconductor behaviour also has consequences on the properties of the metal/polypyrrole contacts. Depending on the doping levels, such metal-semiconductor contacts, can be either an ohmic contact or a Schottky barrier [1,3,7-10].

Charge transfer between conducting regions

The semiconductor theory can explain some, but not all of the electronic properties that are observed for conducting polymers. The discontinuity of the polymer is responsible for other aspects of its behaviour. It was for example found that the temperature dependence of the conductivity is best described by the variable-range hopping model for non-crystalline conductors [1,2,11-14], originally proposed by Mott.

4.1.3 Outline

The fundamental conductivity issues strongly influence the optimal design of a chemo-resistor. This chapter describes experiments which examine some conductivity issues relevant for chemo-resistor design.
In certain cases the influence of vapour will be taken into consideration. The outcome of the various experiments will be discussed in a common conclusion section which leads to a qualitative description of the electrical behaviour of the ppy based chemo-resistors.

4.2 AC Conduction

4.2.1 Introduction

Although the resistance of conducting polymers is often measured with a small DC current, several authors have reported AC impedance measurements [4,15-17]. Such AC measurements can be interesting for sensor application for three reasons.

Firstly, AC measurements will contain a contribution from the dielectric constant of the polymer. At sufficiently high frequencies, not only the ohmic resistance, but also charging effects between the two electrodes will be measured. Measuring the dielectric constant has the potential of increasing the amount of information obtained[10,18,19].

Secondly, an AC voltage removes the barriers between the different polymer chains. Since the material is discontinuous, the electrons have to hop from one conducting region to the other. If these are close to each other, there will be a relatively high capacitance between the chains [20], which will short-circuit the discontinuity above a certain frequency. This then allows intrinsic polymer resistance to be measured.

Lastly, AC characterisation has been reported to improve the noise characteristics of the sensor [15,16]. This is related to the second effect. The charge hopping between the chains causes a 1/f noise contribution, which vanishes at high frequency.

This section describes AC measurements made to examine the frequency response of the chemo-resistors used in this thesis.

4.2.2 Experimental

Chemo-resistors were prepared with bsa doped polypyrrole (5mC) on 5 μm spaced, non-passivated IDA structures according to the procedure described in chapter 3. Because of their structure, a conducting substrate with a thin passivation layer, these substrates have a large parasitic capacitance parallel to the active area (see also chapter 7), making it

difficult to measure any capacitance changes. To circumvent this, chemo-resistors prepared on glass IDAs having a similar electrode design were also characterised.

The frequency dependence of the conductivity of the polymers was measured with a HP4194 impedance/gain-phase analyser. The amplitude of the AC oscillation was set to the minimum of the instrument, 20 mV. The frequency was swept from 100 Hz to 40 MHz. Bode plots were recorded whilst the sensors were exposed to the ambient air and to a methanol sample, which was generated with a 25 ml beaker containing 5 ml methanol and sealed with parafilm®, left at ambient temperature for at least 10 minutes to equilibrate. The sensors were exposed by inserting them in the headspace, through a small hole in the parafilm®.

Obtained Bode plots were fitted to a model composed of a parallel resistance and capacitor using an internal function of the instrument. The same fitting procedure was also performed on data obtained with dummy resistors and IDA substrates without a conducting polymer.

4.2.3 Results and discussion

Bode plots characteristic for an RC circuit were obtained for bsa doped polypyrrole sensors. Fig. 4.1 shows such a bode plot for a bsa doped polypyrrole chemo-resistor. At low frequencies the impedance equals the DC resistance. From the corner frequency it starts to decrease due to the influence of the parallel capacitance.

At the higher limit of the experimental range, a small deviation of ideal RC behaviour can be observed from the phase deviation from the 'ideal' -90°. This deviation may have multiple origins, but since it takes place at the limits of the instrument, it's difficult to interpret, and will not be considered further.

To examine how gas exposure influences the impedance of the chemo-resistor, an equivalent circuit was fitted to the bode plots. The results are presented in Table 4.1. The fitted resistance values correspond to the base-line resistance.

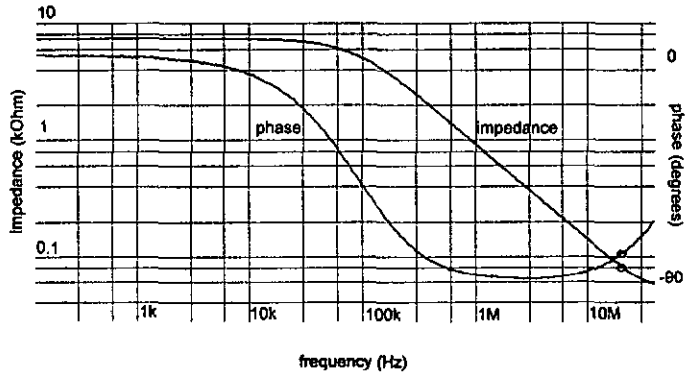

Fig. 4.1: Bode plot of a chemo-resistor (Note that the phase is on a linear scale.)

The value can be seen to increase upon exposure to water, in accord with the *DC* results in chapter 3. The capacitance values remain constant. A control experiment using a resistor and an unmodified IDA substrate showed that this value is the substrate capacitance.

Table 4.1: Fitted values from the Bode plots.

Substrate	Sample	R (kΩ)	C (pF)
silicon	ambient air	8.2	250
silicon	water	8.6	250
glass	ambient air	6.4	5
glass	water	6.8	5

Even on the glass substrates having a capacitance of only 5 pF, allowing the capacitance to be measured more accurately, no changes could be observed on vapour exposure. The dielectric changes in the IDA structure are shorted out by the conductivity of the polymer. With the available equipment it is therefore not possible to measure dielectric effects of the polymer in the IDA chemo-resistor configuration. In chapter 7, it will be demonstrated that without a conducting polymer, the dielectric effects can indeed be measured with an IDA structure.

4.3 Voltage dependency of the resistance

4.3.1 Introduction

Since the resistance of the chemo-resistors is determined by multiple, possibly interfering, mechanisms, its resistance may be voltage dependent [15], for example by Schottky barriers at the metal-polymer interface [9,11], or grain boundaries requiring a minimum voltage for electron tunnelling.
To investigate whether these effects were present over the normal range of operation, the V-I characteristics of a series of bsa doped polypyrrole chemo-resistors were examined.

4.3.2 Experimental

A series of bsa doped polypyrrole chemo-resistors were prepared according to the standard recipe described in chapter 3. They were one by one connected to a D/A-converter HP1328A mounted in a VXI mainframe. The D/A-converter supplied a current between 0 and 100 μA, and the voltage across the sensor was measured with an HP 3440IA multimeter. Both instruments were connected to a personal computer via an HP-IB interface, and were controlled by an application written in HP-VEE.
For characterisation, the sensors were mounted in the flow system and exposed to humidities ranging from 10% to 100% in steps of 10%. At each humidity, the current was increased from 1 to 100 μA in 1 minute duration steps of 1 μA. At the end of each step, the voltage over the chemo-resistor was automatically recorded, and the staircase continued.

4.3.3 Results and discussion

Fig. 4.2 shows the voltage across a chemo-resistor as a function of the applied current at different humidities. The step-like character of the curves is believed to be an artefact of the D-A converter, since this effect was also seen when dummy resistors of a comparable value were examined.

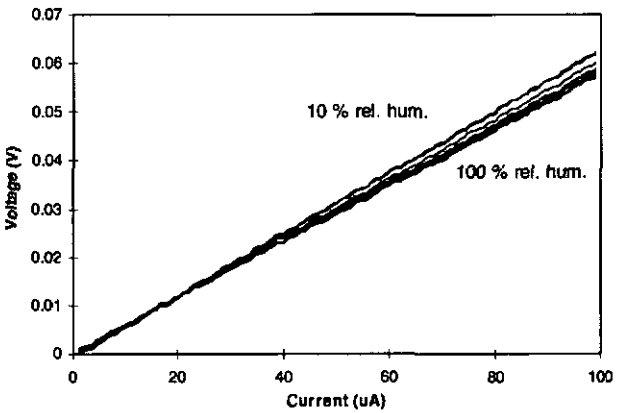

Fig. 4.2: The I-V relation of a bsa doped ppy chemo-resistor for humidities between 10 and 100 %.

It can be seen that a straight line corresponding to a voltage independent resistor was observed over the entire humidity range. This shows that under these conditions neither the polymer, nor the gold-polymer contacts, displayed any non-ohmic properties [8,9]. This is in contradiction with several other reports of non-linearity [21]. However, these measurements were made at a higher current and as has already been suggested, may have been the result of self-heating of the polymer, rather than any inherent property [15]. In conclusion it seems clear that under the measurement conditions used in this thesis, an applied voltage around 10 mV, the chemo-resistors are linear.

4.4 Contact resistance

4.4.1 Introduction

The total resistance measured between the electrodes of a chemo-resistor can be separated in two different contributions. The bulk resistance of the conducting polymer and the contact resistance between the polymer and the electrodes [16]. Using a 4-point measurement, it was examined if the contact resistance shows a different vapour response behaviour than the bulk of the polymer.

Four-point measurements

A common method to measure the intrinsic resistance of a material, without interference from the contact resistance, is a 4-point measurement (Fig. 4.3). In this set-up the resistance is derived from the voltage between the inner two electrodes, whilst a constant current is passed between the two outer electrodes. When the impedance of the voltage measurement circuit on the inner two electrodes is sufficiently high, the current through this circuit can be neglected, and the voltage drop over the contacts vanishes. The resistance between the inner probes can thus be calculated without any influence from the contact resistance.

4.4.2 Experimental

Polymer deposition

The contact resistance experiments were performed on gold micro-band structures. These consisted of 4 parallel gold lines of 5 μm width, 1 mm length and 5 μm apart on a passivated silicon substrate. Polypyrrole doped with bsa was electrodeposited on these electrodes according to the standard recipe (chapter 3). The charge passed for this deposition was 156 μC, which corresponds to 7.8 mC/mm^2.

Electrical set-up

For the four point measurements the outer of the 4 electrodes were connected to the standard current source circuit which was used for the other chemo-resistor measurements (as described in chapter 3). The current was set to 120 nA. The middle 2 electrodes were connected to an instrumentation amplifier type AMP01 from Analog Devices, which was set to amplify 20 times. This device has a typical input current of 1 nA, which is low enough to be neglected. The voltage output from the current source circuit and the outputs of the amplifier were connected to a HPE1313A scanning AD-converter.

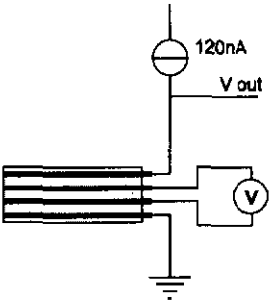

Fig. 4.3: Four point measurements on micro-bands.

The four-point measurements were performed in the flow system, to allow vapour influences to be examined. The carrier stream was kept at 29 % humidity and the sample was a 50 % aqueous methanol solution.

4.4.3 Results and discussion

The 120 nA current resulted in a voltage of 0.173 V and 0.039 V over the outer and the inner electrodes respectively. This corresponds to a resistance of 1.4 MΩ and 325 kΩ respectively. Fig. 4.4 shows the normalised responses of the inner and the outer electrode pair to a 50 % aqueous methanol solution.

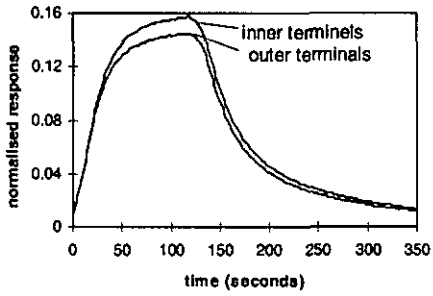

Fig. 4.4: Response to 50% aqueous methanol.

As can be clearly seen, the response of the inner pair is 8% higher then that of the outer. This suggests that the contact resistance has quite a significant influence on the chemo-resistor response, as has been previously observed by Partridge [16].

Extrapolation

In the cross-section shown in Fig. 4.5, it can be seen that the polymer consists of three in principle identical sections. The two outer ones can be considered to be equivalent to the region between the inner electrode pair, which allows the total resistance of the polymer to be estimated as 3*325 kΩ≈1 MΩ. The difference with the total resistance of 1.4 MΩ is thus the total contact resistance, which is 400 kΩ.

Based on this extrapolation, the contact resistance is approximately 29% of the total polymer resistance. The response measured with the 4-point set-up is however only 8% higher than the simple measurement. There are two possible explanations for this phenomena.

Firstly, it is possible that the contact resistance does also change on vapour exposure, but less or more slowly than the bulk resistance, so that the 4-point measurement gives a slightly but not 50% higher response.

Secondly the 4-point measurement is not ideal, due to the relatively large electrodes. This eliminates only a part of the contact resistance, so resulting in an only slightly higher response.

The second possibility is illustrated in Fig. 4.5. The electrodes, which are relatively large compared to the polymer bridges between the electrodes, actually shunt a part of the polymer film, and thus reintroduce a part of the contact resistance in the measurement of the inner voltage. In reality this should be modelled with a transmission line on top of the electrodes, but for simplicity, the effect is here shown with 2 resistors R_C per contact.

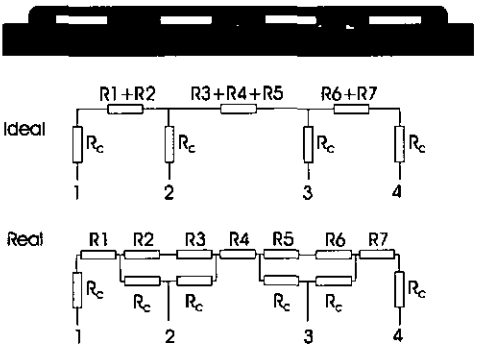

Fig. 4.5: The ideal and the realistic occurrence of the contact resistance in a structure with four micro-bands.

In the ideal situation there is a negligible current passing between terminal 2 and 3. This prevents a voltage drop over the contact resistance, and allows the polymer resistance *R3+R4+R5* to be determined. In reality however, the electrodes shunts a part of the chemo-resistor, which causes part of the current to be passed through the metal, whilst another part passes through the film on top of the electrode. The potential measured between 2 and 3 reflects the polymer resistance R4 plus the shunted current multiplied with the contact resistance.

The partial suppression of the contact resistance with a four point measurement method, results in a larger vapour response. It can from these measurements not be concluded however, if the contact resistance gives a smaller response then the bulk of the polymer, or if it does not respond at all.

4.5 Noise

4.5.1 Introduction

Noise is an inevitable component of all electrical signals [22], also of the measured resistance of chemo-resistors. The detection limit of any sensor is ultimately determined by its noise behaviour. This section will explore the noise behaviour of chemo-resistors. After a brief introduction to noise theory, the results of noise measurements on bsa doped polypyrrole chemo-resistors will be described.

4.5.2 Theory

Two main origins of noise can be distinguished. Firstly, the noise originating from external influences on a circuit, like capacitive coupling to mains cables, hf-disturbance, etc. This type of noise can largely be avoided with a well designed experimental set-up.
Secondly, there is the noise generated in the circuit itself. Electrical current consists of a discrete flow of electrons thus inevitably generating noise. This is the thermal, or so called Johnson, noise. Additionally to this thermal noise, there can be a contribution of flicker noise, or 1/f noise, caused by charge flow in a discontinuous medium.

Calculations

Noise is generally expressed as a power density over a certain band-width. For thermal noise the noise power density is represented by equation (4.1). Because of the random nature of noise signals, it is not the amplitude of the different sources, but their power densities that should be added to allow the determination of the total noise [22]. Therefore it is common to use the notation of equation (4.2) because this notation, with a noise voltage density expressed in [V^2/Hz], allows contributions from different components to be simply added.

$$P = 4kT \cdot \Delta f \tag{4.1}$$

$$v_{thermal}^{\ 2} = 4kTR \cdot \Delta f \tag{4.2}$$

k:	Boltzman's constant	[J/K]
T:	absolute temperature	[K]
Δf:	bandwidth	[Hz]
P:	noise power density	[W]
$v_{thermal}$:	noise voltage	[V]
R:	resistance	[Ω]

Flicker noise is roughly inversely proportional to the frequency f. Assuming a constant power density per octave (pink noise) it can be described by (4.3).

$$v_{Flicker}^{\ 2} = I_B R^2 \cdot K \cdot \frac{\Delta f}{f} \tag{4.3}$$

4.5.3 Experimental

Noise spectra of bsa doped polypyrrole chemo-resistors prepared according to the standard recipe described in chapter 3 were determined. The chemo-resistors had a base-line resistance of approximately 2 kΩ. For the noise measurements the resistor was connected to a 10 V power supply, in series with a metal film resistance of 2 kΩ (the load resistor) according to Fig. 4.6. A spectrum analyser (HP3585A) combined with a low noise amplifier was used to monitor the potential over the sensor. The amplifier had a gain of 100, a bandwidth of 100 kHz and allowed for off-set compensation. The complete electrical set-up was shielded with aluminium foil to minimise external influences.

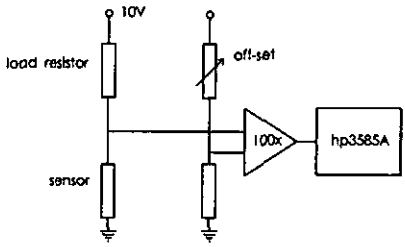

Fig. 4.6: Electrical configuration for noise measurements.

The noise behaviour of the measurement set-up without the chemo-resistor was also tested with a metal film dummy resistor of 2 kΩ in the place of the sensor.

4.5.4 Results and discussion

Dummy

Initially the noise behaviour of the measurement system was determined using a 2 kΩ dummy resistor. This gave a frequency independent noise of 1.3 μV/√Hz. The theoretical thermal noise of a 2 kΩ resistor is $4*k*T*R$ =3.3e-17 V^2/Hz. Together with the load resistor and 100 times amplified, this results in a noise of 100*√2*√3.3e-17= 0.8 μV/√Hz. The rest of the noise can be assigned to the amplifier and associated off-set regulation.

Chemo-resistors

The noise measurements were performed with a voltage of 5 V applied across the chemo-resistor. Although this is significantly greater then the normally used potential, the resistance was nevertheless stable over the period of the experiment. The recorded base-line resistance of the chemo-resistors, and the bias currents calculated, are summarised in Table 4.2.

Table 4.2: Overview of the characterisation conditions and the obtained nose parameters for the chemo-resistors and the dummy.

	I (mA)	R (kΩ)
sensor 1	2.3	2.4
sensor 2	2.4	2.1
dummy	2.5	2.0

The recorded noise spectra from the chemo-resistors are presented in Fig. 4.7 together with the system noise recorded with the dummy resistor. Because the noise recorded for the chemo-resistors was some orders of magnitude larger than the thermal noise of the amplifier and the load resistor, the contribution of the latter to the total noise can be neglected, and does not need to be compensated for.

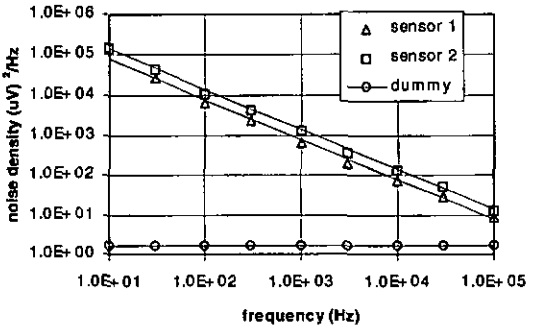

Fig. 4.7: The measured noise densities of two bsa doped ppy sensors and a dummy resistor.

It can be seen that the spectra of the chemo-resistors display a significant 1/f noise. In consequence the signal to noise ratio of the resistance measurements would be significantly improved through the use of AC rather than DC methods.

4.6 Temperature dependence

4.6.1 Introduction

The conductivity of most conducting materials displays a temperature dependence. In the case of a semiconductor material, the temperature dependence originates in both variations in the charge carrier concentration, and in the mobility of the charge carriers [7,11,14]. In the case of conducting polymers, where charge transfer between conducting regions also plays a role, the situation is even more complex. Several authors have successfully used the temperature dependence of the conductivity to characterise charge transfer between the different polymer chains [1,2,9,11,13].

A complete characterisation of the temperature dependence of the chemo-resistors requires specialised equipment, especially for the low temperature range, and falls outside the scope of this project. However, even in the temperature range employed in the flow system, temperature fluctuations may have an important impact. The limited temperature range does then allow a linear modelling [23], which is sufficient to describe the temperature influence in a practical nose system.

4.6.2 Experimental

Butane sulfonic acid doped polypyrrole sensors were mounted in a temperature controlled chamber filled with dry air. Their base-line resistance was recorded at different temperatures.

4.6.3 Results and discussion

Fig. 4.8 shows the resistance as a function of temperature. A temperature dependency of approximately -1%/°C was obtained.

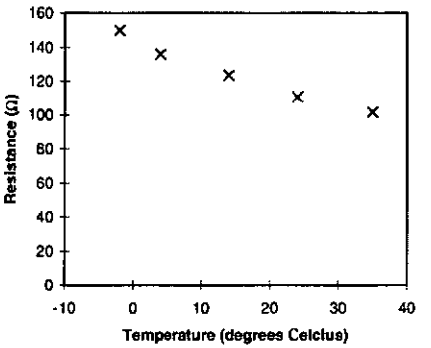

Fig. 4.8: Influence of temperature on the conductivity of the chemo-resistors.

Although these results are obtained over a too limited range to be conclusive, they give increasing conductivity with temperature, comparable with the variable range hopping model [20]. Despite the limited temperature range the results clearly show that temperature induced fluctuations can be significant and that attention to temperature variations should be made to avoid misleading odour responses.

4.7 Conclusions

In this chapter we have investigated several of the electrical characteristics of the chemo-resistors. This study has been motivated by the necessity of understanding which parameters need to be controlled for good measurements, and how the quality of the measurements may be improved. It has been shown that, over the experimental range investigated, AC measurements do not allow any increased information to be obtained, since the devices appear to act as ohmic resistors.

In the event of needing to improve the signal-to-noise performance, it was shown that AC measurements would lead to improved performance. Any frequency below 10 kHz would avoid any influence of the substrate capacitance. However this improvement was too marginal to justify the increased instrumental complexity in the present situation.

Similarly it was shown that 4-point measurements allow bulk and contact resistance to be separated, thus leading to improved performance, but again the improvement doesn't justify the increased complexity.

Perhaps, the most important result from this chapter is the temperature dependence of resistance. This dependence, approximately -1%/°C is large enough to impose a strong requirement on the temperature stability of the flow system.

4.8 References

1. S. Roth, H. Bleier and W. Pukacki, *Charge Transport in Conducting Polymers*, Faraday discuss. Chem. Soc., 88 (1989).
2. G. Wegner and J. Rühe, *The Structural Background of Charge-carrier Motion in Conducting Polymers*, Faraday Discuss. Chem. Soc. 88 (1989).
3. S.M. Sze, Semiconductor devices, physics and technology, Wiley & Sons, New York, 1985.
4. P. Bruschi, F. Cacialli, A. Nannini and Bruno Neri, *Gas and vapour effects on the resistance fluctuation spectra of conducting polymer thin film resistors*, Sensors and Actuators B18-19 (1994) 421-425.
5. R. Singh, R.P. Tandon, V.S. Panwar and S. Chandra, *Low-frequency ac conduction in lightly doped polypyrrole films*, J. Appl. Phys. 69 (1991) 2504-2511.
6. X.B. Chen, J. Devaux, J.-P. Issi and D. Billaud, *The Stability of Polypyrrole Electrical Conductivity*, Eur. Polym. J. 30 (1994) 809-811.
7. C.D. Lokhande, S.S. Kale, U.S. Jadhav and B.G. Wagh, *Studies on metal contact to polyaniline films*, Thin Solid Films 277 (1996) 5-6.
8. O. Inganäs and I. Lundström, *Electronic properties of metal/polypyrrole junctions*, Synthetic Metals 10 (1984/85) 5-12.
9. P.N. Bartlett, J.W. Gardner and R.G. Whitaker, *Electrochemical Deposition of Conducting Polymers onto Electronic Substrates for Sensor Applications*, Sensors and Actuators, A21-A23 (1990) 911-914.
10. F. Musio, M.E.H. Amrani and K.C. Persaud, *High-frequency a.c. investigation of conducting polymer gas sensors*, Sensors and Actuators, B 23 (1995) 223-226.
11. G. Heo, D.H. Lee and K.H. Kim, *Electropolymerization and Physicochemical Properties of Polypyrrole p-Toluenesulfonate*, Journal of Applied Polymer Science 54 (1994) 849-857.
12. A. Bhattacharya, A. De and S. Das, *Electrochemical preparation and study of transport properties of polypyrrole doped with unsaturated organic sulfonates*, Polymer, 37 (1996) 4375-4382.
13. A.J. Heeger, *Charge Transfer in Conducting Polymers*, Faraday Discuss. Chem. Soc. 88 (1989).
14. B. Sixou, N. Mermilliod and J.P. Travers, *Ageing effects on the transport properties in conducting polymer polypyrrole*, Physical Review B 53 (1996) 4509-4521.
15. P.D. Harris, W.M. Arnold, M.K. Andrews, and A.C. Partridge, *Resistance characteristics of conducting polymer films used in gas sensors*, Sensors and Actuators, B 42 (1997) 177-184.
16. A.C. Partridge, P. Harris and M.K. Andrews, High Sensitivity Conducting Polymer Sensors, *Analyst 121 (1996) 1349-1353.*
17. P. Bruschi, A. Nannini and B. Neri, *Vapour and gas sensing by noise measurements on polymeric balanced bridge microstructures*, Sensors and Actuators B 24-25 (1995) 429-432.

18. M.E.H. Amrani, K.C. Persaud and P.A. Payne, *High-frequency measurements of conducting polymers: development of a new technique for sensing volatile chemicals*, Meas. Sci. Technol. 6 (1995) 1500-1507.
19. H. Amrani, R.M. Dowdeswell, P.A. Payne and K.C. Persaud, *An intelligent gas sensing system*, Sensors and Actuators B44 (1997) 512-516.
20. P. Sheng, *Fluctuation-induced tunneling conduction in disordered materials*, Phys. Rev. B 21 (1980) 2180-2195.
21. J. Ouyang and Y. Li, *Enhancement of the electrical conductivity of polypyrrole films on applying higher voltage*, Synthetic Metals 75 (1995) 1-3.
22. A.F.P. van Putten, *Electronic measurement systems*, Prentice Hall, New York, 1988.
23. J.W. Gardner and P.N. Bartlett, *Application of conducting polymer technology in microsystems*, Sensors and Actuators A51 (1995) 57-66.

5 GASFETs

The work described in this chapter has been done in collaboration with Jan Hendrikse from the MESA research institute at the University of Twente (the Netherlands). Parts of it have been presented at CIMTEC'98 [1] and other parts have been published in 'Electrochemical and Solid-State Letters' [2]. Reproduced by permission of The Electrochemical Society, Inc.

5.1 Introduction

5.1.1 General

With the invention of the GASFET in 1975 by Lundström et al. [3], a new type of gas sensors was introduced. After intensive study, the functional behaviour of the hydrogen sensing device proved to be based on a surface modification on the metal-insulator interface[4].
The later development of the suspended gate Field Effect Transistor by Janata allowed work function measurements on different types of materials. With different coatings on the suspended metal electrode directly above an insulted gate, it could be used to measure both variations in the bulk component [5] and in the surface component [6] of the work function. A hybrid technology, allowing for more general coating materials on a similar type of device was published by Flietner et al.[7].
Recently some papers demonstrated that it is also possible to make a gas sensitive device by application of a conducting polymer directly on the gate area [8-12]. Not only does this make the device simpler, it also largely eliminates the surface contribution of the work function changes, which makes the device not only interesting as sensor, but also useful as a tool for studying vapour interactions in the bulk of the polymer.

5.1.2 Outline

After a theoretical section which models the gas behaviour of GASFETs based on well known doping processes in semiconductors [13], this chapter describes the realisation and characterisation of GASFETs having a conducting polymer gate contact. Three different gate materials were used, electrodeposited polypyrrole, doped with bsa or teatfb and dip-coated polyaniline. Experimental data obtained using vapours from several solvents is compared with the model.
Finally the sensors are demonstrated in electronic nose applications, where they were successfully used for the recognition of 4 organic vapours and 4 Swiss cheeses.

5.2 Theory of operation: a simple model

5.2.1 Introduction

This section describes the modelling of a FET having a conducting polymer gate contact. This forms a special type of Insulated-Gate Field-Effect Transistor (IGFET) [13]. The general electrical behaviour of an IGFET is summarised in section 5.2.2, followed, in section 5.2.3, by a brief summary about the related concepts work function and Fermi level.
A model of the gas dependent behaviour of the bulk of the polymer is derived from the doping level of the conducting polymer [14] in section 5.2.4. For the derivation, the doping level is assumed to depend linearly on the fraction of occupied sorption sites, which in turn is assumed to relate to the gas concentration according to a Langmuir sorption isotherm. This Langmuir assumption is justified by the thin nature of the films (see also chapter 6).
Additional to any changes of the work function, the device can also give a response to dipole effects of sorbed gases [6,14]. Although this secondary effect may explain some of the features observed, it is not however expected to be the main mechanism [15] and is not included in the model.

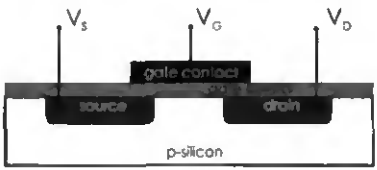

Fig. 5.1: Schematic drawing of an IGFET.

5.2.2 IGFETs and their electrical behaviour.

An IGFET (Fig. 5.1) is a three terminal device in which the current between two terminals, from the drain to the source, can be regulated by the potential applied to the third, the gate, which is isolated from the first two. The general term IGFETs can be used for several specific configurations, such as MOSFETs [13,16] with a metal gate contact for electronic applications, ISFETs where the electrolyte is the gate contact for pH measurements [17], or CHEMFETs where there is a chemically active layer, which can be contacted by an electrolyte [18].
The drain current for an n-channel device is given by equation (5.1).

$$I_D = \frac{K}{2} \cdot \left(2 \cdot V_D \cdot (V_G - V_T) - {V_D}^2\right) \qquad (V_D \le V_G - V_T) \qquad (5.1a)$$

$$I_D = \frac{K}{2} \cdot (V_G - V_T)^2 \qquad (V_D \ge V_G - V_T) \qquad (5.1b)$$

K is a factor depending on the dimensions and material properties of the transistor, V_D and V_G are the voltages applied to respectively the drain and the gate (Fig. 5.1). The source is connected to ground. V_T , the so called threshold voltage, is the voltage required to open a conduction channel between the drain and the source. It depends on the physical and process parameters Q, C_{ox}, ϕ_p, ε_s, N_a, X, q and E_g, which are constant for a given transistor, and the work function of the gate material Φ_{gate} (5.2).

$$V_T = \Phi_{GS} - \frac{Q}{C_{ox}} + 2\left|\phi_p\right| + \frac{1}{C_{ox}}\sqrt{2\varepsilon_s q N_a \left(2\left|\phi_p\right|\right)} \qquad (5.2a)$$

$$\Phi_{GS} = \Phi_{gate} - X - \frac{E_g}{2q} - \phi_p \qquad (5.2b)$$

5.2.3 Work function vs. Fermi level

The work function is the amount of energy required to remove an electron from the bulk of a material and bring it to the vacuum energy level [19]. Since an electron has a fixed amount of charge, the work function of a material can also be expressed as the potential relative to vacuum [13,16,20], instead of the energy. In a semiconductor material, where there is a statistical distribution of energy states, the work function is replaced by the Fermi level, which is the energy level corresponding to a 50% chance of occupation [13].
The Fermi level of a semiconducting material is dependent on the doping concentration. Through this doping, the electrons become more or less tightly bound to the material, resulting in mobile holes or electrons. In the case of polypyrrole, the Fermi level is dependent on the oxidation state and on any additional doping due to charge transfer with sorbed species.
A traditional way of measuring work function is with a Kelvin probe. Recently, IGFET structures have been shown to function as a convenient alternative [19].

5.2.4 Electrochemical potential and the influence of sorbed gas

Oxidised polypyrrole is a p-type conducting polymer (see also chapter 3). When the polymer backbone is oxidised, it becomes conductive due to the formation of mobile electron holes. The positive charge is compensated by a negative counter ion [21], which can also be called a doping ion. In silicon semiconductors, the doping ion itself is, by its low binding energy, the cause of the spontaneous hole generation at sufficiently high temperatures [13].
Despite the differences in origin of the charge carriers between polypyrrole and silicon, in both cases the charge carrier densities are considered to relate to energy levels [13,14] according to equation (5.3). The energy difference between the Fermi level E_f and the top level of the valence band

E_v depends on the doping concentration p, the effective state density N_v, Bolzmann's constant k_B and the absolute temperature T.

$$E_f - E_v = -k_B T \cdot \ln\left(\frac{p}{N_v}\right) \tag{5.3}$$

Additional to an initial doping concentration imposed by the oxidation state of the polymer, a deviation in doping density due to gas interaction can occur [14,22]. The fraction of occupied sites <*gas*> is assumed to change the total doping concentration p linearly with a proportionality factor L according to (5.4).

$$p = p_0 + L \cdot < gas > \tag{5.4}$$

Where p_0 is the doping concentration before gas interaction. The factor L can be positive or negative, depending on whether the electron affinity of the gas is higher (oxidising so positive) or lower (reducing so negative) than that of the polymer.

The absolute Fermi level of the polymer can be an interesting property for the comparison of polymers prepared under different conditions. It can be obtained by comparing the threshold voltage of a polymer coated transistor with the threshold voltage of a MOSFET having a known Fermi level. For this purpose, a MOSFET has to be prepared in the same fabrication process as the sensor substrates, to assure identical transistor parameters.

For gas sorption characterisation however, it is the change in Fermi level due to gas interaction which is important. Equation (5.3) is therefore converted to (5.5).

$$\Delta E_f = k_B T \cdot \left(\ln\left(\frac{p_0}{N_v}\right) - \ln\left(\frac{p}{N_v}\right)\right) \tag{5.5a}$$

$$\Delta E_f = k_B T \cdot \ln\left(\frac{p_0}{p}\right) \tag{5.5b}$$

With equation (5.6), which relates the Fermi level to the potential of the semiconducting polymer Φ_P and the elementary charge q, equation (5.5) can be converted to equation (5.7) which shows the change in polymer potential $\Delta\Phi_P$, depending logarithmically on the ratio of the total doping concentration and the initial doping concentration.

$$E_f = -q \cdot \Phi_P \tag{5.6}$$

$$\Delta\Phi_P = \frac{k_B T}{q} \cdot \ln\left(\frac{p}{p_0}\right) \tag{5.7}$$

Equation (5.8) is obtained by substituting equation (5.4) into equation (5.7).

$$\Delta\Phi_P = \frac{k_B T}{q} \cdot \ln\left(\frac{p_0 + L \cdot < gas >}{p_0}\right) \tag{5.8}$$

The site occupancy is assumed to follow a Langmuir isotherm (chapter 6), according to equation (5.9).

$$< Gas >= \frac{k \cdot [gas]}{1 + k \cdot [gas]} \tag{5.9}$$

Where $[gas]$ is the gas concentration in the air, k is the sorption constant which is the ratio between the sorption and de-sorption rate constants. Combining (5.8) and (5.9) results in (5.10).

$$\Delta\Phi_P = \frac{k_B T}{q} \ln\left(1 + \frac{L}{p_0} \cdot \frac{k \cdot [gas]}{1 + k \cdot [gas]}\right) \tag{5.10}$$

Equation (5.10) can be simplified to (5.11).

$$\Delta\Phi_P = \frac{k_B T}{q} \ln\left(1 + B \cdot \frac{k \cdot [gas]}{1 + k \cdot [gas]}\right) \tag{5.11}$$

B is the dimensionless constant of the combination of L and p_0. Because a negative effective doping concentration p (5.4) would mean electron conductivity in the polymer, which cannot occur for polypyrrole, B should always be larger then -1.

5.2.5 The model

The model described above is the result of an attempt to include the sorption behaviour in the work function response. The final equation (5.11) can be generalised to equation (5.12). A summary of the meaning of the variables in the derived model is given below.

$$\Delta\Phi = A \cdot \log\left(1 + B \cdot \frac{k \cdot [gas]}{1 + k \cdot [gas]}\right) \tag{5.12}$$

k: Ratio between sorption and de-sorption rates. Determines the amount of sorbed gas in a polymer in equilibrium with a certain gas concentration. The variable k is always positive.

A: Slope of the logarithmic relation between the potential and the doping concentration. It is comparable with the slope of the Nernst equation [23]. The variable A has a value of RT/nF which gives 59 mV for a single electron transfer.

B: The proportionality parameter relating the concentration of sorbed gas to the doping concentration change. It is negative for reducing species, and positive for oxidising species. The value of B should be larger then -1.

5.3 Fabrication

5.3.1 Silicon substrate

The GASFETs (Fig. 5.2) were realised on a FET substrate without a gate contact, but with the gate area surrounded by a Pt electrode. The same type of structure has been previously used as an integrated sensor actuator system, where the Pt film was used as a pH actuator. Details of the fabrication can be found in the articles related to this structure [24]. The gate area of the FET is 15 µm long and 500 µm wide. The surrounding Pt electrode has a 20 µm wide slot which leaves the gate exposed.

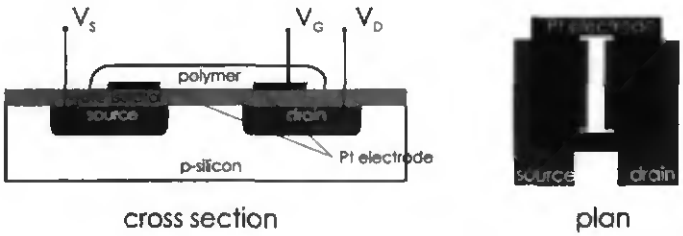

Fig. 5.2: Schematic drawing of the GASFET. (For clarity the polymer is not shown in the plan).

The structures were mounted on a PCB, wire-bonded and encapsulated with epoxy resin.

5.3.2 Deposition

Electrochemical

Conducting polymers were electrochemically deposited over the gate area. Before each deposition, the platinum electrodes were pre-treated by cyclic voltammetry in 1.0 M H_2SO_4 as follows: four sweeps at 100 mV/s, with the first and the last being over the range -0.2 to 1.2 V vs. SCE, whilst for the middle two the anodic limit was increased to 2.0 V. Pyrrole was

purified by passage down a neutral aluminium oxide column immediately before use. Polypyrrole (ppy) films were electrodeposited from 0.1 M pyrrole monomer dissolved in either a 0.1 M aqueous butane sulfonic acid (bsa) solution or in dry acetonitrile containing 0.1 M tetraethylammonium tetrafluoroborate (teatfb). The deposition was performed using a potentiostatic pulse train. In the case of the non-aqueous electrolyte this consisted of 2 s long 1.5 V vs. SCE pulses, separated by 5 s at 0.0 V, whilst in the aqueous electrolyte the pulses were 0.5 s at 1.1 V separated by 5 s at 0.0 V. The pulse train was applied until the required charge was passed, which was 8 mC for aqueous bsa and 6 mC for teatfb in acetonitrile, which corresponds to 8 and 6 mC/mm^2 respectively. All chemicals used were obtained from Aldrich.

Dip-coating

In the case of dip-coating, an already encapsulated FET structure was dipped in pure ORMECON 9000132 polyaniline dispersion (Ormecon Chemie, GmbH & Co. KG, Ferdinand-Harten-Strasse 7, D-22949 Ammersbek, Germany). The coated structure was then left for 1 hour at room temperature to dry, followed by baking for 1 hour at 100° C. This procedure resulted in a relatively thick film.

5.3.3 **Resulting structures**

The bsa doped films displayed good adhesion, whilst the teatfb doped films showed a limited adhesion to the underlying metal. With careful handling both types could be used for gas measurements. Although no effort has yet been made to optimise the adhesion, it is believed that it can be improved by, for example, modification of the metal surface or of the pulse sequence.

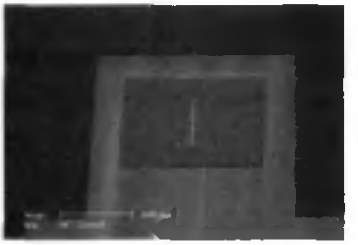

Fig. 5.3: SEM photo of the active area of a finished structure with a bsa doped ppy film..

Fig. 5.3 shows a SEM picture of a finished device. In Fig. 5.4, which is a zoom on the top end of the gate area, it can be observed that the polymer deposits not only on the metal electrode, but that it also spreads out and completely covers the gate area.

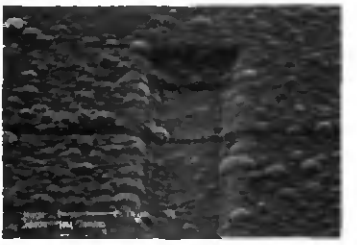

Fig. 5.4: A SEM photograph showing the edge of the gate. The different layers of the transistor passivation outside the transistor gate and the metal electrode are clearly visible.

The lateral growth, which is essential to obtain functioning structures can be clearly observed in Fig. 5.5. This SEM image shows a magnification of the edge of the platinum electrode. On the right hand side the lateral spread-out of the ppy on the substrate can be observed.

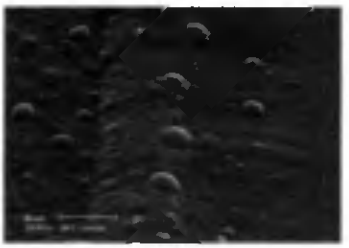

Fig. 5.5: An enlargement of the edge of the polymer coverage on the edge of the metal electrode.

Before deposition of the polymers, the feedback-loop of the FET amplifier did not stabilise, showing that the Pt electrode is sufficiently far from the gate area to prevent interference with the work function measurement. In contrast, after deposition of the polymer, a stable threshold voltage representative for the polymer work function could be measured, indicating the correct functioning of the polymer film as a gate contact.
The resulting structures were not only used for GASFET applications described in the following section, but were also successfully used as ^{E}mosfets [20].

5.4 Characterisation of vapour response

5.4.1 Experimental

The realised GASFETs were mounted in the flow system (chapter 2) and connected to a FET amplifier to measure the work function of the polymer due to gas interactions, which is equal to the shift in V_T (equation 5.2). The current was set at 100 μA, and V_{DS} was set at 0.2 Volt. The gate was connected to ground, so the work function changes (equation 5.12) could thus be directly obtained from the measured V_S in the feedback loop of the amplifier. All characterisations were performed at 25°C.

Vapour characterisation

The sensors were exposed to 5 minutes pulses of water, methanol, ethanol, isopropanol and acetonitrile vapours at various concentrations, separated by a 1.5 hour purge with a dry air stream at a flow rate of 1 l/min.

Odour recognition with cheese

When applied to chemo-resistors, the polymer materials used have proven to give a good distinction between various swiss cheeses [25]. To demonstrate the feasibility of an electronic nose with FET-based sensors, an array of FETs, of the three different types realised, was exposed to different samples of Swiss cheese. Samples of Gruyere, Emmentaler, Roquefort and Tilsiter were freshly purchased from the local CO-OP supermarket. Wash bottles were filled with 50 grams of freshly grated cheese.
The cheese measurements were performed under 2 humidity conditions. Under fully wet conditions 5 ml water was added to all the samples and the carrier humidity was kept at 100%, using a wash bottle filled with water upstream of the two mass flow controllers (Fig. 2.3).

In a second series, no water was added to the cheese, and the carrier was kept at 29% rel. hum. using a wash bottle filled with an aqueous $CaCl_2$ (sat.) solution placed upstream of the two mass flow controllers.
Together with the cheese samples, a water sample was tested, to estimate the influence of humidity on the recognition. In the second series, this sample was also diluted with the 29% carrier stream to result in a sample with a humidity of 65%. For all the experiments the flow rate of the nose was set at 0.5 l/min instead of the usual flow of 1 l/min, to minimise the composition changes in the sample headspace.

5.4.2 Vapour responses

All three types of FET based sensor showed responses to the applied test vapours. Depending on the vapour, two types of response peaks could be distinguished. The first type of response is a simple on-off curve and the second a more complex multi-phasic curve. To illustrate this, the two typical response types are shown in Fig. 5.6.

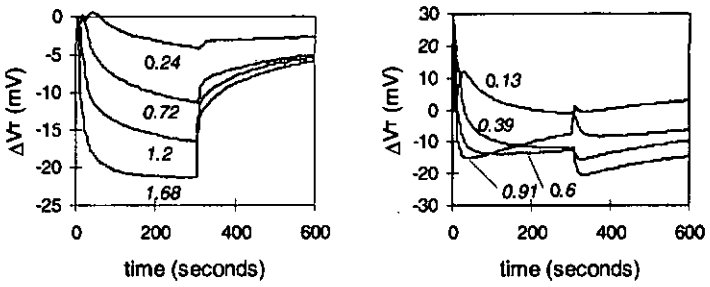

Fig. 5.6: Response curves of the teatfb doped polypyrrole sensor for different concentrations of isopropanol (left) and water (right). Vapour concentrations in mmol/l are shown in italics on the graphs.

The threshold voltage shifts after 300 s were plotted against the vapour concentration to result in the calibration curves shown in Fig. 5.7 - Fig. 5.9. Simple, continuously rising or descending curves are

seen for ethanol, isopropanol and acetonitrile, whilst for water and methanol more complex curves were obtained.

The continuously rising calibration curves result from the on-off type of response curves (left-hand plot of Fig. 5.6). The more complex calibration curves result from the two-phasic response curves (right-hand plot of Fig. 5.6). These are thought to stem from another process additional to work function changes, possibly a dipole effect on the polymer-gate interface [14,15].

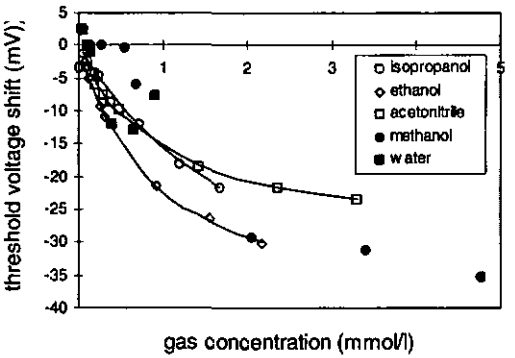

Fig. 5.7: Calibration curves of the teatfb doped polypyrrole GASFET.

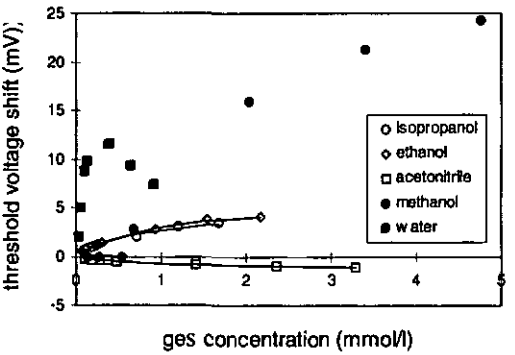

Fig. 5.8: Calibration curves of the bsa doped polypyrrole GASFET.

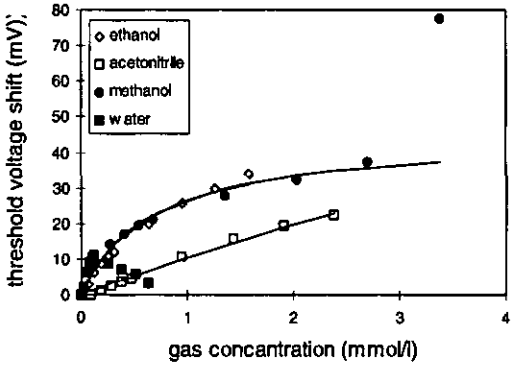

Fig. 5.9: Calibration curves of the polyaniline GASFET.

Curve fitting

Also shown in Fig. 5.7 - Fig. 5.9 are the fits of the continuously rising responses to equation (5.12). The parameters resulting from these fits are collected in Table 5.1.

Table 5.1: Summary of the parameters obtained from the fits to equation (5.12).

		A (mV)	B	k (l/mmol)
teatfb doped polypyrrole	isopropanol	241	-0.39	0.59
	ethanol	280	-0.29	1.32
	acetonitrile	187	-0.31	1.39
bsa doped polypyrrole	isopropanol	80	0.16	1.1
	ethanol	87	0.17	0.96
	acetonitrile	43	-0.07	1.14
polyaniline	ethanol	301	0.56	0.69
	acetonitrile	551	1.0	0.047
	methanol	257	0.49	1.23

Because of the limited amount of data available care must be taken with the interpretation of the data resulting from the fits. Nevertheless some

observations can be made. The bsa doped polymer shows an *A* value in the same order of magnitude then the 59 mV for complete electron transfer. The polyaniline and the teatfb doped polypyrrole show much larger *A* values than the bsa doped polypyrrole. This suggests a partial electron transfer [15,22].

Selective recognition of vapours

To demonstrate the suitability of these sensors for use in an electronic nose system, the calibration curves for 5 GASFETs of the 3 types described (2 of each polypyrrole GASFETs and 1 polyaniline GASFET), were combined and projected onto a two-dimensional space using principle component analysis (Fig. 5.10). This figure shows that different vapours, starting from a common 'zero point' follow a distinct trajectory through the projection, allowing such a system, at least for these simple vapours, to be used to obtain information about species and concentration.

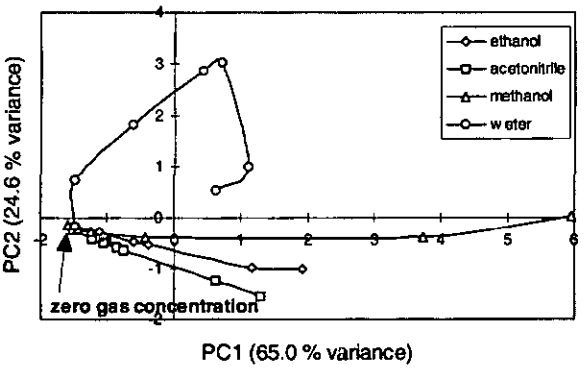

Fig. 5.10: PCA plot of the threshold voltage shift after 300 s of several concentrations of the different vapours. Vapour concentrations corresponding to dilution of 10, 20, 30, 40, 50 and 60% of the vapour pressure.

5.4.3 Cheese recognition.

Under fully wet conditions poor results were obtained. Although initially the cheeses could be distinguished, the performance of the system rapidly deteriorated. This is caused by the rapid spoiling of the cheese under wetted conditions at 25 °C. Also for the human nose, the spoiled cheeses smelled very similar when they were disposed of after the experiment.
With a 29% rel. hum. carrier, and no water added to the samples, better results were obtained. Fig. 5.11 shows a PCA plot of the first two components.

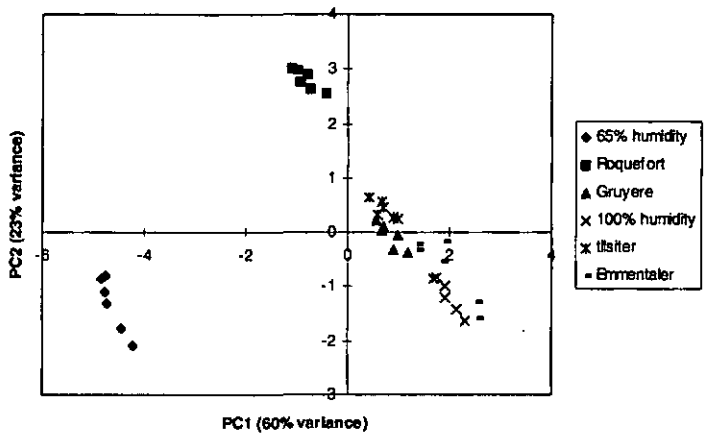

Fig. 5.11: Principle component analysis of normalised data of 3 sensors.

The Roquefort can clearly be distinguished from the other 3 types of cheeses which were all typically Swiss hard cheeses. With exception of the Emmentaler, which gives unstable results, the hard cheeses can be distinguished in their individual groups. It is interesting to note that the water controls appear to fall on a line almost perpendicular to the cheeses, suggesting that the separation of the cheeses is not due to humidity.

5.5 Conclusions

GASFETs with a conducting polymer gate contact have been realised. The lateral growth of the pyrrole in a standard electrodeposition was great enough to cover a gate area surrounded by a platinum contact electrode.
The realised devices were characterised with several test vapours at different concentrations. A reversible sensor signal was obtained. For several of the vapours the gas-response characteristics of the GASFETs could be fitted to a simple model based on a Langmuir isotherm.
The devices have been demonstrated as sensors in an electronic nose set-up. A PCA of the responses of a set of 5 of these sensors allows the various concentrations of 4 different solvents as well as a series of Swiss cheeses to be distinguished. The experiments with the cheese showed that adding water to the samples is not a suitable method to suppress any humidity influences, since it stimulates spoiling making odour characterisation impossible.

5.6 References

1. M.G.H. Meijerink, M. Koudelka-Hep, N.F. de Rooij, D.J. Strike, J. Hendrikse, W. Olthuis and P. Bergveld, *Gas sensing with a conducting polymer on an isolated gate field effect transistor*, 9th CIMTEC Conference, abstract SIX-1:P25, Florence, Italy (1998).
2. M.G.H. Meijerink, M. Koudelka-Hep, N.F. de Rooij, D.J. Strike, J. Hendrikse, W. Olthuis and P. Bergveld, *Gas-Dependent Field Effect Transistor with an Electrodeposited Conducting Polymer Gate Contact*, Electrochemical and Solid-State Letters 2 (1999) 138-139.
3. K.I. Lundström, M.S. Shivaraman and C.M. Svensson, *A hydrogen-sensitive Pd-gate MOS transistor*, J. Appl. Phys. 46 (1975) 3876.
4. I. Lundström, C. Svensson, A. Spetz, H. Sundgren and F. Winquist, *From hydrogen sensors to olfactory images - twenty years with catalytic field-effect devices*, Sensors and Actuators B13-14 (1993) 16-23.
5. M. Josowicz and J. Janata, *Suspended Gate Field Effect Transistor Modified with polypyrrole as Alcohol Sensor*, Anal. Chem. 58 (1986) 514-517.
6. G.F. Blackburn, M. Levy and J. Janata, *Field-effect transistor sensitive to dipolar molecules*, Appl. Phys. Lett. 43 (1983).
7. B. Flietner, T. Doll, J Lechner, M. Leu and I. Eisele, *Reliable hybrid GasFETs for work-function measurements with arbitrary materials*, Sensors and Actuators B22 (1994) 109.
8. M. Liess, D. Chinn, D. Petelenz and J. Janata, *Properties of insulated gate field-effect transistors with a polyaniline gate electrode*, Thin solid films 286 (1996) 252-255.
9. J.V. Hatfield and K.S. Chai, *A Conducting Polymer GasFET*, Eurosensors XI conference proceedings (739-742).
10. J.V. Hatfield, J.A. Covington and J.W. Gardner, Chemical Sensors Conference, abstract 707, China (1998).
11. K. Domansky, J. Li and J. Janata, *Selective Doping of Chemically Sensitive Layers on a Multisensing Chip*, J. Electrochem. Soc. 144 (1997) L75.
12. V. Meister and K Potje-Kamloth, *Polymer-Oxide-Silicon-Field-Effect-Transistor (POSFET) as sensor for Gases and Vapors*, Joint ECS, ICE meeting, Paris 1997, abstract 672.
13. S.M Sze, Semiconductor Devices, Physics and Technology, Wiley & Sons, New York, 1985.
14. J. Janata, *Chemical Modulation of the Electron Work Function*, Anal. Chem. 63 (1991) 2546-2550.
15. D. Blackwood and M. Josowicz, *Work Function and Spectroscopic Studies of Interactions between Conducting Polymers and Organic Vapors*, J. Phys. Chem 95 (1991) 493-502.
16. R.S. Muller and T.I. Kamins, Device electronics for integrated circuits, Wiley & Sons, New York, 1977.
17. P. Bergveld, IEEE Trans. Biomed. Eng., BME-17 (1970) 70.
18. P. van der Wal, *The development of a durable potassium sensor based on fet-technology*, Ph.D. Thesis, University of Twente, Enschede, 1991.

19. J. Janata and M. Josowicz, *A Fresh Look at Some Old Principles: The Kelvin Probe and the Nernst Equation*, Anal. Chem. 69 (1997) 293A.
20. J. Hendrikse, *The EMOSFET, A potentiometric transducer based on chemically induced work function changes of electrochemically active films*, Ph.D. Thesis, University of Twente, the Netherlands, 1998.
21. M. Josowicz, *Applications of Conducting Polymers in Potentiometric Sensors*, Analyst 120 (1995) 1019-1024.
22. J. Janata and M. Josowicz, *Nernstian and non-nernstian potentiometry*, Solid State Ionics 94 (1997) 209-215.
23. A.J. Bard and L.R. Faulkner, Electrochemical methods, fundamentals and applications, Wiley & Sons, New York, 1980.
24. B.H. van der Schoot, *Coulometric sensors, Integration of a chemical sensor-actuator system*, Ph.D. Thesis, University of Twente, the Netherlands, 1986.
25. D.J. Strike, *Unpublished results.*

6 Response modelling

6.1 Introduction

6.1.1 General

The study of a theoretical model of the behaviour of a sensor often allows to improve understanding of the functional behaviour of the device, and can therefore be a valuable tool for sensor development. In the case of gas sensors in an electronic nose system, a model can furthermore be useful for an improved feature extraction from the transient sensor response [1]. Multiple authors report attempts to describe the behaviour of conducting polymer based sensors with a mathematical formula [2-4]. Most of these publications are however limited to the plateau value of the response. In this chapter a transient model for conducting polymer responses will be derived, and verified with experimental data obtained from both chemo-resistors and a Quartz Crystal Microbalance (QCM).

6.1.2 Conduction modulation due to vapour interaction

The interaction between conducting polymers and vapours is a complicated issue, and the exact mechanism of the response remains unclear. It is likely that there is not one single mechanism of operation, but several, possibly acting in different directions.

The main mechanism is believed to be partial electron transfer [5,6] between conducting polymers and the vapour (see also chapter 5). Other proposed mechanisms include swelling [7] and interface effects [8]. It is also possible that some of the observed features, such as history effects result from the displacement or interaction of the sample vapour with already sorbed environmental species. Such effects are reported for metal oxide sensors [9]. Table 6.1 gives a short summary of the mechanisms which are generally accepted as the dominant. The vapour sensitivity in

most polymers is likely to be a combination of two or more of the proposed mechanisms.

Table 6.1: Interactions between vapours and conducting polymers.

1	(partial) electron charge transfer
2	swelling
3	interaction at the metal/polymer interface
4	modulation of sorbed environmental gas

To begin its interaction with the polymer, a gaseous species must sorb [10]. The sorbed vapour then eventually diffuses further into the polymer to interact in the whole volume of the polymer. The sorption process and the spatially devised interaction with the polymer then combine to a variant of the classical problem of combined diffusion and chemical reaction [11]. Gardner et al. [4,12] used this approach to calculate sorption profiles in the polymer under different boundary conditions of diffusion and sorption. Bartlett et al. [3] have demonstrated that the experimentally determined saturation-values of conducting polymer chemo-resistor responses could best be described by a model based on a Langmuir sorption isotherm. This implies that diffusion is fast enough to be disregarded. This then reduces the issue to a problem of vapour sorption.

6.1.3 Outline

This chapter starts with the derivation of a theoretical model for the sensor response in section 2. In section 3, the sorption behaviour will be verified with a Quartz Crystal Microbalance. Section 4 compares the model to experimental chemo-resistor data. This is then expanded to the case of two-phasic responses in section 5. Section 6 finally discusses the temperature dependence of the chemo-resistor response in relation to the sorption theory.

6.2 Sorption theory

6.2.1 Introduction

Depending on the boundary conditions and simplifying assumptions taken, sorption can be described with several mathematical models. The simplest model, the Langmuir isotherm, is based on the assumption of a fixed amount of sorption sites in the solid material, which are all freely exposed to the gas, and do not interact with each other. Other models like the Temkin isotherm and the Freundlich isotherm account for a change in adsorption enthalpy with the pressure, using a linear and a logarithmic function respectively [13]. Models can furthermore be completed by accounting for the influence of diffusion [4].
In this chapter, the simplest isotherm, the Langmuir isotherm, will be used. Although in reality the situation will be more complex, it is desirable to begin with the simplest model, to obtain a minimum number of parameters (degrees of freedom) in the fitting procedure. Where this results in errors, this will be pointed out.

6.2.2 Langmuir isotherm [13]

According to a Langmuir isotherm, the sorption state is defined by the dynamic equilibrium [4,13] between sorption (6.1) and de-sorption (6.2).

$$[Gas] + < Site > \xrightarrow{k_a} < Gas > \tag{6.1}$$

$$< Gas > \xrightarrow{k_d} [Gas] + < Site > \tag{6.2}$$

k_a:	forward reaction rate	[m^3/s.mol]
k_d:	backward reaction rate	[1/s]
[*Gas*]:	gas concentration in the air	[mol/m^3]
<*Site*>:	concentration of empty sites	[1/m^3]
<*Gas*>:	concentration of occupied sites	[1/m^3]

When the sorption process is redefined with a parametcr representing the fraction of occupied sites θ=<*gas*>/(<*site*>+<*gas*>), a differential equation (6.3) for the state of the process can be defined.

$$\frac{\delta\theta}{\delta t} = k_a \cdot [Gas] \cdot (1-\theta) - k_d \cdot \theta \tag{6.3}$$

The solution of this differential equation with the boundary condition $\theta(0)=0$ (i.e. initially no sorbed gas) is given in (6.4).

$$\theta(t) = \left(\frac{1}{1+K}\right) \cdot \left(1 - e^{-kt}\right) \tag{6.4}$$

Where the constants K and k are defined as :

$$K = \frac{k_d}{k_a \cdot [Gas]} \tag{6.5}$$

$$k = k_a \cdot [Gas] + k_d \tag{6.6}$$

If the gas concentration is assumed to be 0 during de-sorption, only (6.2) has to be taken into account, which results in a 0 value for the first term of (6.3). The solution of the differential equation (6.3) is in that case given by (6.7).

$$\theta(t) = \theta(0) \cdot e^{-k_d \cdot t} \tag{6.7}$$

The equations (6.4) and (6.7) can be combined (6.8) to model the site occupation caused by a step in gas concentration [*Gas*] from $t_0<t<t_1$ under the condition of a constant temperature.

$$\theta(t) = \begin{cases} \frac{1}{1+K} \cdot \left(1 - e^{-k \cdot t}\right) & t_0 \le t \le t_1 \\ \theta(t_1) \cdot e^{-k_d \cdot (t - t_1)} & t_1 < t \end{cases} \qquad (6.8)$$

t_0: start sample

t_1: switch back to carrier

6.2.3 Drift compensation

Conducting polymer chemo-resistors inevitably show some drift [14,15]. There is a slow increase in base-line resistance, likely due to oxidation of the polymer in contact with the ambient air [16]. Normalisation can eliminate a large part of this drift, but not all. This results in an incomplete recovery of the base-line after vapour exposure.

For some vapours, a drift in the inverse direction is observed, as an undershoot of the response when the sensors are purged with the carrier [16]. This might be caused by either the facilitation of the removal of residual vapours from previous exposures, or by a reducing effect of the vapour, dependent on the vapour and the polymer.

Because of the small amplitudes of the drift, it can to a first approximation be considered linear, and is in the model described by equation (6.9).

$$drift = a \cdot t \qquad (6.9)$$

Where a is a rate constant [1/s], t is the time from the start of the exposure, and *drift* is the dimensionless drift added to the response caused by the vapour influence (equation 6.8).

6.2.4 Mass changes

For the derived model to be applied to mass changes of the polymer due to sorption, the fraction of occupied sites has to be converted to mass according to equation (6.10).

$$M = A \cdot \theta \tag{6.10}$$

The variable A represents a constant corresponding to the product the molecular mass of the gas, and the total amount of sites. The mass increase due to sorption is described by (6.11).

$$M(t) = \begin{cases} \dfrac{A}{1+K} \cdot \left(1 - e^{-k \cdot t}\right) & t_0 \le t \le t_1 \\ M(t_1) \cdot e^{-k_d \cdot (t - t_1)} & t_1 < t \end{cases} \tag{6.11}$$

6.2.5 Resistance changes.

Assuming a relative resistance change proportional to the amount of sorbed gas (6.12), the sorption model can also be used to describe a resistance change according to equation (6.13).

$$\frac{\Delta R}{R} = B \cdot \theta \tag{6.12}$$

$$\frac{\Delta R}{R}(t) = \begin{cases} \dfrac{B}{1+K} \cdot \left(1 - e^{-k \cdot t}\right) & t_0 \le t \le t_1 \\ \dfrac{\Delta R}{R}(t_1) \cdot e^{-k_d \cdot (t - t_1)} & t_1 < t \end{cases} \tag{6.13}$$

The dimensionless variable B represents the relative resistance change per occupied site ratio. The chemo-resistor drift can eventually be modelled by adding a term $a \cdot t$ according to equation (6.9) to both terms of equation (6.13).

6.2.6 Fitting of the lumped or the physical parameters

For the fit of the model to the experimental data, two different strategies are possible. The first possibility is a direct fit of the parameters k_d, k_a, and B to the transient response curve (6.13) after substitution of equation (6.5) and (6.6). A second possibility is a fit with the lumped parameters $B/(1+K)$ and k, which represent an amplitude - and time constant, to equation (6.13). In both cases the de-sorption constant k_d is obtained directly from the decay curves. The fits can furthermore eventually be complemented with a drift component a.

The first method has the advantage that the physical parameters are unambiguously defined when the fit is successful. A disadvantage of this method is the appearance of the parameters k_d and k_a in both the amplitude constant D and the time constant k of the exponential curve. This requires more calculation during the iterations and can cause convergence problems.

The lumped parameter fit, with one amplitude - and one time constant, needs less calculation during the iteration. However, the post-extraction of k_d and k_a from the in this case obtained constants D and k can give inconsistent results which can be difficult to interpret.

For the QCM experiments the 'lumped parameter fit' was used. For the chemo-resistors both methods were evaluated.

6.3 Quartz Crystal Microbalance

6.3.1 Introduction

A Quartz Crystal Microbalance (QCM) is an instrument which allows mass changes to be detected by means of the change in the oscillation frequency of a quartz crystal. It is commonly used for the control of the layer thickness in metal evaporation apparatus. When the crystals are coated with a polymer, they can act as detectors for gas sorption [17] and have already found application in electronic nose systems [18-22]. Here the QCM will be used, not as an electronic nose element directly, but as a second, independent measure of the gas sorption. As such it will allow the effects of gas sorption to be measured, independent from electronic effects which will later be measured with the chemo-resistors.

6.3.2 Experimental

QCM experiments were performed at the department of Inorganic, Analytical and Applied Chemistry of the University of Geneva. The microbalance employed 5 MHz AT-cut crystals having a mass sensitivity of 18.5 ng/Hz. The oscillation frequency was measured with a frequency counter which was connected to a personal computer to allow the transient response of the crystals to be recorded during gas exposures. Initially, the sampling time was 5 s, but this was later decreased to 2.5 seconds to obtain a better resolution of the transients.

Deposition

Butane sulfonic acid doped polypyrrole was deposited on the gold electrodes of the crystals by electrochemical deposition according to the standard recipe (chapter 3). During deposition, the contact areas of the crystal were protected by scotch tape. After deposition this was peeled off, leading to crystals coated only on the 0.38 cm^2 central area. Depositions

were performed with a total charge of 30 or 40 mC corresponding to 0.79 or 1.05 mC/mm^2 respectively, which is relatively low compared to the chemo-resistors.

Gas exposures

The resonating crystals were mounted in a glass flow cell having an estimated volume of approximately 200 ml. Two mass flow controllers and a bubbler allowed different vapour concentrations to be prepared according to the same principle as in the IMT nose (Fig. 2.3). The stepwise concentration changes were applied with the use of two electric valves. Argon and synthetic air were used as carrier gases at a flow rate of 0.72 l/min. Assuming ideal mixing in the sample cell, the flow system is estimated to have a time constant of 17 s. Since this is too slow to characterise the transient of the sorption behaviour, the crystal was mounted directly in front of the gas inlet of the flow cell so that the inlet gas blows directly onto the crystal, before it mixes in the chamber. This assured an almost stepwise concentration change on the crystal surface.

Curve fitting

All the curves were fitted with the lumped parameters $A/(1+K)$, k and k_d without any drift compensation. The fit was performed by the minimisation of the square error with the solver function in Microsoft Excel©. The direct fitting strategy was not applied because of the limited amount of experimental data. This strategy will be discussed in detail in the following section dealing with chemo-resistors.

6.3.3 Results and discussion

The crystals coated with polypyrrole showed a stable resonance frequency which could be recorded to a resolution of 0.1 Hz. All the response peaks were normalised by subtracting the base-line frequency value just before the start of the vapour exposure.
The frequency of the crystal was found to be flow dependent as described in the literature [20]. This is believed to be due to the pressure dependent damping of the crystal. This effect was circumvented by performing all measurements at the same flow rate.

Blank

Initially a blank, uncoated crystal was examined. Fig. 6.1 shows the response to a sample of 3.4 mmol/l methanol in argon. The small frequency shift observed is believed to be combination of surface absorption of the vapour and a variation in damping due to the density variation of the passed gas (i.e. the carrier with methanol is more dense than the pure carrier).

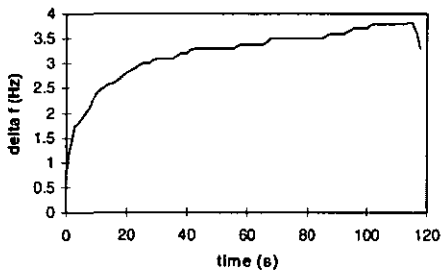

Fig. 6.1: The frequency response of an uncoated crystal to a 120 s long exposure to 3.4 mmol/l methanol.

However, this frequency change is insignificant compared to the frequency shifts observed for polymer coated crystals described further on, which confirms that the measured changes are indeed due to gas sorption in the polymer layer.

Polymer coated crystals

The responses of a crystal coated with 40 mC of polypyrrole, to 120 s exposures of various concentrations of methanol, ethanol and water are shown in Fig. 6.2 - Fig. 6.4. For methanol and water the curves fit well to equation (6.11).

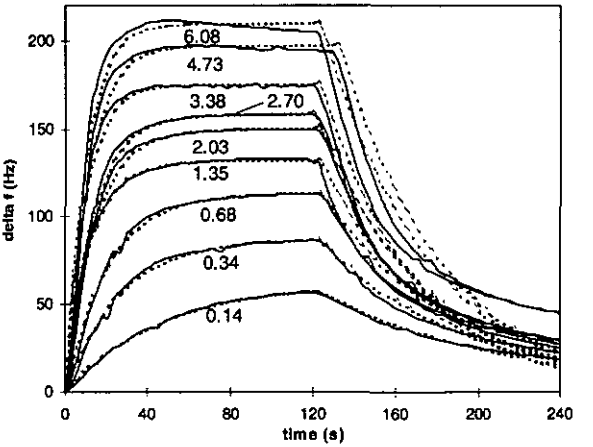

Fig. 6.2: Methanol sorption in a 40 mC polypyrrole film. Vapour concentrations in mmol/l are shown under the curves. The solid line is the experimental data, the dashed line is the fit.

The response peaks for the higher concentrations of methanol do not show a constant plateau but a slow decrease. This is thought to be due to cooling of the sample during the evaporation of relatively large amounts of methanol from the sample bottle. The temperature was observed to drop by as much as a few degrees Celsius, causing a lower vapour pressure and therefore a lower response. To avoid this problem in subsequent experiments, the sample vessel was thermostatted at ambient temperature (22°C).

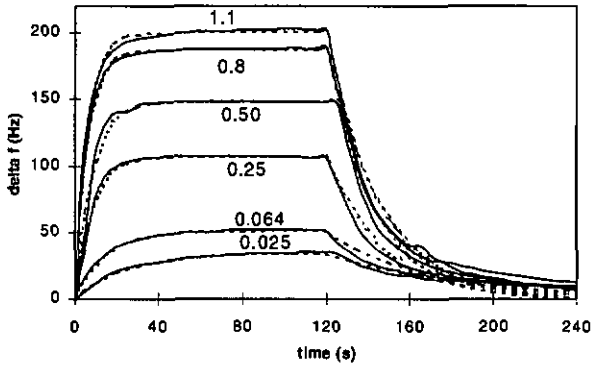

Fig. 6.3: Water sorption in a 40 mC polypyrrole film. Vapour concentrations in mmol/l are shown under the curves. The solid line is the experimental data, the dashed line is the fit.

Although a good fit between data and model was observed with methanol and water, ethanol showed a more complex behaviour, consisting of a rapid initial increase followed by a second, much slower, increase possibly due to the lower diffusion constant of ethanol in the polymer film.

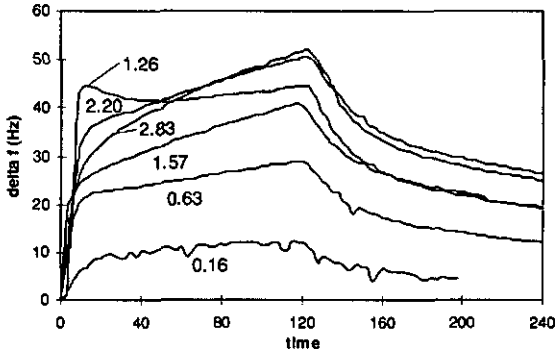

Fig. 6.4: Ethanol sorption in a 40 mC polypyrrole film. Vapour concentrations in mmol/l are shown under the curves. The solid line is the experimental data, the dashed line is the fit.

The application of 'drift compensation' was not suitable to solve this problem. In that case the transients could reasonable be followed by the fit, but the resulting parameters did not show the theoretical concentration trend as can be observed in Fig. 6.7 and Fig. 6.8. This clearly shows the limitations of the Langmuir isotherm based model.

A particular feature can be observed on the 1.26 mmol/l response curve. Since this was the first ethanol response curve in the series, the overshoot in the response may be an artefact, due to the interaction with remaining water from the previous water exposure series with the ethanol.

The methanol response of a crystal coated with a thinner polypyrrole film (30 mC) was also investigated (Fig. 6.5).

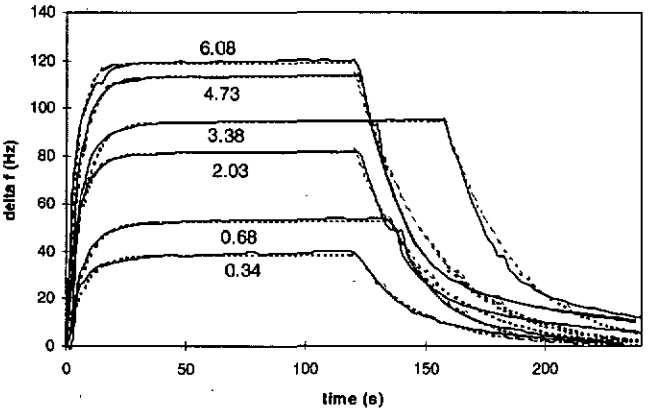

Fig. 6.5: Methanol sorption in a 30 mC film. Vapour concentrations in mmol/l under the curves. The solid line is the experimental data, the dashed line is the fit.

A much faster response with a smaller amplitude than for the thicker film (Fig. 6.2) was observed. The smaller amplitude is not in contradiction with the Langmuir isotherm model. The thinner film can have a smaller number of sorption sites. However, the time constants should in the case of an ideal Langmuir behaviour be the same (equation 6.6). The fact that the thinner film shows faster sorption indicates that there is a diffusion influence on the sorption behaviour.

The crystals were also exposed to vapours in a synthetic air carrier instead of argon. Fig. 6.6 shows two typical response peaks obtained for methanol. The slightly heavier argon gives a slightly larger and faster response. This might be caused by the fact that, due to the higher molecular weight, the argon displaces the vapours more efficient than air. The shape of the response is the same for the two carrier gases, indicating that there is no important oxygen influence, as is the case for SnO_2 gas sensors [9].

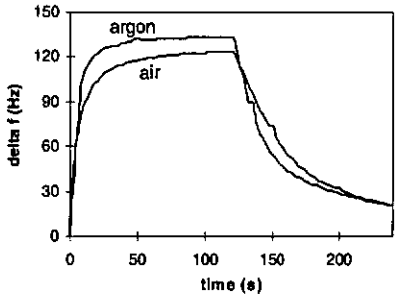

Fig. 6.6: A 50% methanol exposure with two different carrier gases.

Post-extraction of parameters

As expected from theory (equation (6.5) & (6.6)), the fitted values of $A/(1+K)$ and k obtained from the various response peaks of different crystals (Fig. 6.2, Fig. 6.3 and Fig. 6.5) are gas concentration dependent. In Fig. 6.7 and Fig. 6.8 the parameters obtained from the various fits are presented as a function of vapour concentration.

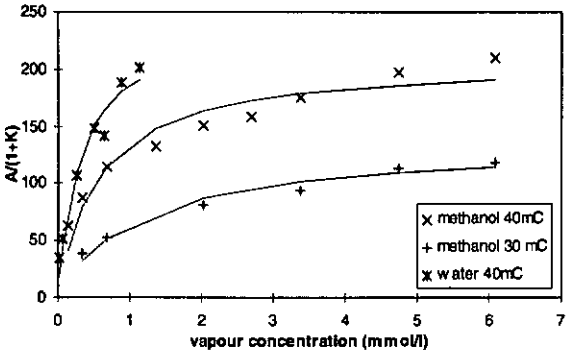

Fig. 6.7: The fitted amplitude of the vapour response.

After the substitution of K according to equation (6.5), the data points in Fig. 6.7 were fitted to the term $A/(1+K)$ from equation (6.11).

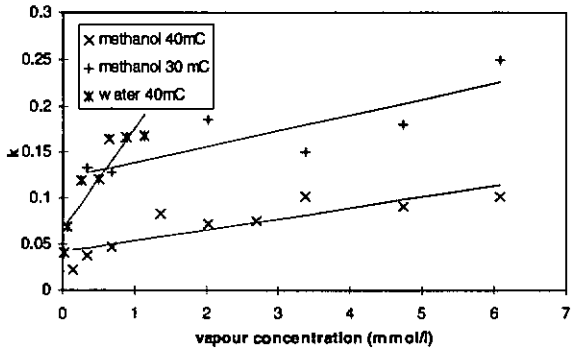

Fig. 6.8: The time constants of the sorption together with their fit to equation (6.6).

The ratio k_d/k_a could also independently obtained from a fit of equation (6.6) to Fig. 6.8. The resulting values for A, the ratio k_d/k_a, together with the values of k_d, which were obtained directly from the decay fits in Fig. 6.2, Fig. 6.3 and Fig. 6.5 are collected in Table 6.2. Relatively large differences are observed for the parameter values obtained from different sources. This is likely to be due to the observed diffusion influences which are not taken into account in the model.

However, it can be observed that for both parameter sources, the thickness variation of the polymer film has the same influence on the obtained time constants, i.e. k_d is roughly a factor 3 higher for the thinner film, k_a is a factor 1.5 higher, to result in a k_d/k_a ratio which is a factor 2 higher for the thinner film, independent of the fitting method.

Table 6.2: The sorption constants for the different vapours on the two crystals.

Charge [mC]	vapour	k_d/k_a [mol/m^3]		k_a [m^3/s.mol]	k_d [1/s]		A [Hz]
		from amplitude (Fig. 7)	from timing (Fig. 8)	from timing (Fig. 8)		direct from decay	from amplitude (Fig. 7)
40	MeOH	0.080	0.51	0.08	0.042	0.010	207
40	water	0.24	0.49	0.14	0.067	0.036	242
30	MeOH	0.16	1.07	0.11	0.122	0.035	135

It is also important to notice that the obtained time constants (Fig. 6.8) are, for concentrations above 2 mmol/l, larger than 0.06 (=1/17 s), which would be the time constant if the response was restricted by mixing. This confirms the effectiveness of mounting the sensor directly behind the gas inlet of the flow chamber to limit the influence of mixing.

6.4 The model applied to chemo-resistors

6.4.1 Experimental

Fitting experiments were performed on the series of bsa doped polypyrrole chemo-resistors of different thicknesses, similar to those described in section 3.5. The charge, taken as a measure for thickness, varied between 2 and 7 mC. Also hexane sulfonate (hsa) and decane sulfonate (dsa) doped polypyrrole sensors (see section 3.6) were examined. All the sensors were exposed to 1 minute pulses of various concentrations of water and organic vapours, using the flow system.

Fitting strategies

The resulting transients consisting of the exposure and 2 minutes of the decay were normalised according to the standard procedure (section 1.1), and fitted to equation (6.13). Fits were performed with lumped parameters and directly with the substituted physical parameters (see section 6.2.6). The influence of 'drift compensation' (section6.2.3) was also examined.

Software

Curve fitting of the transient files was done using a fitting procedure written as a set of m-files for the MATLAB® environment. The Matlab internal minimisation procedure 'fmins', which uses a Nelder-Mead type simplex search method, was used to minimise the mean square error. The termination tolerance was set to 1e-10 for the parameters, and to 1e-15 for the function values. The maximum number of iterations was 10,000. The m-files specially written for this procedure are given in Appendix B. The post-extraction of the physical parameters from the lumped fitting results was performed by minimisation of the square error with the solver of Excel©.

6.4.2 Water response of bsa doped ppy sensors

Lumped parameters with and without 'drift compensation'

Fig. 6.9 shows the transients for the thinnest of the chemo-resistors (prepared with 2 mC) together with the lumped fits to equation (6.13). Except for the lowest concentration, were convergence was not obtained, a good fit between the experimental curve and the model was observed for the exposure part of the curve. For the decay part, the fit was less good. This is considered in the next section.

The transients at lower concentrations show a slight time delay. This is inherent to the flow-system used to generate the different vapour concentrations, and was therefore observed for all vapours. The lower concentrations require a low flow rate through the sample bottle which causes a delay between the sample valve and the mixing point with the bypass flow (Fig. 2.3). No attempt to correct for this was made.

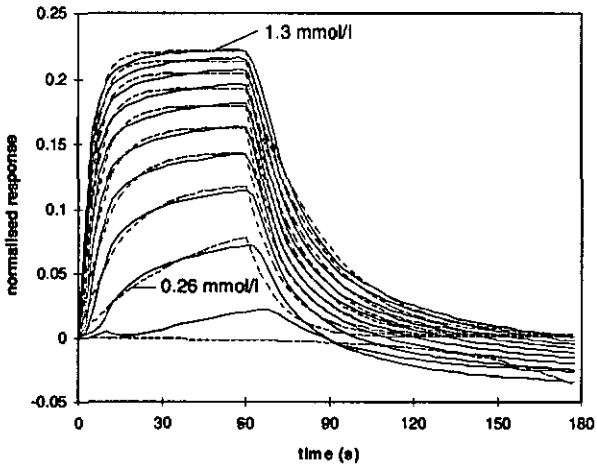

Fig. 6.9: Water responses of a 2 mC bsa doped ppy film. Water concentrations between 0.13 and 1.3 mmol/l with steps of 0.13 mmol/l. The continuous curves are experimental data, the dotted curves are the fits

Drift compensation

The poor fit of the decay part of the curve is believed to be caused by a drift component. A 'drift compensation' according to equation (6.9) was therefore introduced. Fig. 6.10 shows one of the transients from Fig. 6.9, together with fits according to equation (6.13) with and without drift compensation. As can be seen, the 'drift-compensation' leads to a better fit, especially on the decay part of the curve, and was employed during fitting of chemo-resistor data.

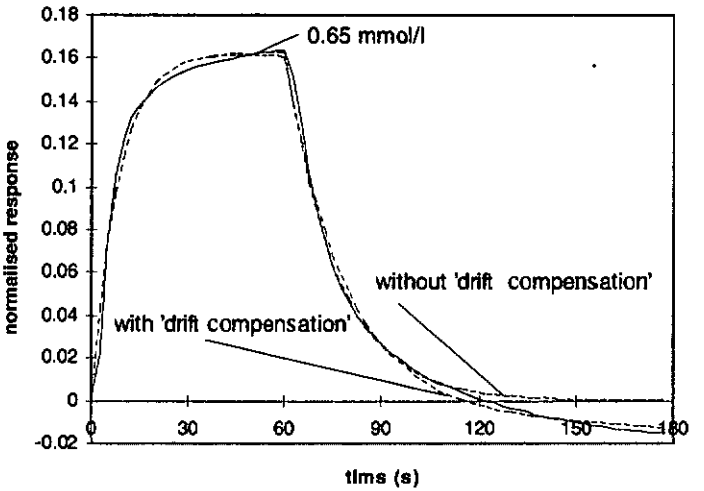

Fig. 6.10: Evaluation of 'drift' compensation on a 0.65 mmol/l water responses of a 2 mC bsa doped ppy film. The continuous curve is experimental data, the dotted curves are the fits.

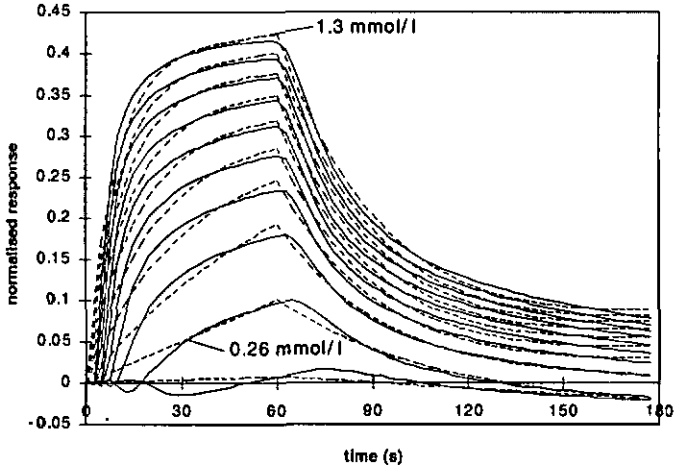

Fig. 6.11: Fits of the water responses of a 7 mC bsa doped ppy film with drift compensation. Water concentrations between 0.13 and 1.3 mmol/l with steps of 0.13 mmol/l. The continuous curves are experimental data, the dotted curves are the fits.

Fig. 6.11 shows the experimental and fitted curves for a thicker polymer film, which displayed a slower but larger response. The fitting procedure was also performed on all the sensors with intermediate charges. The so obtained parameters are displayed graphically in Fig. 6.12 and Fig. 6.13.

Extraction of physical parameters

The calculated fit parameters in Fig. 6.12 were used to extract the parameters B and k_d/k_a which represent respectively the interaction strength and sorption dynamics. This was done by fitting Fig. 6.12a to the term $B/(1+K)$ with equation (6.5) substituted for K. The so obtained values for B are presented Fig. 6.14a for the various thicknesses. The value for k_d/k_a is presented in the curve labelled 'amplitude' in Fig. 6.14b.

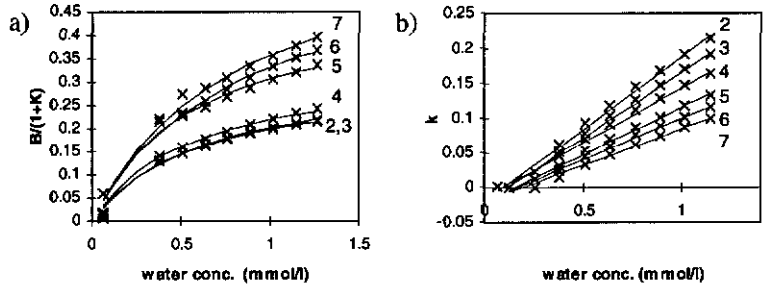

Fig. 6.12: Graph of the fitted amplitude and time constants as a function of the vapour concentration. The crosses correspond to fitted data of different film thicknesses. The corresponding deposition charge in mC is plotted on the graph. Together with this data, fits to respectively B/(1+K) and equation (6.6) are shown in the graph a) and b) respectively.

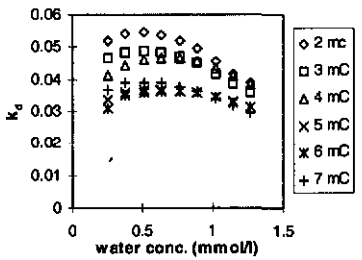

Fig. 6.13: Graph of k_d values as a function of the vapour concentration. The corresponding sensor deposition charge in mC is given in the legend.

Fig. 6.12b was fitted to equation (6.6) to result in values of k_d and k_a. Their ratio, labelled with 'raise', is also plotted in Fig. 6.14b. The last curve labelled 'decay' in Fig. 6.14b represents the k_d/k_a ratio for k_d values obtained from the decay part as presented in Fig. 6.13. The values estimated from these curves were divided by k_a values obtained from the fits to Fig. 6.12b.

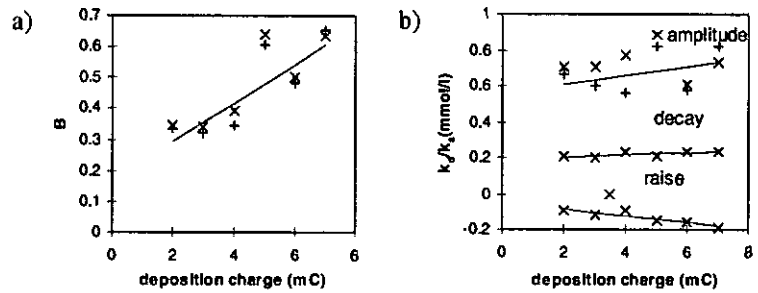

Fig. 6.14: Obtained physical parameters from the fit to Fig. 6.12. See text for the origin of the various curves. The data obtained with drift compensation are marked with x signs and the results without drift compensation are marked with + signs.

Also shown in Fig. 6.14 are regression lines to the various data points obtained from Fig. 6.12 and Fig. 6.13. Due to the larger response of the thicker films, the variable B rises with increasing thickness. This implies a bulk response with a relatively small contribution of surface effects [23]. The k_d/k_a ratio, which differs depending on the way it was obtained, is for all these methods rather thickness independent.

As for the QCM measurements, the differences in data obtained from the different parameters is believed to be mainly due to the influence of diffusion on the sorption process. This is confirmed by the fact that in Fig. 6.14b the difference between the data obtained in the different ways does decrease for thinner films, which obviously suffer from less diffusion limitation than the thicker films.

The mixing behaviour of the sensor cell is another factor which may cause deviating behaviour. At a flow rate of 1 l/min, the sensor cell with a volume of 32 ml has a time constant of 2 s. This is only one order of magnitude higher than the de-sorption time, which is approximately 25 s, and can therefore not be fully neglected.

All k_d values extracted from the constant k were found to be negative, which has no physical sense. The resulting 'raise' curve in Fig. 6.14b can therefore be omitted, and the physical k_d/k_a ratio is therefore expected to

be between the values observed from the 'amplitude' and 'decay' curve in Fig. 6.14b. This results in an estimated value between 0.2 and 0.5. This corresponds well with the values obtained with the QCM (Table 6.2).

The influence of 'drift compensation' on the obtained parameters.

The same parameter extraction with figures similar to those presented in Fig. 6.12 and Fig. 6.13 was also performed on the fitted data without 'drift compensation'. The so obtained parameter values were very similar to the values obtained with drift compensation. Where different, they were marked in Fig. 6.14.
From the good similarity it can be concluded that the extra degree of freedom in the fit of the transient curves does not result in degraded fitting parameters. To the contrary, because of the much better transient fits, the method with drift compensation can be considered superior.

Direct fits

The parameters k_d, k_a, B and a, can also be fitted directly to the transient curves. With a few exceptions, especially at low concentrations, this resulted in similar curves to the ones shown in Fig. 6.10. This is expected, because the curve shape of the two mathematical expressions is exactly the same. The small differences which were observed at lower concentrations are likely to be caused by local minima, or rounding errors in the end condition. The ending criterion is an absolute error, and since K and k are larger than k_d and k_a this results in a larger relative error for the direct fits.

Evaluation of parameters from 'direct fits'

The parameters obtained by direct fitting to the concentration curves, as in Fig. 6.10 and Fig. 6.11, are collected in Fig. 6.15 and Fig. 6.16. The obtained values for B do agree with the values in Fig. 6.14. The k_d values with exception of the lowest concentration values do agree withFig. 6.13.

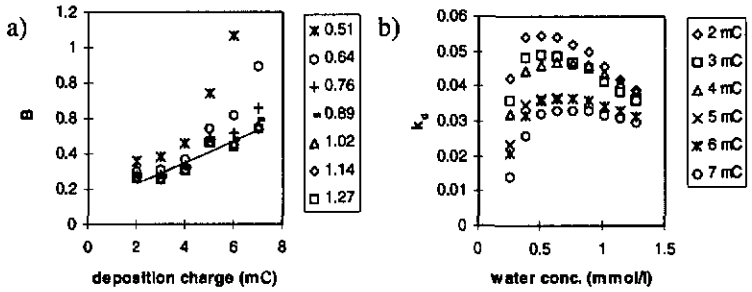

Fig. 6.15: Fitted values of B an k_d as a function of film thickness at different water concentrations. The regression line for the highest concentration is also shown.

The $k_a \cdot [Gas]$ curves of Fig. 6.16 do not go through the origin. This is likely to be related to the mixing properties in the sensor chamber, which results in a lower time constant than in case of a step-wise gas concentration. The obtained parameters do however fall an a straight line, the obtained slopes are presented in Fig. 6.16b. They are somewhat concentration dependent, but considering a k_d value of approximately 0.04 (Fig. 6.15b) this results in k_d/k_a values between 0.2 and 0.4 which is in good agreement with the lumped fitting values inFig. 6.14.

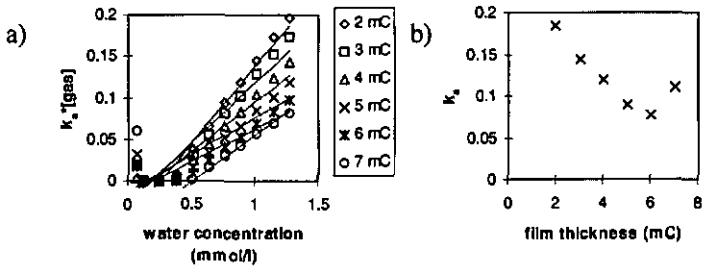

Fig. 6.16: Fitted values for $k_a \cdot [Gas]$ (a) and the extracted values for k_a (b), obtained with direct fits.

All estimated numerical values, together with those from the lumped fits, are collected in Table 6.3. It can be observed that the direct fits result in a lower value for k_a which occurs together with a lower B value. This can be explained by mixing and diffusion, resulting in apparent k_a and k_d values which are lower than their physical values.

Table 6.3: Overview of the water sorption parameters of bsa doped ppy. For the various k values an estimated range is given. The B values were found to be charge dependent. The estimated formula is given.

	B	k_a [m3/s.mol]	k_d [1/s]	k_d/k_a [mol/m^3]
fitting strategy		**timing values**		**amplitude values**
Lumped	0.17+0.06*charge	0.1-0.2	0.03-0.05	0.6
Direct	0.11+0.06*charge	0.08-0.18	0.03-0.05	

Diffusion and mixing will however not influence the equilibrium value (the plateau) of the response. The amplitude of the exponential curve which is presented by the lumped variable $B/(1+K)$ (equation 6.13) is therefore a more accurate parameter than k_d, k_a and B obtained from the direct fits, because these are influenced by the time constant. The values for k_d/k_a and B can later be derived from the $B/(1+K)$ values over the concentration gradient. This does however only give a reliable value for the ratio k_d/k_a, and not for the individual values.

6.4.3 Methanol response of bsa doped ppy sensors

The fitting procedure with 'drift compensation' was also performed on methanol transients recorded at various concentrations. The results for chemo-resistors prepared with a charge of 2mC are presented in Fig. 6.17.

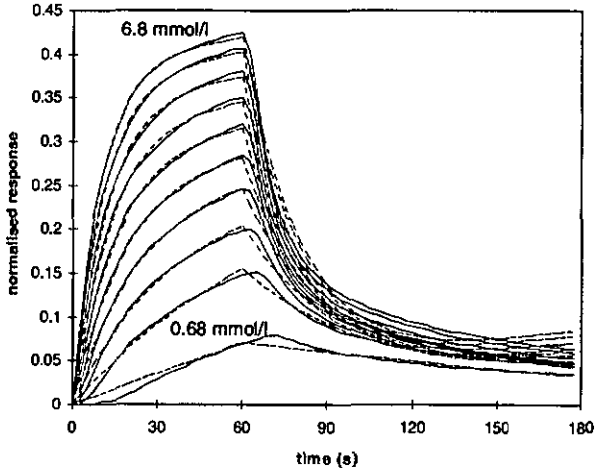

Fig. 6.17: Fits of the methanol responses of a 2 mC bsa doped ppy film with drift compensation. The concentration step size is 0.68 mmol/l.

It can be clearly seen that the methanol responses are much slower than the water responses (Fig. 6.10). So slow that for the sensors with a polymer layer of more than 3 mC the saturation value could not be determined. However, the transients can in this case still be described well by the model. This is illustrated for a 7 mC film in Fig. 6.18. Contrary to the water response, there is in case of methanol a tendency to smaller response amplitudes for thicker films. This might be related to the fact that equilibrium is not reached within the 1 minute exposure.

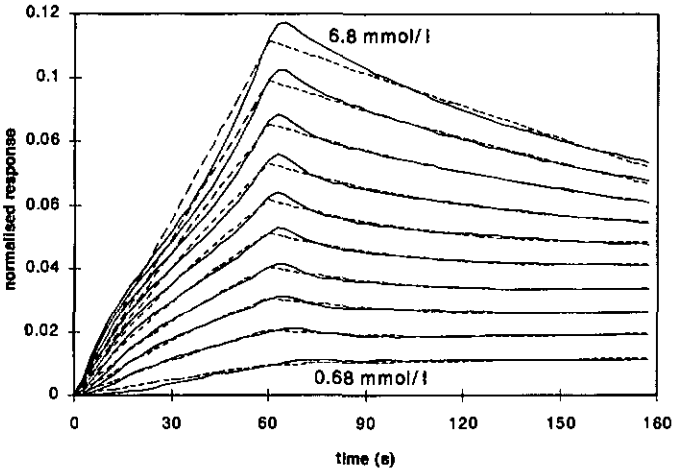

Fig. 6.18: Fits of the methanol responses of a 7 mC bsa doped ppy film with drift compensation. The vapour concentration for the various curves steps up with 10 steps of 0.68 mmol/l starting from 0.68 mmol/l.

The fitted parameters from Fig. 6.17, Fig. 6.18 and similar curves obtained for other sensors with intermediate deposition charges, are collected in Fig. 6.19 and Fig. 6.20.

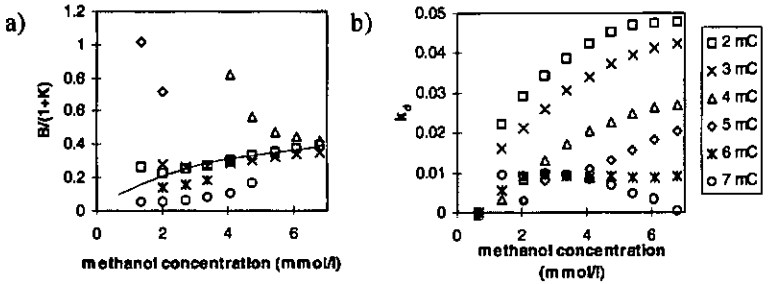

Fig. 6.19: Graph of the fitted amplitude - and de-sorption time constants as a function of the vapour concentration. The deposition charge is given in the legend. For the 2 mC film, the fit is presented in Fig. o).

With the exception of the chemo-resistors with the 2 and 3 mC films, no trend can be observed in the $B/(1+K)$ plots (Fig. 6.19a), and consequently the fitted parameters can not be used for the extraction of the physical parameters B and k_d/k_a. The lack of a plateau value in the response does apparently cause a lot of freedom for the parameters, which results in inaccurate values.

The k values for the thinner films follow a straight line which allows for the estimation of k_a (Fig. 6.20a). For the thicker films, the values are very small, and there is no obvious pattern (Fig. 6.20b). The estimated response parameters for methanol in the 2 mC bsa doped ppy films are collected in Table 6.4.

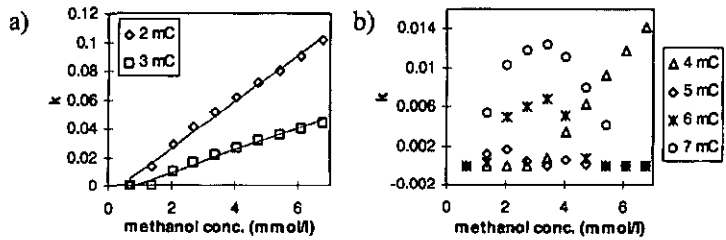

Fig. 6.20: The fitted time constants as a function of vapour concentration for various thicknesses of polymer films. The deposition charge corresponding to the different curves is given in the legend.

The methanol responses were also fitted with the 'direct fit' method. However this does give less accurate results then the 'lumped' fits, and is not shown.

6.4.4 Other vapours and other sensor materials

To investigate the general utility of the model, it was further tested with several vapours and differently doped polymers. The tested vapours, which were pyrrole, aniline, tripropylamine and ethanol, were chosen since they represent a range of chemical functionalities.

Figure 6.21 - Fig. 6.24 illustrate these measurements with a hsa doped ppy sensor.

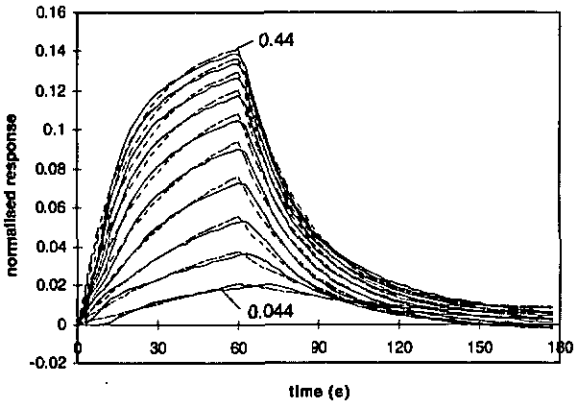

Fig. 6.21: The response of a hsa doped ppy sensor to pyrrole vapour. Concentrations between 0.044 and 0.44 mmol/l with steps of 0.044 mmol/l.

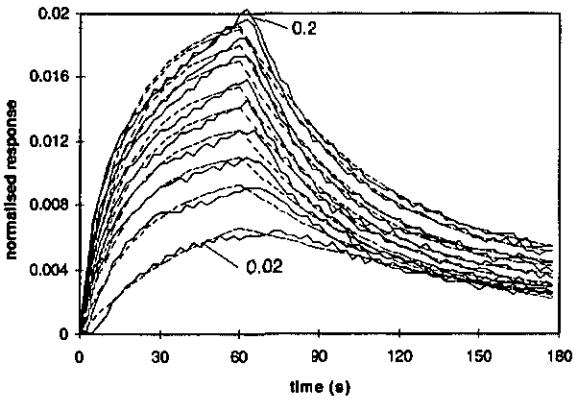

Fig. 6.22: The response of a hsa doped ppy sensor to tripropylamine vapour. Concentrations between 0.02 and 0.2 mmol/l with steps of 0.02 mmol/l.

For pyrrole and tripropylamine, the responses and the corresponding fits look almost ideal. For aniline and ethanol vapours there are some recovery problems. The response was observed to undershoot, especially at the higher concentrations.

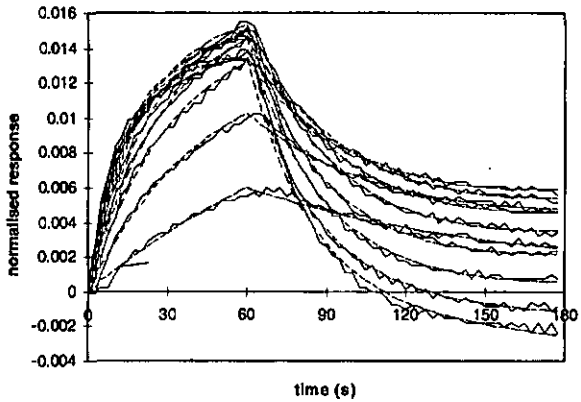

Fig. 6.23: The response of a hso doped ppy sensor to various concentrations of aniline vapour.

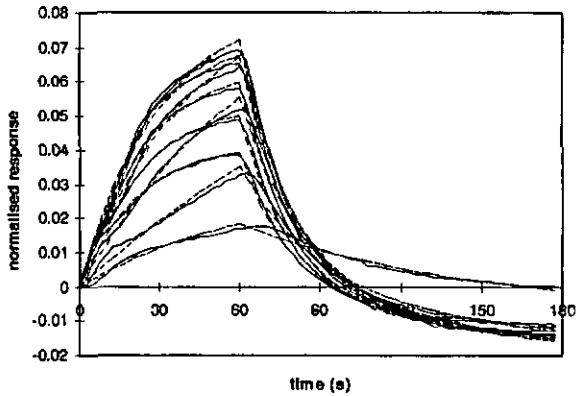

Fig. 6.24: The response of a hsa doped ppy sensor to various concentrations of ethanol vapour.

Where possible, the parameter values for the different vapours and polymers were estimated from lumped fits to the responses. The k_d values were taken from the decay curves, the k_a values from the slope of the time constant as a function of concentration. The parameters are collected in Table 6.4.

It can be observed that for all sensors and all vapours, the k_d values are rather similar. This is related to the mechanism of sorption. De-sorption is largely thermally activated [24], and the required energy to free the vapour molecule from the polymer is, due to apparently rather similar interactions between the different vapours and the polymer, similar for all the vapours. The sorption rate shows much more variation between the different vapours and polymers, because parameters like sorbate mass and the number of sites, which can differ considerably for the different vapours and polymers, are involved (see also section 6.6).

Table 6.4: Overview of the estimated sorption parameters.

Vapour		bsa (2mC)	hsa	dsa
Water	B	0.25	0.28	0.2
	k_a [m^3/s.mol]	0.15	5	3.5
	k_d [1/s]	0.04	0.04	0.04
Methanol	B	0.6	0.73	1.07
	k_a [m^3/s.mol]	0.01	0.05	0.38
	k_d [1/s]	0.04	0.015	0.05
Pyrrole	B		0.20	0.082
	k_a [m^3/s.mol]		0.1	0.06
	k_d [1/s]		0.04	0.035
Aniline	B		0.016	0.004
	k_a [m^3/s.mol]		2	1
	k_d [1/s]		0.03	0.04
Tripropylamine	B		0.021	
	k_a [m^3/s.mol]		0.2	
	k_d [1/s]		0.02	
Ethanol	B			0.03
	k_a [m^3/s.mol]			0.02
	k_d [1/s]			0.04

6.4.5 Discussion

Depending on the vapour and the sensor type, different fitting agreements were obtained for the different methods. The best results for all fitting methods were obtained for water vapour. This is believed to be related to the small size and the polar character of the molecule which causes a fast diffusion and a strong interaction with the polymer.

The lumped fitting method, in which the two lumped parameters according to equation (6.5) and (6.6) rather then directly the physical parameters were fitted, proved to function better because it is more robust against the influences of diffusion. The extraction of the physical parameters can in this case be obtained by post-extraction from the lumped parameters over a range of concentrations.

In order to obtain a successful fit, it is desirable to continue the vapour exposure until an equilibrium value is reached. An additional linear drift correction was found to greatly enhance agreement between theory and experiment.

6.5 Two-phase responses

6.5.1 Introduction

Various polymer materials were found to exhibit two-phasic responses to certain vapour mixtures [25]. This section will examine to what extent the previous model can be adapted to allow the description of these responses. The modelling of more complicated response curves may be performed by a model with two exponential components [1,26]. In this section the two exponentials are assumed to be independently occurring Langmuir sorption curves, i.e. two species are assumed to sorb and interact completely independently.

6.5.2 Experimental

Measurements

In this case, the examined sensors were teatfb doped polypyrrole chemoresistors (see section 3.2.3). The sensors were mounted in the flow system, and exposed to the vapour generated from various dilutions of aqueous methanol between 0 and 50%. The carrier humidity was kept at 30% by means of a wash bottle with a sat. $CaCl_2$ solution. The flow rate was 0.5 l/min and the exposure period was 1 minute.
The vapour concentration of water and methanol resulting from the different solutions was calculated from equation (A1.10) in appendix A.

Fitting procedure

The normalised response was fitted to two superimposed exponential curves (6.13) resulting in equation (6.14). The subscript w stands for water, m for methanol. The variables k and K consist of the individual parameters k_d and k_a according to equation (6.5) and (6.6).

$$\frac{\Delta R}{R} = \begin{cases} \dfrac{B}{1+K_m}\cdot\left(1-e^{-k_m t}\right)+\dfrac{B}{1+K_w}\cdot\left(1-e^{-k_w t}\right) & 0 \le t \le t_1 \\ \dfrac{B}{1+K_m}\cdot\left(1-e^{-k_m t_1}\right)\cdot e^{-k_{dm}(t-t_1)} + & \\ \qquad \dfrac{B}{1+K_w}\cdot\left(1-e^{-k_w t_1}\right)\cdot e^{-k_{dw}(t-t_1)} & t_1 < t \end{cases}$$

(6.14)

The six parameters (k_d, k_a, and B for both water and methanol) were fitted directly to equation (6.14) using the Excel Solver. For this purpose the errors of the six transient curves were taken together to result in one error term. Because of the large freedom in the fit (6 parameters) which result in many local minima, the fit had to be started close to the end-point.
For this purpose, the response curve of water alone was first fitted to estimated the values of the water related parameters. Then the 3 methanol parameters were fitted to all data. Finally all 6 parameters were fitted to minimise the total error using the previously obtained values as starting values.

6.5.3 Results and discussion.

Fig. 6.25 shows the response curves obtained from the exposures to the different mixtures along with the fits to equation (6.14). A good agreement between the experimental and the fitted curve was observed, especially at the lower methanol concentrations.

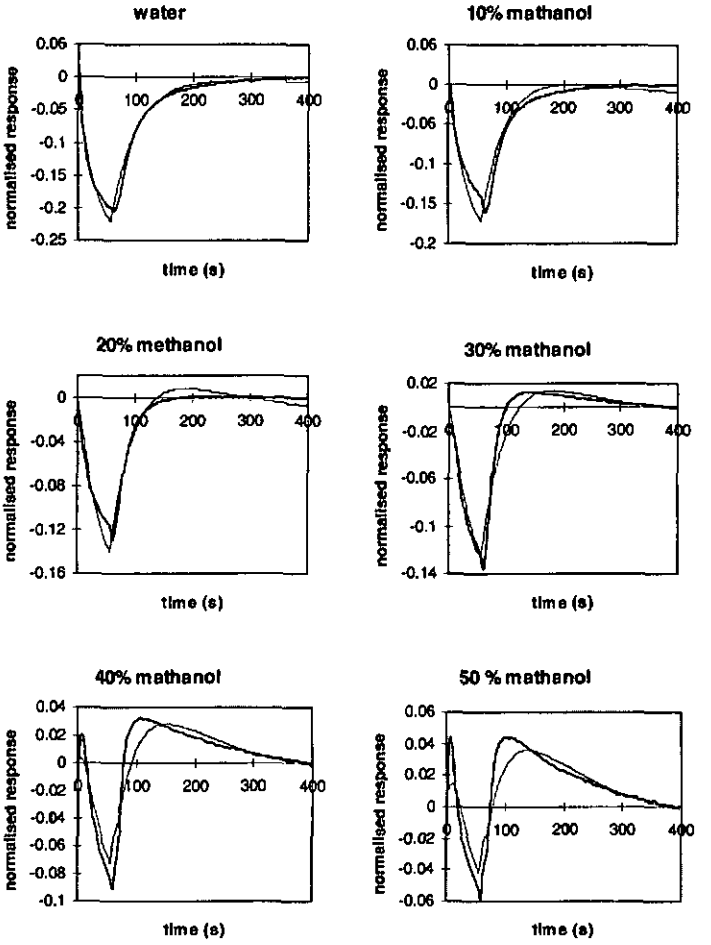

Fig. 6.25: Responses and simulations of a teatfb doped polypyrrole sensor to different alcohol concentrations. The thick line corresponds to the experimental data, the thin line is the fit. Note that the scale on the y-axis is not the same for all graphs.

Deviation for the higher methanol concentrations might be related to interaction between water and methanol. The superimposition of the two experimental curves assumes that the two vapours do fully independently sorb and interact with the polymer. For the lower methanol concentrations, where the site occupation ratio is relatively low, this assumption is probably in better agreement with reality than for the higher concentrations.

Table 6.5: The fitted parameters for the aqueous methanol solutions.

	water	methanol
k_a [m3/s.mol]	0.002	0.014
k_d [1/s]	0.026	0.0115
B	-2.76	0.20

The parameters obtained with the fit are summarised in Table 6.5. Because this is a different sensor type from the sensors used in previous paragraph, care must be taken with the comparison of the data in this table to that in Table 6.4. It can however be observed that the obtained parameters for methanol do largely agree with the methanol values of the bsa doped polypyrrole sensor. However, the water responses are contrary to all the sensors in Table 6.5 negative. Furthermore the k_a value obtained here is smaller for water then for methanol whereas k_a values in Table 6.4 were for all polymers larger for water then for methanol.

6.6 Studying kinetics by temperature ramping

6.6.1 Introduction

During the modelling using the Langmuir isotherm at the beginning of this chapter, isothermal conditions were assumed. The sorption behaviour of gases in solids however, is temperature dependent [17,24]. This section reports experiments made to examine this temperature dependence.

6.6.2 Theory [24]

Assuming attractive forces between the vapour and the polymer, the desorption is related to the average time τ during which the gas molecules stay at the interface between the solid and gaseous phases. This depends on the ratio of the interaction energy Q between the solid and the absorbed gas, and the thermal energy of the gas molecule, according to equation (6.15). The variable R is the gas constant, τ_0 is the molecular vibration time.

$$\tau = \tau_0 \cdot e^{\frac{Q}{RT}} \tag{6.15}$$

The de-sorption constant k_d is inversely proportional to this value, so the temperature dependency of the backward sorption relation can be described by (6.16).

$$k_d = \frac{1}{\tau_0} \cdot e^{-\frac{Q}{RT}} \tag{6.16}$$

The sorption constant k_a depends on the number of impacts of volatile gas molecules on the solid according to equation (6.17), which is defined by the kinetic gas theory [13,24].

$$k_a = \frac{N_0 \sigma^0}{(2\pi MRT)^{0.5}} \tag{6.17}$$

σ^0:	site area	[m^2]
N_0:	number of sites	
M:	sorbate mass	[kg/mole]

6.6.3 Experimental

To examine the influence of temperature on the behaviour of bsa doped ppy, the sensors were mounted in a thermostatted flow cell (Fig. 6.26). This flow cell replaced the sensor chamber of the IMT electronic nose (Fig. 2.3). This set up does not allow the temperature to be exactly controlled, because the gas stream is not at the same temperature as the cell wall. To correct for this, a temperature sensor was mounted in the flow chamber.

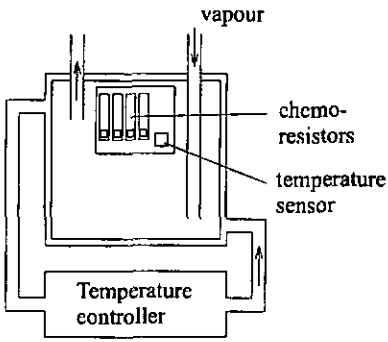

Fig. 6.26: Experimental set-up for vapour exposures at various temperatures.

The vapour generating part of the system was operated at ambient temperature. Concentrations were kept low to prevent condensation of the vapour in the cool areas of the sensor chamber. Various water concentrations were obtained from a saturated $CaCl_2$ solution in a wash bottle at 25°C. The resulting air was diluted with dry air from 10% to 100% to give vapour containing water concentrations between 0.04 and 0.4 mmol/l. The concentration change due to the temperature difference between the sensors chamber and the sample generation was compensated for with the gas-law (equation A1.1).
The flow was 1.0 l/min, since the flow cell had a 2 dl volume, this should be low enough for a minimal influence of the carrier gas on the temperature in the chamber.

6.6.4 Results and discussion

The different response amplitudes at different temperatures are presented in Fig. 6.27. It is clearly observed that the sensor responses decreases with temperature. This can be explained by increase de-sorption at elevated temperatures leading to a lower amount of sorbed gas and a lower response [27].

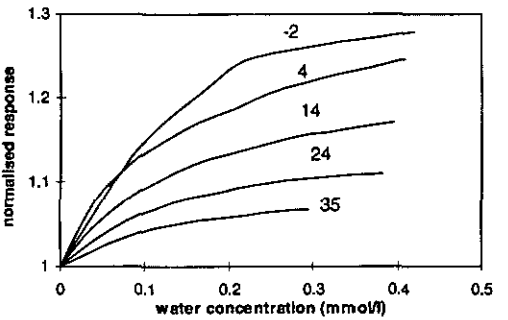

Fig. 6.27: Sensor responses as a function of water concentration. The temperatures in °C are given above the curves.

Another possible origin of the lower response at elevated temperatures might be a change in vapour - polymer interaction. At higher temperatures, the polymers become intrinsically more conducting (see also section 4.6). This might cause a lower vapour sensitivity of the polymer conductivity. Since there is to the author's knowledge no mention of such effects in literature, sorption phenomena are here expected to be the origin of the temperature dependency.

6.7 Conclusions

This chapter has demonstrated that for most vapours the transient behaviour of conducting polymer chemo-resistors can be successfully described by a simple sorption based model. As described at the beginning of this chapter, the vapour response of the conducting polymer is likely to be the result of several mechanisms, and this is perhaps the reason for the limited accuracy of the so obtained fitting parameters. It was particularly noticeable that water gave the best fit, perhaps due to its small size, leading to fast diffusion in the polymer.

From the QCM measurements, and the temperature dependence of the vapour response, it is clear that sorption is a dominating mechanism in the transient behaviour of a chemo-resistor. This explains the observed influence of for example film thickness in chapter 3, and can be used for new designs of chemo-resistors.

The de-sorption parameter k_d was found to be very similar in all cases. This would suggest that the interaction between the vapour and the polymer was similar in all the cases. In contrast the sorption parameter k_a was found to be much more variable.

Extending the model to simple mixtures in which the two components were found to interact independently was found to work only at low concentration of one of the components, presumably since under these conditions the interaction between the components was minimised.

6.8 References

1. T. Eklöv, P. Mårtensson and I. Lundström *Enhanced selectivity of MOSFET gas sensors by systematical analysis of transient parameters*, Anal. Chem. Acta 353 (1997) 291-300.
2. E. Stussi, R. Stella and D. De Rossi, *Chemoresistive conducting polymer-based odour sensors: influence of thickness changes on their sensing properties*, Sensors and Actuators, B43 (1997) 180-185.
3. P.N. Bartlett and S.K. Ling-Chung, *Conducting Polymer Gas Sensors Part II: Response of Polypyrrole to Methanol Vapour*, Sensors and Actuators 19 (1989) 141-150.
4. J.W. Gardner, P.N. Bartlett and K.F.E. Pratt, *Modelling of gas-sensitive conducting polymer devices*, IEEE Proc.-Circuits Devices Syst. 142 (1995) 321-333.
5. M. Josowicz, J. Janata, K. Ashley and S. Pons, *Electrochemical and Ultraviolet-Visible Spectroelectrochemical Investigation of Selectivity of Potentiometric Gas Sensor Based on Polypyrrole*, Anal. Chem. 59 (1987) 253-258.
6. D. Blackwood and M. Josowicz, *Work Function and Spectroscopic Studies of Interactions between Conducting Polymers and Organic Vapors*, J. Phys. Chem 95 (1991) 493-502.
7. J.M. Slater, E.J. Watt. N.J. Freeman, I.P. May and D.J. Weir, *Gas and Vapour Detection With Poly(pyrrole) Gas Sensors*, Analyst 117 (1992) 1265-1270.
8. J.W. Gardner and P.N. Bartlett, Electronic Noses, Principles and Applications, Oxford Science Publications, Oxford, 1999.
9. H.V. Shurmer, J.W. Gardner and H.T. Chan, *The application of discrimination techniques to alcohols and tobaccos using tin-oxide sensors*, Sensors and Actuators, 18 (1989) 361-371.
10. E. Kress-Rogers, Handbook of Biosensors and Electronic Noses, CRC Press, Inc., Boca Raton (U.S.A.) 1997.
11. J.W. Gardner and P.N. Bartlett, *Design of Conducting Polymer Gas Sensors: Modelling and Experiment*, Synthetic Metals, 55-57 (1993) 3665-3670.
12. P.N. Bartlett and J.W. Gardner, *Diffusion and binding of molecules to sites within homogeneous thin films*, Phil. Trans. R. Soc. Lond. A 354 (1996) 35-57.
13. P.W. Atkins, Physical Chemistry, Oxford University Press, Oxford (GB), 1979.
14. J.M. Slater, J. Paynter and E.J. Watt, *Multi-Layer Conducting Polymer Gas Sensor Arrays for Olfactory Sensing*, Analyst 188 (1993) 379-384.
15. X.B. Chen, J. Devaux, J.-P. Issi and D. Billaud, *The Stability of Polypyrrole Electrical Conductivity*, Eur. Polym. J. 30 (1994) 809-811.
16. J.P. Blanc, N.Derouiche, A. El Hadri, J.P. Germain, C. Maleysson and H. Ropert, *Study of the Action of Gases on a Polypyrrole Film*, Sensors and Actuators B1 (1990) 130-133.
17. S. Zhang and S.F.Y. Li, *Detection of Organic Solvent Vapours and Studies of Thermodynamic Parameters Using Quartz Crystal Microbalance Sensors Modified With Siloxane Polymers*, Analyst 121 (1996) 1721-1726.
18. Z. Cao, H.G. Lin, B.F. Wang, D. Xu and R.Q. Yu, *A perfume odour-sensing system using an array of piezoelectric crystal sensors with plasticized PVC coatings*, Fresenius J. Anal. Chem. 355 (1996) 194-199.

19. C. di Natale, J.A.J. Brunink, F. Bungaro, F. Davide, A. d'Amico, R. Paolesse, T. Boschi, M. Faccio and G. Ferri, *Recognition of fish storage time by a metalloporphyrins-coated QMB sensor array*, Meas. Sci. Technol. 7 (1996) 1103-1114.
20. Z. Cao, H.-G. Lin, B.F. Wang, K.-M. Wang, and R.Q. Yu, *Piezoelectric Crystal Sensor Array Used as an Organic Vapor Sensing System*, Microchemical journal 52 (1995) 174-180.
21. B.W. Saunders, D.V. Thiel and A. Mackay-Sim, *Response Kinetics of Chemically-modified Quartz Piezoelectric Crystals During Odorant Stimulation*, Analyst 120 (1995) 1013-1018.
22. Sugimoto, M. Nakamura and H. Kuwano, *Sensitive, selective chemical-sensing layers produced by plasma organic film technology*, Sensors and Actuators B37 (1996) 163-168.
23. W. Göpel, *Supramolecular and polymeric structures for gas sensors*, Sensors and Actuators B24-25 (1995) 17-32.
24. Arthur W. Adamson, Physical Chemistry of Surfaces, Fourth edition, Wiley & Sons, New York 1982.
25. H. Nagase, K. Wakabayashi and T. Inmanaka, *Effect of doping anions in polypyrrole gas sensors*, Sensors and Actuators B13-14 (1993) 596-597.
26. E. Llobet, X. Vilanova, J. Brezmes, J.E. Sueiras and X. Correig, *Transient response of thick-film tin oxide gas-sensors to multicomponent gas mixtures*, Sensors and Actuators B47 (1998) 104-112.
27. A.L. Kukla, Y.M. Shirshov and S.A. Piletsky, *Ammonia sensors based on sensitive polyaniline films*, Sensors and Actuators B37 (1996) 135-140.

7 Dielectric sensors

7.1 Introduction

7.1.1 General

Although diclectric sensors arc mostly used for mcasuring humidity [1,2], there is also a series of papers which discusses their application for the measurement of organic vapours [3-7]. They can therefore also be interesting for application in electronic nose systems. Advantages include the ease of integration with electronics on a single chip [8], and the large variety of polymers, available to modify its selectivity [3,9,10]. This chapter examines the feasibility of the application of the IDA structures used throughout this thesis, for dielectric gas measurements.

7.1.2 Outline

Section 2 of this chapter gives theoretical consideration of the IDA capacity. The capacities of the different part of the structure will be calculated and summarised, and the influence of ohmic conduction and dielectric loss will be discussed. Section 3 describes impedance measurements over the complete frequency range. Section 4 demonstrates practical capacitive vapour measurements with simple interface electronics.

7.2 Theory

7.2.1 General

The capacity of an isolated conducting body is the ratio of the electric charge that must be added to the body per unit increase in its potential [11]. A parallel plate capacitor (Fig. 7.1) is the most simple capacitor configuration.

Fig. 7.1: A parallel plate capacitor.

When boundary effects are neglected by taking $A>>d$, its capacity is given by equation (7.1). For all types of more complicated electrode configurations the capacity can be obtained by integrating the electrode distance over their surface area in a suitable co-ordinate system.

$$C = \varepsilon_0 \varepsilon_r \cdot \frac{A}{d} \tag{7.1}$$

The equivalent capacity of two parallel capacitors is calculated by summarising the contribution from the individual capacitors. This relation can conveniently be used for calculation of the capacity of a complex structure. The structure can simply be split up in different parts, which can be added up to calculate the total capacity.

7.2.2 Planar interdigitated capacitors

The capacity of the IDA structures can be split up in two main parts (Fig. 7.2). One on top of the electrodes through the air, and one under the electrodes through the substrate. The first one is the actual sensing capacity, the second will remain constant.
A third contribution can appear if a significantly thick dielectric layer, i.e. a polymer [3] or a significantly thick inert passivation layer [1] is applied on top of the electrodes. Because solids have a dielectric constant of at least two orders of magnitude larger then gases, this contribution can be quite significant.

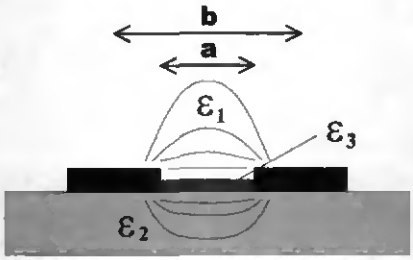

Fig. 7.2: A section of the planar capacitor with the two contributions to the capacity. The black areas are the metal electrodes.

For an interdigitated set of electrodes without passivation, the capacity per unit length [3] of electrode is given by (7.2).

$$C1_U + C2_U = \varepsilon_0 \cdot \frac{\varepsilon_1 + \varepsilon_2}{2} \cdot \frac{K\left[\left(1-\left(\frac{a}{b}\right)^2\right)^{0.5}\right]}{K\left[\frac{a}{b}\right]} \qquad (7.2)$$

$$K(k) = \int_0^{\frac{\pi}{2}} \frac{1}{\sqrt{1 - k^2 \sin^2(x)}} dx \tag{7.3}$$

Where b is the cell length, and a is the electrode spacing (Fig. 7.2). In the case of the 2 µm spaced IDAs used, b and a are 4 µm and 2 µm respectively. $K[k]$ is the elliptic integral of the first kind according to equation (7.3). An eventually present additional passivation layer with a thickness h will result in an additional 3rd part of unit capacity according to (7.4).

$$C3_U = \varepsilon_0 \varepsilon_r \cdot \frac{h}{a} \tag{7.4}$$

To obtain the total capacity C of the interdigitated structure the unit capacity $C_U = C1_U + C2_U + C3_U$ has to be multiplied with the number of fingers N minus one, and their length l according to (7.5).

$$C = (N - 1) \cdot l \cdot C_U \tag{7.5}$$

Substrate capacity

Initial experiments were performed on readily available IDA structures on a silicon substrates, which are conducting. This makes the contribution of the second part (Fig. 7.2) different. The substrate capacity will in this case not exist of the capacity between two electrodes, but of half the capacity between 1 electrode and the substrate according to equation (7.1).

7.2.3 Theoretical capacity of IDAs

The different contributions to the total capacity of an IDA with 2 µm wide electrodes with 2 µm spacing [12] were calculated and are summarised in Table 7.1. The substrate capacity of silicon was obtained from equation

(7.1) by substituting a nitride thickness of 200 nm and an electrode area of 1.25 mm^2 (including connection leads). The contribution of the capacity through the air, or through glass is calculated with equation (7.2).

Table 7.1: The different contributions to the IDA capacity

Geometric part of the structure	Capacity contribution (pF)
elliptic integral through air	1.4
elliptic integral through glass (ε_r=5)	7.0
substrate capacity (silicon with nitride (ε_r=8) passivation)	221

The total capacitance of such a structure can, dependent on whether the substrate is glass or silicon, be calculated by addition of the value from the first row together to that on the second or third row respectively.

7.2.4 Dielectric loss and surface conductivity

A change in gaseous environment will not give a pure dielectric effect for two reasons. Firstly no dielectric is ideal. There will always be a certain charge loss which is represented by the loss angle [5,11], which results in a frequency dependent dielectric according to (7.6).

$$\varepsilon_c = \varepsilon - j\frac{\sigma}{\omega} \tag{7.6}$$

Secondly, the surface absorbed vapour will form a conductive layer on the electrodes [1]. This results in an increase of apparent dielectric loss of planar capacitors (equation 7.6). From impedance curves, the two phenomena cannot be distinguished, and they will in this chapter therefore be taken together.

7.3 Impedance measurements on IDA structures

7.3.1 Introduction

An ideal capacitor has a frequency independent capacity. However, due to the dielectric loss and the surface conduction, the IDA based vapour sensor will not be an ideal capacitor. The measured characteristics of the device will be frequency dependent. This section will demonstrate this effect with impedance measurements over a wide frequency range.

7.3.2 Experimental

The impedance measurements were performed with a HP 4194A Impedance Analyser. The sensors were directly connected to a set of HP16048C test wires, and the frequency was scanned between 100 Hz and 40 MHz.

Vapour samples were generated with a 25 ml beaker filled with 5 ml solvent and sealed with parafilm®. They were left at ambient temperature for at least 10 minutes to equilibrate. The sensors were exposed by inserting them in the headspace in the beaker, through a small hole in the parafilm®.

The impedance characteristics of an IDA were also defined whilst the sensor was dipped demineralised water.

7.3.3 Results and discussion

Fig. 7.3 shows the Nyquist plots for a 2 μm Au IDA under different conditions. Note that the instrument plots the imaginary axis negatively. The polar plots were independent of the oscillation amplitude between 0.5 V and 50 mV. At low frequencies a large phase noise is observed.

In ambient air, the real component is frequency independent and the imaginary component decreases with increasing frequency. In this case the structure behaves purely like a capacity. When exposed to vapours or liquid water, the polar plot becomes more complex. For liquid water, a semi-circle can be distinguished, which corresponds to a capacitance with a parallel resistance [13]. For the case of water and methanol vapour, the semi-circles can to some extent also be observed. This is believed to be due to a combination of dielectric loss and surface conductivity as described in previous section.

These measurements show that under vapour exposure, the capacity is frequency dependent up to frequencies as high as 40 MHz. Measured capacity changes therefore have to be interpreted with great care.

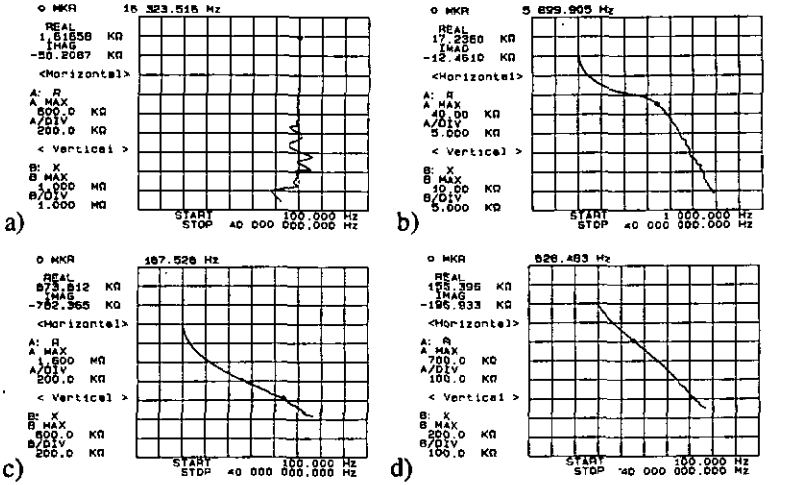

Fig. 7.3: Nyquist plots for a 2 μm Au IDA under different conditions. a) in lab air b) in demineralised water. c) in ethanol vapour d) in water vapour. The imaginary axis is plotted in the negative direction.

The impedance analyser was also used to measure the real capacity of the sensors in dry air (similar to section 4.2). This resulted in a capacity of 212 pF, which is in good agreement (5%) with the calculated value presented in Table 7.1.

7.4 Towards practical application

7.4.1 Introduction

For an eventual application of dielectric sensors in an electronic nose, the interface electronics is a critical issue. The interface needs to be simple, reliable and multiple of these need to be operated in parallel.
This section evaluates 2 possible solutions. The simplest is an oscillator, which frequency is determined by the required time to charge and discharge the sensing capacitor. The second is an Amplitude Modulator (AM), which measures the impedance of the sensor.

7.4.2 Theoretical

Oscillator

An op-amp can in combination with three resistors and a capacitor be used to build an oscillating circuit (Fig. 7.4). The capacitor C is loaded through resistor R_3 until its potential equals the potential on the positive entry of the op-amp. At that moment, the op-amp switches the sign of its output potential. Consequently the capacitor is unloaded and loaded in the inverse direction, until it reaches again half the output, then the op-amp switches back. The process then starts from the beginning. The resulting output potential of the op-amp is a square wave which frequency is defined by the capacity.

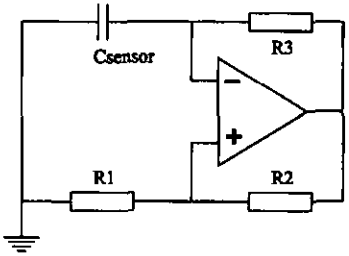

Fig. 7.4: An astable multivibrator with an ascillation frequency proportional to C.

In case R_1=R_2 and an ideal op-amp, the oscillation frequency of the circuit is given by equation (7.7). Which allows the capacity to be calculated from (7.8).

$$f = \frac{1}{2 \cdot R_3 \cdot C \cdot \ln(3)} \tag{7.7}$$

$$C = \frac{1}{2 \cdot \ln(3) \cdot R_3 \cdot f} \tag{7.8}$$

The capacity change due to the vapour interaction can be calculated by normalisation with the baseline signal according to (7.9) which can be rearranged to (7.10).

$$\Delta C = \frac{1}{2 \cdot \ln(3) \cdot R_3 \cdot f} - \frac{1}{2 \cdot \ln(3) \cdot R_3 \cdot f_0} \tag{7.9}$$

$$\Delta C = \frac{f_0 - f}{2 \cdot \ln(3) \cdot R_3 \cdot f_0 \cdot f} \tag{7.10}$$

The oscillator circuit has in the past successfully been used in combination with capacitive pressure sensors [14,15]. Advantages include the simple operation and the digital output signal, which eliminates the need for analogue signal processing.

Depending on the size of the to be measured capacitance changes, the base-line frequency can change quite significant, which can be disadvantageous for frequency dependent detectors. Another disadvantage is the rather high potential the sensor has to be exposed to for proper functioning of the op-amp.

AM modulator

Capacity measurements can be performed with a very high accuracy with an AM modulator (Fig. 7.5). This has previously been demonstrated with an accelerometer by Lötters [16]. For capacitive pressure sensors [14] this measurement strategy resulted in a better signal to noise ratio then the previously described oscillators.
The impedance of the sensor was used to modulate the amplitude of an AC signal from a function generator. The Op-Amp is used for a virtual earth connection of the output terminal of the sensor and the amplification. This set-up is particularly advantageous, because the virtual earth connection eliminates the influence of the wire capacitance, which can be quite significant compared to the small sensor capacitance (Table 7.1).

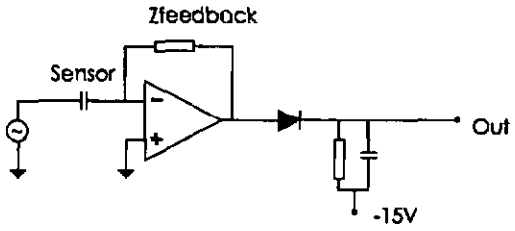

Fig. 7.5: The AM modulator for capacity measurements.

The output of the Op-Amp which is an AC signal with an amplitude proportional to the impedance of the sensor Z_{sensor} is given by (7.11). The variable V is the amplitude of the applied sine wave.

$$V_{out} = V \cdot \frac{Z_{feedback}}{Z_{sensor}} \tag{7.11}$$

When this sensor is assumed to be purely capacitive according to (7.12), the apparent capacity can be calculated from (7.13) which is obtained by rearranging the substitution of (7.12) in (7.11).

$$Z_{sensor} = \frac{1}{j\omega C} \tag{7.12}$$

$$\Delta C = \frac{\Delta V_{out}}{V \cdot j\omega \cdot Z_{feedback}} \tag{7.13}$$

Advantages of this circuit include a freely adaptable measurement amplitude, a constant characterisation frequency and a sine wave potential on the sensor, which makes it easier to interpret combined resistive and capacitive effects. A disadvantage of the circuit is the need for off-set regulation. The feedback has to be adapted to every sensor, with a trimmer or a potentiometer, to avoid clipping of the op-amp.

7.4.3 Experimental

Oscillator

The oscillator circuit was constructed around an LF356 operational amplifier with R_1=R_2=10 kΩ. The charging resistor R_3 was chosen 10 kΩ or 100 kΩ dependent on the desired characterisation frequency. To minimise the influence of parasitic capacities, all the components were soldered as close to each other as possible. The circuit was operated with a power supply of -2.0 and +2.0 V. The resulting square wave at the output of the op-amp was monitored on an HP 54600A oscilloscope and proved to have an amplitude of 1.0 V. This means that the sensor is exposed to voltages up to 0.5 V.

The circuit was realised in threefold to allow for the simultaneous characterisation of 3 sensors. The 3 frequencies were measured with a HP5335A 2 channel counter and a HP34401A multimeter, both connected to a PC over an HP-IB interface. The instruments were controlled by a virtual instrument running in the HP-VEE environment. The counters were all operated with a gate time of 0.5 s.

Without any external capacitor connected to the circuit, and a charging resistor of 100 kΩ, this resulted in an oscillation frequency of 165 kHz due to parasitic capacity on the PCB. Connection of the standard flow cell, which adds a certain wire capacity, lowers this frequency to 143 kHz. This corresponds to a parasitic capacity of 27.6 pF and a total capacity including the flow cell of 31.8 pF.

AM-modulator

The circuit shown in Fig. 7.5 was realised around an LF356 operational amplifier. The filter at the outlet consisted of a 100nF capacitor and a 100kΩ resistor to result in a cut-of frequency of 16 Hz. The function generator was operated at an amplitude of 100mV, at frequencies between 4 an 100 kHz.

The feedback impedance in the original circuit of Lötters consisted of capacitor and a resistance in parallel, operated at a frequency well above the cut-off frequency of the two, so that the impedance is determined by the capacitor. The resistance is only required for stability of the feedback loop.

This set-up, which results in a frequency independent amplification, was initially copied. Experiments were performed with a feedback impedance of 22pF//10M which results in a corner frequency is 725 Hz. The system was operated well above this frequency, so the capacity change can in this case be calculated from (7.14).

$$\Delta C = \frac{\Delta V \cdot C_{feedb}}{V} \tag{7.14}$$

For later measurements with the sensors on glass substrates, having a low capacity, a 10 MΩ simple resistor was taken as a feed-back. The output is in this case frequency dependent, and the capacitance changes were calculated from equation (7.13).

The output of the circuit was fed to a HPE1313A 16 bit scanning A/D converter. The scanner was read out with a virtual instrument written in HP-VEE.

Flow system

The different types of flow cells were connected in the standard flow system (Fig. 2.3) to allow the sensors to be exposed to a concentration range of different vapours.

IDAs and coating

Measurements were made with 2 μm spaced uncovered Au IDAs. Platinum electrodes and coated structures were also tested to see how the electrode material or an additional coating influences the vapour response. Hexamethyldisilazane (HMDS) was applied on the structures by dipping the structures in pure HMDS and drying them in laboratory air. Solutions of 3 and 30 mg/ml PVC in tetrahydrofurane (THF) were prepared with high molecular weight PVC (Fluka 81392). With a micro-pipette 10 μl of these solutions were dispensed on the substrates as well on glass microscope plates, for a visual inspection of the so obtained layer. The structures were dried in laboratory air.

7.4.4 Results and discussion

Oscillator

With a 2 μm IDA on a silicon substrate, and a feedback resistance of 100 kΩ, the circuit oscillates at a frequency of 18 kHz. According to equation (7.8), this corresponds to a total capacity of 252 pF. When the wire and component capacitance (section 7.4.3) of 30 pF is subtracted, a very good agreement with the calculations of 222.4 pF in Table 7.1 is obtained.

The dielectric sensors gave a fast and reproducible responses to different vapours. Fig. 7.6 shows a typical response curve obtained for exposure to saturated water vapour. For lower concentrations and other vapours, similarly shaped responses were obtained. Compared to previously presented conducting polymer response curves, especially the fast response followed by an even faster recovery are attractive features of this sensor type.

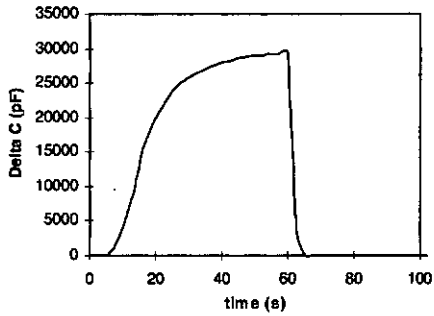

Fig. 7.6: Transient water response.

The relative dielectric constant of liquid water is 78.5. The measured capacity does, compared to the baseline of 222.4 pF, change with a factor 100 though. This means that the large apparent capacity change represented in Fig. 7.6 cannot be purely caused by a change in dielectric constant of the vapour according to equation (7.1). Even if water condenses on the sensor surface, the capacity can change only with a factor 78.

This larger response is caused by the change of the characterisation frequency to values as low as 150 Hz during the vapour exposure. This low frequency causes a relatively important ohmic part in the measured capacitance (equation 7.6), which causes a leakage current whilst charging the resistor making the capacitor look larger then it actually is.

Although the response is not only the consequence of capacitance change, a calibration curve with apparent capacitance changes was obtained. Fig. 7.7 shows 5 consecutive responses of an 2 μm gold IDA to a range of

concentrations of methanol and water. Note the logarithmic scale of the sensory response. A very good reproducibility is observed for concentrations above 0.1 mmol/l. For lower vapour concentrations the signal disappears in the noise.

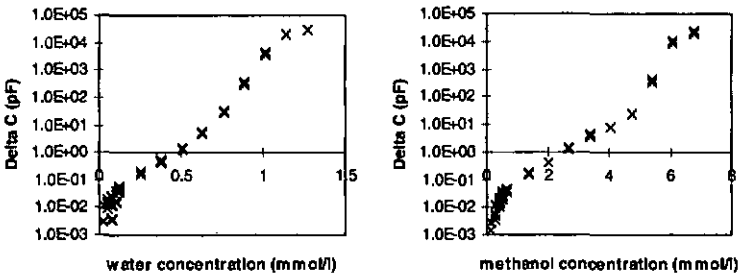

Fig. 7.7: Calibration curve water response of 5 repeated series of exposures.

For intermediate concentrations of both vapours the sensor responds logarithmically. Above a certain concentration the slope does sharply increase and then follows about the original direction for even higher concentrations. The slope variations are, just like the very high responses, believed to be caused by the frequency dependence of the sensor.

Calibration curves were also obtained at a higher base-line frequency. This was obtained by changing the 100 kΩ charging resistor for a 10 kΩ resistor. This resulted in a base-line frequency of 120 kHz. The experiment was simultaneously performed on three similar sensors. Fig. 7.8 shows the responses of 3 different sensors to water and methanol at the two different base-line frequencies.

It can be seen that the increased sensitivity at higher concentration is for most of the sensors suppressed at the higher base-line frequency. This confirms that the high responses at higher concentrations are an artefact of the low frequency. A good reproducibility between sensors can furthermore be observed, especially at moderate vapour concentrations.

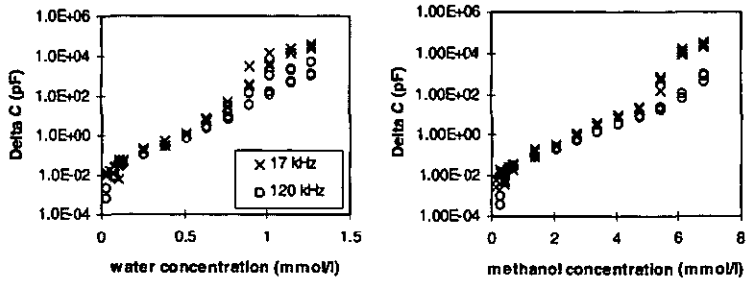

Fig. 7.8: Water ond methanol response curve of 3 Au IDAs at two different frequencies. The base-line frequencies are marked in the plot. However, during exposures the frequency is considerably lower then this value.

AM measurements

A 2 µm Au IDA on a silicon substrate was characterised with the AM circuit with a feedback of 22pF//10MΩ at frequencies of 100kHz and 4 kHz. The response values after 60 seconds are presented in Fig. 7.9.

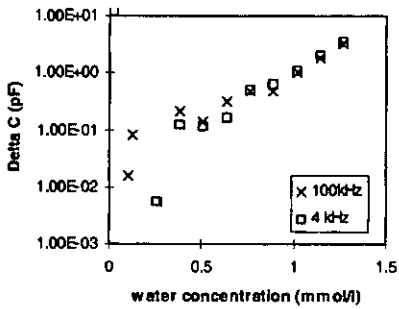

Fig. 7.9: Water responses of a 2 µm Au IDA at 4 and 100 kHz.

The resulting calibration curves were quite similar. Apart from some noise at low vapour concentrations, a straight line without any saturation at higher vapour concentrations was obtained. The characterisation at a constant frequency shows that the previously observed slope variations on

a logarithmic scale are indeed due to frequency changes, and that the sensor response is in fact logarithmic.
The figure also shows that the AM circuit can be operated at a wide range of frequencies. The detection limit of the system however, is troublesome. This was mainly caused by the primitive set-up of the actual circuit.
The same electric circuit was constructed fourfold in a more thorough way, with a metal shielding of the signal carrying part of the circuit. The new circuit was operated at 100 kHz. The high freqency allows to lower the feedback resistor to 100 kΩ, whilst equation (7.14) remains valid. The shielded circuit with a lower impedance showed an improved noise behaviour. Results with this circuit are shown in Fig. 7.10.

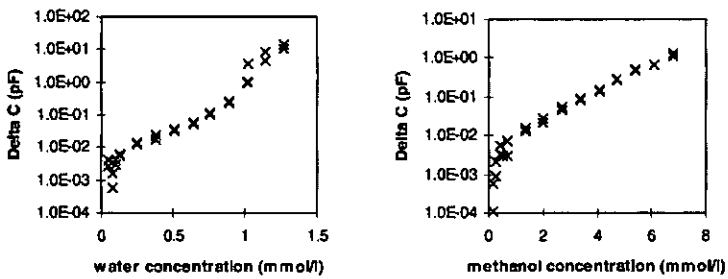

Fig. 7.10: Response of a 2 μm Au IDA with the shielded circuit to 2 repeated series of exposures to water (left) and methanol (right).

For the water response, the higher concentration points are not reproducible. This may be caused by an earlier reported hysteresis in the surface sorption [1], also observed in one of the sensors in Fig. 7.8. For methanol this is not observed. In contrary, for this vapour a reproducible response was obtained over the whole concentration range.

Glass structures

The parallel resistance through the silicon substrate is believed to lower the detection limit considerably. Dielectric measurements were therefore also performed on IDAs fabricated on glass substrates.
The capacity of IDAs on the glass structures was measured with the gain-phase analyser as described in section 7.3 and proved to be 8.7 pF in good agreement with the calculations summarised inTable 7.1.
The structures were characterised with the AM circuit. The small sensor capacitance in this case, needs a high impedance in the feedback loop, to keep a reasonable signal level. This means that the feedback capacitance should be smaller then 8 pF, which is impossible, because the parasitic capacity on the PCB is already higher then this value. The capacitive feedback was therefore removed, and a 10 MΩ resistor was used as a feedback. The frequency had to be lowered to 45 kHz, to lower the influence of the parasitic capacitance on the PCB and get a reasonable output signal level.
There was a cross-talk problem whilst using multiple AM circuits in parallel, and therefore only one set was used at a time. Cross talk can for future measurements easily be eliminated by constructing the interface circuits for the individual sensors on thoroughly shielded individual printed circuit boards. The sensor characteristics of the glass IDAs exposed to water and methanol are shown in Fig. 7.11.

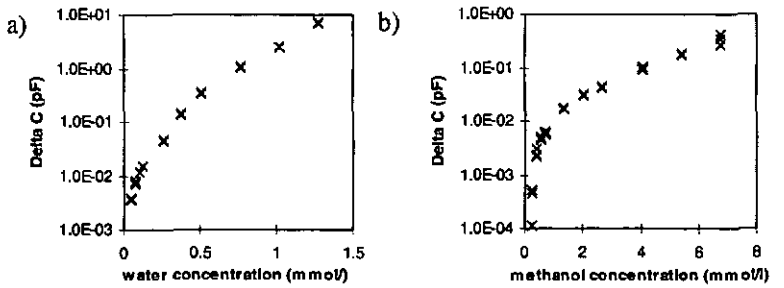

Fig. 7.11: Capacity shifts of 2 µm Au IDAs for 3 repeated series of exposures to a) water and b) methanol.

The electrode configuration of the IDAs on glass is identical to those on the silicon substrates. In consequence, the capacity changes obtained, are in good agreement with the results presented in Fig. 7.10. The lower parasitic capacity does however improve the signal to noise ratio considerably, which results in a good reproducibility between the three consecutive series of concentration.

Sensor modification

Although the presented sensory responses look promising, the responses for water and methanol do unfortunately look very similar. Gas sensors for electronic nose applications do not have to be 100% selective, but for a successful odour recognition, a certain amount of selectivity is required. The possibility of the modification of the sensor properties was therefore examined before further effort to improve the detection limit.
The chemical state of the surface was modified with an HMDS treatment. This treatment of one of the sensors had no effect. It responded similar to hexanol, ethanol, water, methanol and acetonitrile vapour before and after the treatment. The HMDS may have no influence, or it may simply be washed of by one of the vapours it was exposed to. The exact cause was not further examined because the sensors need to be robust to have any practical application.

A sensor modification with PVC films was more successful. Fig. 7.12 shows calibration curves for 4 different organic vapours detected with 3 different sensors. The first is an untreated 2 µm gold IDA as previously used. The second is similar IDA with an additional PVC layer, and the last one is a 2µm Pt IDA.

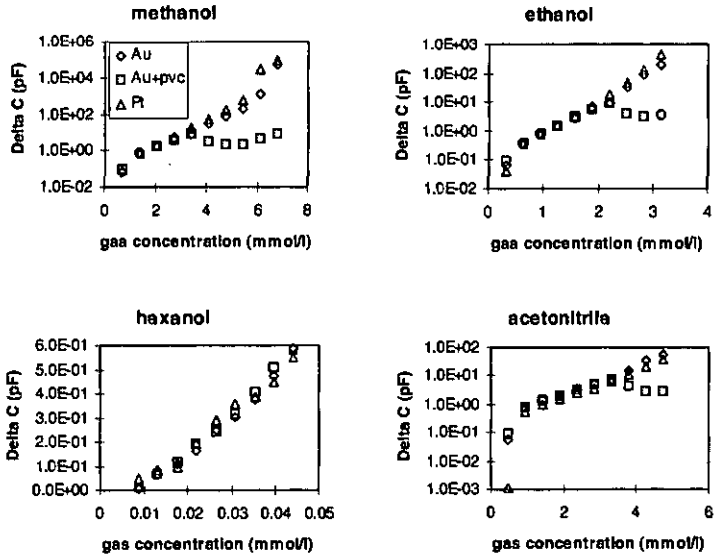

Fig. 7.12: Responses of different sensors to different organic vapours. Note the linear scale for the hexanol vapour.

All the sensors respond very similar at low vapour concentrations. At higher vapour concentrations it can be observed that the PVC membrane suppresses the responses to all the tested vapours, except for the hexanol. This might be caused by the low vapour pressure of hexanol, which does not allow the concentration to be risen enough to see the response suppression. Furthermore it can be observed that there is no significant difference between gold and platinum electrodes.

7.5 Conclusions and outlook

It was clearly demonstrated that the IDA structures are suitable for dielectric vapour measurements. Since the vapour detection is frequency dependent, the oscillator circuit has a limited performance in this application. However, the AM circuit, especially combined with the IDAs on a glass substrate, resulted in a system with a rather low detection limit. Furthermore a good reproducibility between sensors was observed.
Selectivity of the sensors is poor, but an initial experiment with PVC showed that a polymer membrane can change the characteristics drastically. Since there is a wide range of polymer available for such surface modifications, it is believed that it should be possible to fabricate an array with a sufficiently high selectivity.
A next step towards practical application will involve the application of polymer layers on the glass structures, and the development of other polymer membranes, which will provide the required selectivity.

7.6 References

1. R.S. Jachowicz and S.D. Senturia, *A thin-film capacitance humidity sensor*, Sensors and Actuators 2 (1981/82) 171-186.
2. P.P.L. Regtien, *Solid-State Humidity Sensors*, Sensors and Actuators, 2 (1981/82) 85-95.
3. H.E. Endres and S. Drost, *Optimization of the Geometry of Gas-sensitive Interdigital Capacitors*, Sensors and Actuators B, 4 (1991) 95-98.
4. R. Zhou, A. Hierlemann, U. Weimar and W. Göpel, *Gravimetric, dielectric and calorimetric methods for the detection of organic solvent vapours using poly(ether urethane) coatings*, Sensors and Actuators B34 (1996) 356-360.
5. F. Josse, R. Lukas, R. Zhou, S. Schneider and D. Everhart, *AC-impedance-based chemical sensors for organic solvent vapors*, Sensors and Actuators B35-36 (1996) 363-369.
6. K. Alberti and F. Fetting, *Zeolites as sensitive materials for dielectric gas sensors*, Sensors and Actuators B21 (1994) 39-50.
7. M. Haug, K.D. Schierbaum, G. Gauglitz and W. Göpel, *Chemical sensors base upon polysiloxanes: comparison between optical, quartz microbalance, calorimetric, and capacitance sensors*, Sensors and Actuators B11 (1993) 383-391.
8. H. Baltes, D. Lange and A. Koll, *The Electronic Nose in Lilliput*, IEEE Spectrum (1998) 35-38.
9. W. Göpel, *New materials and transducers for chemical sensors*, Sensors and Actuators B18-19 (1994) 1-21.
10. J.W. Grate and M.H. Abraham, *Solubility interactions and the design of chemically selective sorbent coatings for chemical sensors and arrays*, Sensors and Actuators B3 (1991) 85-111.
11. D.K. Cheng, Field and Wave Electromagnetics, Addison-Wesly, Massachusetts (1989).
12. J.C. Fiaccabrino, *Thin-Film Microelectrode Arrays: Materials & Designs*, Ph.D. Thesis, University of Neuchâtel, Switzerland, 1996.
13. R. Greef, R. Peat, L.M. Peter, D. Pletcher and J. Robinson, Instrumental Methods in Electrochemistry, Ellis Horwood Ltd. Chichester, United Kingdom (1985).
14. M.G.H. Meijerink, *Development on an IC-compatible capacitive pressure sensor*, Master's Thesis, Faculty of electrical engineering, University of Twente 1996.
15. M. Pedersen, M.G.H. Meijerink, W. Olthuis, P. Bergveld, *An IC-compatible polyimide pressure sensor with capacitive readout*, Sensors and Actuators A63 (1997) 163-168.
16. J. Lötters, *A Highly Symmetrical Capacitive Triaxial Accelerometer*, Ph.D. Thesis, University of Twente, 1997.

8 Conclusions and outlook

In this thesis several methods for characterising conducting polymer based gas sensors have been described. Polypyrrole doped with bsa was chosen as a model conducting polymer. This polymer displayed a greater deposition reproducibility and stability than many other materials investigated, and so allowed a quantitative overview of the influence of several parameters to be obtained.

Perhaps the most important results were obtained in relation to the materials' humidity response. It was demonstrated that replacing the bsa with a more hydrophobic counter ion can reduce the relative sensitivity to water. Furthermore it was found that as the thickness of the bsa doped polypyrrole films increased, the water sensitivity was increasing, whilst the response to more hydrophobic organic vapours decreased. It was also seen that as the film thickness increased, the response time increased. Together, these results strongly suggest that it is preferable to use thin polypyrrole films.

A study of the electrical parameters of the chemo-resistors revealed that a 4-point measurement, which suppresses the contact resistance, resulted in increased responses. It was also shown that low frequency AC measurements could be used to reduce the noise in the resistance measurements. However, additional sensory information, as some authors have reported for AC measurements, could not be observed.

As well as the chemo-resistor system, GASFETs and QCM systems were investigated. For the GASFET measurements a simple fabrication method for the conducting polymer gate contact was developed. Using the GASFETs responses, very similar results to those obtained with chemo-resistors were obtained, which strongly supports the idea that partial charge transfer is the main response mechanism in conducting polymer based gas sensors.

A simple model based upon a Langmuir isotherm was developed. Comparison of experimental data obtained from chemo-resistors and QCM devices, with the model showed that for small molecules and thin films sorption was the limiting step in the response. The results also showed that under certain conditions the close parallel between model and experiment was rapidly lost. This reflects the complexity of the conducting polymer/gas interaction and supports the proposition that overall no mechanism is dominant. The simple model was able to explain the temperature dependency of the sensor responses.

Although the measurements performed here have concentrated upon bsa doped polypyrrole, there is no reason that the techniques can not be extended to other conducting polymers.

Finally, considering the commercial instruments based solely around conducting polymer sensors, it must be said that conducting polymers appear to be on the wane. They may, however, find a use in the mixed technology, hybrid, noses currently under development. In the longer term electronic noses based upon mass spectrometry (MS) are beginning to become commercially available. The presence of data libraries for MS illustrate the stability if this method. It seems therefore probable that, unless the problems such as drift and stability that currently plague conventional electronic nose systems are rapidly solved, the MS based systems will dominate in all but the most specialised markets.

Appendix A

Headspace equilibration theory

For pure chemical components and mixtures of those, the equilibrium vapour concentration can be calculated from the vapour pressure.

The Gas-law

In static conditions (i.e. in a closed vessel in the absence of flow) a liquid sample will evaporate into the air above it until the vapour pressure is reached. Assuming the gases and vapours to behave as ideal gases is reasonable, because the pressure is in all our applications close to ambient pressure [6.13]. From this vapour pressure the gas concentration can be calculated by applying the general gas law equation (A1.1).

$$\frac{pV}{nT} = R \tag{A1.1}$$

p: Pressure [Pa]
V: Volume [m^3]
R: Gas constant (8.31 [J/(mol K)])
n: amount of gas [mol]

Single components

For a single liquid component the equilibrium between liquid and gas in a closed volume is represented by equation (A1.2).

$$n + n_{vapour} = \frac{V}{R \cdot T} \cdot \left(p + p_{vapour}\right) \tag{A1.2}$$

n_{vapour}: amount of vapour present in the headspace [mol]

p_{vapour}: the vapour pressure of the liquid [Pa]

Subtracting the initial present amount of gas from both sides of equation (A1.2) results in equation (A1.3) which can be rearranged to result in equation (A1.4) which represents the equilibrium concentration of the sample in the headspace in particles per volume.

$$n_{vapour} = \frac{p \cdot V}{R \cdot T} - n + \frac{V}{R \cdot T} \cdot p_{vapour} \tag{A1.3}$$

$$C = \frac{n_{vapour}}{V} = \frac{p_{vapour}}{R \cdot T} \tag{A1.4}$$

At a defined pressure, gas concentrations can also be expressed as a molecular ratio. This is commonly expressed as part per million (PPM) according to equation (A1.5).

$$C_{rel} = 10^6 \cdot \frac{p_{vapour}}{p} \tag{A1.5}$$

At ambient temperature (25°C) and pressure (10^5 Pa), the gas concentration in moles per m^3 can, under the assumption of ideal gas conditions, be converted to the mole fraction in PPM with equation (A1.6).

$$C_{rel} = 2.47 \cdot 10^4 \cdot C \tag{A1.6}$$

Mixtures

The vapour pressure above a mixtures of two liquids is described by Raoult's law according to equation (A1.7).

$$p_{total} = p_A \cdot x_A + p_B \cdot x_B \tag{A1.7}$$

p_X: vapour pressure of pure liquid X.
x_X: mole fraction of substance X in the liquid.

The concentration of the two species together (A1.8) can be calculated from the total vapour pressure in the same way as equation (A1.4).

$$C_{total} = \frac{n_{total}}{V} = \frac{p_{total}}{R \cdot T} \tag{A1.8}$$

Dalton's Law (A1.9) shows that the concentration of one species in the mixture can be calculated by taking the ratio of the vapour pressures according to the mixing ratio in the liquid[6.13].

$$y_A = \frac{p_A \cdot x_A}{p_{total}} \tag{A1.9}$$

y_A: mole fraction of substance A in the vapour.
p: the total pressure.

The concentration of one fraction can therefore be calculated with equation (A1.10) which is obtained by combining (A1.8) and (A1.9).

$$C_A = y_A \cdot C = \frac{p_A \cdot x_A}{RT} \tag{A1.10}$$

Appendix B

This appendix gives the 4 most important m-files which were used for the normalisation of chemo-resistor data from the acquisition and the fit of the model to the normalised data. When different normalisation procedures were used, or different models were fit, a new set of m-files with small variations were used.

```
% nossdatafit.m
clear
echo on

% processes a datafile data.txt
% with boundary conditions timing.txt from the nose directory.

% load datafile and parameterfile
load data.txt
[x,y]=size(data)
load timing.txt

% assign values from parameterfile to constants
begin=timing(1,1)
sampling=timing(2,1)
delay=timing(3,1)
number=timing(4,1)
purge=timing(5,1)
eerstesensor=timing(6,1)
sensors=timing(7,1)

% discard empty columns from datafile
datawithoutzero(:,1)=data(:,1);
for m=1:sensors
      datawithoutzero(:,m+1)=data(:,eerstesensor+m);
end
size(datawithoutzero)
clear data

% calll cutper, which returns a matrix with normalised
% responses
matrix=cutper(begin,sampling,delay,number,purge,datawithoutzero
);
save normpesk.txt matrix -ascii

% plot individual untrested response curves
figurecounter=0
for k=1:sensors
      figure(k+figurecounter)
      plot(0.0001*datawithoutzero(5:x,1),
       [datawithoutzero(5:x,1+k)])
end
figurecounter=figurecounter+k+1
% plot untreated response curves in one graph
figure(figurecounter)
plot([datawithoutzero(5:x,2:sensors+1)])
```

```
%plot individual normalised response curves
[x,y]=size(matrix)
for k=1:sensors
      figure(figurecounter+k)
      plot (matrix(3:x,1+k))
end
figurecounter=figurecounter+k+1

% plot normalised response curves in one graph
figure(figurecounter)
      plot([matrix(3:x,2:sensors+1)])

% call fitting procedure
parameters=simplefi(matrix,number,sampling,delay);
```

```
function matrix=cutper(begin,sampling,delay,
number,purge,input)

% cutper(begin,sampling,delay,number,purge,input)
% Normalise every response peak separately
%
% Gives zeros in the first two rows of the output matrix
% Normalises the response peak on the 10 measuring points
% before and gives the response peaks in the rest of the lines
%
% The time in the first column starts with two zeros in the
% first rows
% On every sample row there is the absolute time shifted so
% every sample starts at t=0

echo on
[m,column]=size(input)

% for all response peaks
for m=1:number

% generate first column with time values
matrix(3+(m-1)*(delay+1)*sampling:
2+m*(1+delay)*sampling,1)=input(begin+(m-
1)*(purge+sampling):begin-1+(m-
1)*(purge+sampling)+(1+delay)*sampling,1)-input(begin+(m-
1)*(purge+sampling),1);

% for all sensors
for k=2:column

% calculate baseline from 10 previous values
claverage=0.1*sum(input(begin-10+(m-1)*(purge+sampling):begin-
1+(m-1)*(purge+sampling),k));

% normalise
matrix(3+(m-1)*(delay+1)*sampling:2+m*(1+delay)*sampling,k)=
(input(begin+(m-1)*(purge+sampling):begin-1+(m-1)*
(purge+sampling)+(1+delay)*sampling,k)/claverage)-1;

end
end
```

```
function parameters=simplsfi(matrix,number,sampling,delay)

% simplefi(matrix,number,sampling,delay) performs a fit with
% a single rc curve and 'drift compensation'
%
% the input format is a n*m matrix with
% m-1 sensors. The first two rows are empty the next rows
% contain number * (1+delay) *sampling samples
% see also cutper.m; needs funcsimp.m

%options(1)=1;          %echo's iteration
options(2)=1.0e-10;     %x
options(3)=1.0e-15;     %f(x)
options(14)=10000;      %maxnumber

% define the important parameters global to allow
% them to be accessed by funcsimp.m
global N;
global K;
global MATRIX;
global LENGTH;
global SAMPLING;

% assign values to the globsl variables
SAMPLING=sampling;
LENGTH=(1+delay)*sampling;
MATRIX=matrix;

% check the amount of available data
[rows,columns]=size(matrix);
clear rows;

% for all sensors
for K=2:columns
        K;
% for all response peaks
        for N=1:number
                N;

% define start values for the fitting paramters
                c=0.05;
                raise=0.02;
                decay=0.005;
                slope=.01;
                a=100*K+N

% call fitting procedure
a=fmins('funcsimp',[c,raise,decay,slope],options);

% copy parameters obtained from 'funcsimp'
                parameters(1+(K-2)*4:(K-1)*4,N)=a';
        end
end
```

```
function y=funcsimp(a)

% belongs to simplefi.m

% define global variables
global N;
global K;
global MATRIX;
global LENGTH;
global SAMPLING;

% calculate the simulated response from the parameters
% in the vector a, which comes from the minimisation procedure
yaim=a(1)*(1-exp(-a(2)*MATRIX(3+(N-1)*LENGTH:3+(N-
1)*LENGTH+SAMPLING,1)));
yaim(SAMPLING+2:LENGTH)=yaim(SAMPLING+1)*exp(-
a(3)*(MATRIX(4+SAMPLING+(N-1)*LENGTH:2+N*LENGTH,1)-
MATRIX(3+SAMPLING+(N-1)*LENGTH,1)));

% add 'drift compensation' to the response peak
yaim=yaim+0.001*a(4)*MATRIX(3+(N-1)*LENGTH:2+N*LENGTH,1);

% calulate the difference between simulation and data
error=yaim-MATRIX(3+(N-1)*LENGTH:2+N*LENGTH,K);

% take the aquare of all the errors and return to 'aimplefi.m'

y=error'*error;
```

Appendix C

"Detection limits for different gas sensor technologies"

C.1 Introduction

C.1.1 General

This thesis describes different aspects of, mainly conducting polymer based, gas sensors for electronic nose applications. During the sensor characterisation, the noise level proved not to be the limiting factor in the performance of the devices. Consequently the detection limits have not been experimentally determined.
There is however a growing awareness that for many applications the detection limits of sensors are an important factor in the feasibility of the implementation of electronic nose technology. Especially in the case where the system needs to be able to detect outliers containing a single polluting component (for example herbicide in food) the feasibility of the electronic nose implementation critically depends on the detection limit of the sensors used.

C.1.2 Detection limit

The lowest possible concentration that can be detected with a particular sensor depends on different sensor properties. Assuming perfectly repeatable experimental data, it is the limit at which the signal can be distinguished from the noise. A common measure is 3 or 5 times the noise level.
In the particular case of the gas sensors examined here, there is furthermore a considerable drift. Although this does not directly influence the lowest concentration which gives a detectable signal, it does make it difficult to quantify the vapour concentrations and therefore indirectly influences the detection limit. Another problem in the determination of the

detection limits is that the repeatability with which a sensor can be exposed to a defined vapour concentration is not known.

C.2 Experimental

The experiments in this thesis were not performed with the intention of the determination of the detection limit. To have some indication of experimental values, detection limits were estimated by extrapolation of the modelled sensor response to the concentrations where the model response equals the estimated experimental noise level.
Detection limits are given in mmol/l following the convention throughout this thesis. It should be kept in mind that at 25 °C a vapour concentration of 1 mmol/l corresponds to 24.7e3 ppm (Appendix A).

C.3 Estimation of detection limits

C.3.1 Chemo-resistors

The physical noise density in chemo-resistors (mainly 1/f noise) at 10 Hz and a bias of 2.5 mA was found to be typically 1e5 $\mu V^2/Hz$ (Fig 4.7). During sensor operation the current is kept at 5 μA, so the noise level at a bandwidth of 10 Hz, will be approximately $10Hz \cdot \frac{5e-6A}{2.5e-3A} \cdot 1e5\mu V^2/Hz = 2000\mu V^2$. This corresponds to a noise amplitude of 44 μV.
The observed electrical noise on the sensors typically corresponded to 0.1 % of the sensor signal (3 times the noise amplitude in for example Fig. 6.23). At a sensor bias of typically 10 mV this corresponds to 10 μV, in reasonable agreement with the 44μV from the theory.
The interface circuit apparently does not contribute significantly to this noise. The response characteristics summarised in Table 6.4 were extrapolated to a response of 0.1%.

The results are presented in Table C.1.

Table C.1: Detection limits in mmol/l extrapolated from Table 6.4.

analyte	bsa	hsa	dsa
water	0.002	0.002	0.002
methanol	0.006	0.006	0.010
pyrrole		0.0008	0.0063
aniline		0.00015	0.0053
tripropylamine		0.0018	
ethanol			0.00025

C.3.2 Conducting polymer GasFETs

The noise in the GasFET measurements was estimated to be 0.2 mV. Response curves in Table 5.1 were extrapolated to this value, to result in the detection limits given in Table C.2. Since for the GasFETs there was more data available, not only the detection limits, but also the variation in these detection limits could be estimated.

Table C.2: Detection limits of the conducting polymer GasFETs in mmol/l for various vapours.

Analyte	teatfb	bsa
isopropropanol	0.1+0.07	0.07±0.04
ethanol	0.04±0.03	0.1±0.07
acetonitrile	0.05±0.04	0.2±0.1
water	0.02±0.01	0.001
methanol	0.09±0.05	0.4±0.3

C.3.3 Dielectric sensors

The best dielectric measurements in this thesis, which are the AM measurements on glass substrates, showed a detection limit of about 0.05 mmol/l for water and 0.4 mmol/l for methanol.

C.3.4 Acoustic Devices

The noise limit of the QCM used in chapter 6 is approximately 0.4 Hz. The response values of table 6.2 were extrapolated to this level. This results in detection limits summarised in Table C.3.

Table C.3: Detection limits in mmol/l of a QCM covered with 40 mC polypyrrole.

methanol	0.001
water	0.0005

The functional behaviour of the acoustic devices is well known from literature. Consequently, the theoretical detection limits, in mass loading per surface area are known from literature [1]. This is however quite difficult to translate to the practice because the relation between vapour concentration and mass loading strongly depends on the sorption properties of the coating material used.
The theoretical sensitivity of the frequently used Surface Acoustic Wave (SAW) devices is one order of magnitude higher then that of QCM devices. With the Lamb wave technology even higher sensitivities can be obtained. For example the Flexural Plate Wave (FPW) technology which is a particular type of Lamb wave, has a sensitivity which is again one order of magnitude higher [1] then the SAW technology. To the authors' knowledge the lamb wave technology has however not yet been applied in electronic noses.

C.3.5 Mass spectrometry

Quadrupole based Mass Spectrometers are being increasingly used in electronic nose applications mainly due to their inherently high stability. They have a typical detection limit of 1e-9 gram [2]. At a sample volume of 1 ml, this corresponds in the case of water vapour to a concentration of 5.6e-5 mmol/l, roughly 1 ppm.

C.4 Discussion

This appendix gives an overview of the detection limits of various gas sensor technologies. Detection limits proved to be dependent on the particular vapour considered. Especially water, a small and polar molecule, proves to have very low detection limits for all sensor technologies.
Care must however be taken with the interpretation of the given values. Since at the time of the experiments no special attention was paid to the detection limits, rather large errors can occur in the estimated values. For certain technologies the observed noise might for example be largely due to the noise originating from the interface electronics, and therefore not fundamentally limiting to the particular sensor technology.
Keeping the limitations in mind, the estimated values show a rather good performance of the conducting chemo-resistors, compared to the FET and dielectric sensors. They approach the detection limit of the used acoustic devices (0.001 mmol/l corresponding to 25 ppm).
Considering other possible technologies, the quadrupole mass-spectrometer gives a rather similar detection limit. However the SAW and the FPW devices have a potential of a lower detection limit when they can be operated in a set-up which guarantees a sufficient stability of the sensor signal.
It is clear that in electronic nose applications where the system is used as a surveillance system which should warn for a frequently occurring event of one single contaminant, the detection limits of the sensors should be low enough to detect this particular vapour. However, the detection limit is not in all cases the critical factor for the performance of an electronic nose system. Especially in the case of complex odours, the concentration of the individual components of the odours might lie well below the detection limit, but the sensor responses which are the sum of all the responses to all the individual vapours may still be usable.

C.5 References

1. Ballantine, R.M. White, S.I. martin, A.J. Ricco, E.T. Zellers, G.C. Frye and H. Wohltjen, Acoustic wave sensors, Theory, Design, and Physico-Chemical Applications, In the series Applications of modern acoustics, edited by R. Stern and M. Levy, Academic Press, San Diego, 1997.
2. W.E. Morf, *personal communication.*

Acknowledgements

This work would not have been possible without the help of a lot of people, some of which I would like to mention here. First of al Prof. Milena Koudelka-Hep and Prof. Nico de Rooij who gave me the possibility to work in their group for 3 years. It was a great pleasure to work in this large and multidisciplinary group.

I would like to thank Dr. David Strike who was my daily supervisor. Apart from the introduction in the secrets of electrochemistry and especially conducting polymers, he also revealed other secrets, like the way to IKEA in Lausanne, which helped a lot to get settled in Neuchâtel. Furthermore I want to thank him a lot for correcting this thesis and many other documents on both scientific and grammatical errors.

Another important person was Dr. Peter van der Wal with whom I shared an office for more then 3 years. He was there to respond on basic chemistry question I often had, and to ask critical questions to keep me on the right track. He also corrected a part of the drafts for this thesis.

The third person in our office was PD Dr. Werner Morf. His pleasant discussions and stimulating ideas were highly appreciated.

Dr. Jean-Charles Fiaccabrino introduced me in the IMT clean-room, the secrets of IDA fabrication and supplied me with some SEM pictures of them. For the device fabrication I would like to thank the technical staff (Mr. Sylvain Jeanneret, Mr. Pierre-André Clerc, Mrs. Sabina Jenny and Mr. Giani Mondin) for their support. Special thanks goes to Ms. Sylviane Pochon for dicing and encapsulating of the many devices I used during this thesis.

Dr. Pierre-François Indermühle and Mr. Gregor Schürmann introduced me in the world of AFM. Pierre Thiébaud made SEM photographs of the GASFETs with the conducting polymer gate contact and Dr. Terunobu Akiyama belped me with the noise measurements. Dr. Bart van der Schoot corrected a chapter of this thesis. I would like to thank these and all the other collaborators of the SAMLAB group of IMT very much. I highly

appreciated the pleasant working ambience and the many trips in bars of Neuchâtel and on mountains in Switzerland.
Outside the university of Neuchâtel I would like to thank Dr. Jan Hendrikse (University of Twente) for the pleasant collaboration on the FET measurements as well as Dr. Milan Fedurco and Dr. Piotr Kedzierzawski (University of Geneva) for the assistance with the QCM measurements.
The Swiss Centre for Electronics and Microtechnology (CSEM) is acknowledged for their financial support of this thesis. From the CSEM I especially would like to thank Dr. Victor Neumann, who also agreed to be co-examiner, for useful discussions and Dr. Mario El-Khoury for the support and the enthusiastic discussions during the beginning of this project.
Finally I would like to thank Prof. W. Schuhmann for kindly agreeing to be co-examiner.

List of publications

Related to this thesis:

M.G.H. Meijerink, M. Koudelka-Hep, N.F. de Rooij, D.J. Strike, J. Hendrikse, W. Olthuis and P. Bergveld, *Gas sensing with a conducting polymer on an isolated gate field effect transistor*, 9th CIMTEC Conference, June 1998, Florence (Italy), abstract SIX-1:P25.

J. Hendrikse, W. Olthuis, P. Bergveld, M.G.H. Meijerink, M. Koudelka-Hep, N.F. de Rooij and D.J. Strike, *A novel potentiometric transducer for use in aqueous solutions based on a FET having a polypyrrole gate contact*, 9th CIMTEC Conference, June 1998, Florence (Italy), abstract SIX-1:L10.

M.G.H. Meijerink, M. Koudelka-Hep, N.F. de Rooij, D.J. Strike, J. Hendrikse, W. Olthuis and P. Bergveld, *Gas-Dependent Field Effect Transistor with an Electrodeposited Conducting Polymer Gate Contact*, Electrochemical and Solid-State Letters 2 (1999) 138-139.

D.J. Strike, M.G.H. Meijerink and M. Koudelka-Hep, *Electronic Noses, A Mini-Review*, Accepted for publication in Fresenius' Journal of Analytical Chemistry.

M.G.H. Meijerink, D.J. Strike, N.F. de Rooij and M. Koudelka-Hep, *Modelling of conducting polymer gas sensors*, "Transducers 99" conference, June 7-10, Sendai, Japan, conference proceedings, pp. 432-435.

M.G.H. Meijerink, D.J. Strike, N.F. de Rooij and M. Koudelka-Hep, *Fabrication of Gas Sensitive Chemo-Resistors with Commercially Available Polyaniline*, Accepted for presentation at the "Eurosensors XIII" conference, September 12-15, The Hague, the Netherlands.

In other areas:

D.J. Strike, P. Thiébaud, Ph. Arquint, M. Koudelka-Hep, N.F. de Rooij and M.G.H. Meijerink, *Glucose and Urea Measurement using micromachined open tubular heterogeneous enzyme reactors*, DECHEMA Monographs Vol. 132 VCH Verlagsgesellschaft, Frankfurt am Main (Germany) 1996, pp. 125-137.

D.J. Strike, M.G.H. Meijerink, P. Thiébaud, Ph. Arquint and N.F. de Rooij, *Micromachined Enzymatic Reactors*, MST News Number 17/96, July/Aug. p. 4, 1996

M. Pedersen, M.G.H. Meijerink, W. Olthuis and P. Bergveld, *An IC-compatible polyimide pressure sensor with capacitive readout*, Sensors and Actuators A63 (1997) 163-168.

M. Pedersen, M.G.H. Meijerink, W. Olthuis and P. Bergveld, *A capacitive differential pressure sensor with polyimide diaphragm*, J. Micromech. Microeng. 7 (1997) 250-252.